

AD-A168 394

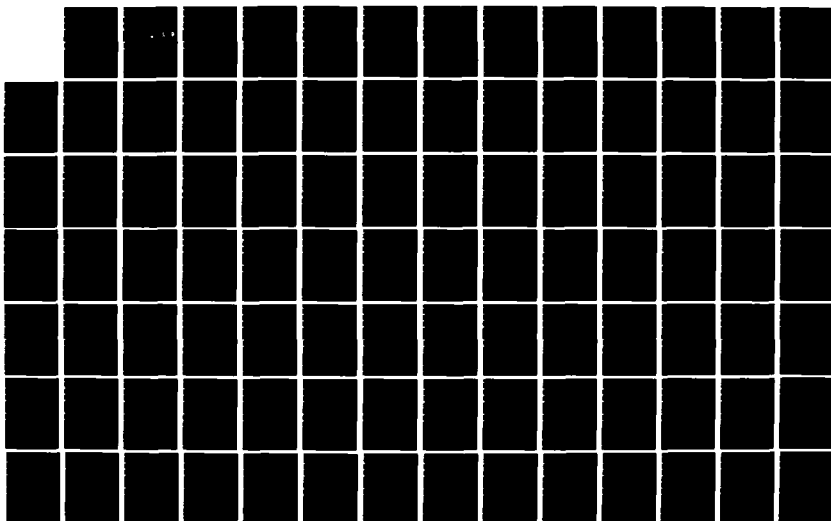
SATELLITE TRACKING AND OBSERVABILITY(U) NAVAL
POSTGRADUATE SCHOOL MONTEREY CA M G MORT MAR 86

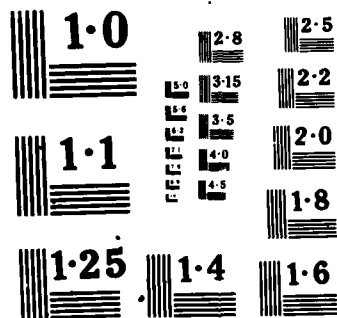
1/2

UNCLASSIFIED

F/G 22/3

NL





NATIONAL BUREAU OF STANDARDS
MICROCOPY RESOLUTION TEST

AD-A168 394

NAVAL POSTGRADUATE SCHOOL
Monterey, California



DTIC
ELECTE
JUN 10 1986
S D

THESIS

SATELLITE TRACKING AND OBSERVABILITY

by

Michele G. Mort

March 1986

Thesis Advisor:

Srbijanka Turajlic

Approved for public release; distribution is unlimited.

86 6 2 080

unclassified

SECURITY CLASSIFICATION OF THIS PAGE

A168394

REPORT DOCUMENTATION PAGE

1a. REPORT SECURITY CLASSIFICATION unclassified			1b. RESTRICTIVE MARKINGS	
2a. SECURITY CLASSIFICATION AUTHORITY			3. DISTRIBUTION / AVAILABILITY OF REPORT Approved for public release; distribution is unlimited.	
2b. DECLASSIFICATION / DOWNGRADING SCHEDULE				
4. PERFORMING ORGANIZATION REPORT NUMBER(S)			5. MONITORING ORGANIZATION REPORT NUMBER(S)	
6a. NAME OF PERFORMING ORGANIZATION Naval Postgraduate School		6b. OFFICE SYMBOL (If applicable)	7a. NAME OF MONITORING ORGANIZATION Naval Postgraduate School	
6c. ADDRESS (City, State, and ZIP Code) Monterey, California 93943-5000			7b. ADDRESS (City, State, and ZIP Code) Monterey, California 93943-5000	
8a. NAME OF FUNDING / SPONSORING ORGANIZATION		8b. OFFICE SYMBOL (If applicable)	9. PROCUREMENT INSTRUMENT IDENTIFICATION NUMBER	
8c. ADDRESS (City, State, and ZIP Code)			10. SOURCE OF FUNDING NUMBERS	
			PROGRAM ELEMENT NO.	PROJECT NO.
			TASK NO.	WORK UNIT ACCESSION NO.
11. TITLE (Include Security Classification) SATELLITE TRACKING AND OBSERVABILITY				
12. PERSONAL AUTHOR(S) Mort, Michele G.				
13a. TYPE OF REPORT Master's Thesis		13b. TIME COVERED FROM July 85 to Mar 86	14. DATE OF REPORT (Year, Month, Day) 1986 March	15. PAGE COUNT 151
16. SUPPLEMENTARY NOTATION				
17. COSATI CODES			18. SUBJECT TERMS (Continue on reverse if necessary and identify by block number)	
FIELD	GROUP	SUB-GROUP	Satellite, Satellite Tracking, Observability, Observers, Non-linear Observers, Tracking Models, Non-linear Models	
19. ABSTRACT (Continue on reverse if necessary and identify by block number) The purpose of this thesis is to study the availability of targets moving on or near the earth's surface when viewed by an orbiting satellite. A discussion of basic orbital mechanics is presented as well as a development of a suitable coordinate system. An analysis of non-linear observability is then provided. Lastly an observer is designed and successfully simulated.				
20. DISTRIBUTION / AVAILABILITY OF ABSTRACT <input checked="" type="checkbox"/> UNCLASSIFIED/UNLIMITED <input type="checkbox"/> SAME AS RPT <input type="checkbox"/> DTIC USERS			21. ABSTRACT SECURITY CLASSIFICATION unclassified	
22a. NAME OF RESPONSIBLE INDIVIDUAL Srbijanka Turajlic			22b. TELEPHONE (Include Area Code)	22c. OFFICE SYMBOL Code 621C

Approved for public release; distribution is unlimited.

Satellite Tracking and Observability

by

Michele G. Mort
Lieutenant, United States Navy
BA, Lycoming College, 1977

Submitted in partial fulfillment of the
requirements for the degree of

MASTER OF SCIENCE IN ELECTRICAL ENGINEERING

from the

NAVAL POSTGRADUATE SCHOOL
March 1986

Author:

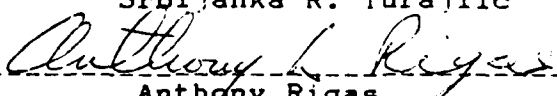


Michele G. Mort

Approved by:



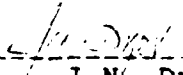
Srbiyanka R. Turajlic



Anthony Rigas



Harriett Rigas, Chairman, Department of
Electrical and Computer Engineering



J. N. Dyer,
Dean of Science and Engineering

ABSTRACT

The purpose of this thesis is to research the availability of targets moving on or near the earth's surface when viewed by an orbiting satellite. A discussion of basic orbital mechanics is presented as well as a development of a suitable coordinate system. An analysis of non-linear observability is then provided. Lastly an observer is designed and successfully simulated.

TABLE OF CONTENTS

I.	INTRODUCTION	7
II.	THE SATELLITE IN ORBIT	9
A.	SHAPE OF THE EARTH	9
B.	GREAT AND SMALL CIRCLES	10
C.	ORBITAL MOTION	15
1.	Gravity	15
2.	The Center of Mass	18
3.	Equations of Motion	20
4.	Uniform Circular Motion	23
5.	Equations of Motion in Polar Coordinates	25
D.	SATELLITE SENSORS	28
III.	SATELLITE COVERAGE AND COORDINATE SYSTEMS	34
A.	GENERAL SATELLITE COVERAGE	34
1.	Geometric Swath Width	34
2.	Ground Track and Coverage	38
3.	Spherical Triangle	41
B.	COORDINATE SYSTEMS	43
1.	Position Variables θ and ϕ	43
2.	Use of Variables θ and ϕ	45
3.	The Projected Orbit Technique	47
IV.	OBSERVABILITY	55
A.	OBSERVABILITY OF NON-LINEAR SYSTEMS	57
B.	JACOBIANS AND NON-LINEAR ANALYSIS	61

V. OBSERVERS	71
A. LINEAR LUENBERGER OBSERVERS	71
B. NON-LINEAR OBSERVER	74
C. DEVELOPMENT OF SATELLITE OBSERVER	78
VI. SIMULATION RESULTS	83
A. THE BASIC CONTINUOUS OBSERVER	83
B. THE DISCRETE OBSERVER	85
1. Full Non-Linear Observer	87
2. Redefined Non-Linear Model	89
3. Redefinition of State Variables	91
4. Model Decoupling	94
5. Subsystem Two	94
VII. CONCLUSIONS AND RECOMMENDATIONS	101
APPENDIX A: ELEMENTS OF ORBIT	103
APPENDIX B: RELATIVE MOTION	107
APPENDIX C: ORIGINAL MODEL SIMULATION RESULTS.....	110
APPENDIX D: DECOUPLED MODEL SIMULATION RESULTS	126
LIST OF REFERENCES	148
BIBLIOGRAPHY	149
INITIAL DISTRIBUTION LIST	150



Accession For	
NTIS CRA&I	<input checked="" type="checkbox"/>
DTIC TAB	<input type="checkbox"/>
Unannounced	<input type="checkbox"/>
Justification	
By	
Distribution /	
Availability Codes	
Dist	Avail and/or Special
A-1	

ACKNOWLEDGEMENTS

I would like to thank Professor Srbijanka Turajlic for her strong support and outstanding guidance throughout the development of this thesis. Her superior knowledge, engineering intuition and encouragement enabled me to complete the necessary research. Professor Turajlic's helpful advice and technical expertise proved instrumental in the development of the latter part of this work.

I would also like to thank Professor Anthony Rigas for his support and helpful suggestions. His excellent English rhetoric skills and proof reading aided the completion of this thesis. I would also like to extend my appreciation to Professor Harriett Rigas for her administrative support of my thesis goals and processing.

This thesis was originally part of a long term project researching satellite tracking under the guidance of Professor R. R. Mohler, Oregon State University. It is hoped that the results obtained by my research will contribute to this project.

I would like to acknowledge the much appreciated assistance of Captain James Kesler, USMC, for his aid in processing this thesis. This thesis would not be possible without the support of staff, faculty and fellow students.

I. INTRODUCTION

This thesis deals with satellite tracking of relatively low altitude targets. The long term goal of this project is to determine an effective general-coverage satellite orbital pattern. The short term goal of this thesis is to explore the possible use of various coordinate systems and to design a satellite observer. A target such as a slow moving aircraft is assumed for the basic development.

Chapter 2 contains an overview of basic satellite mechanics and dynamics as well as a brief discussion of satellite detection and tracking equipment. Equations regarding orbital motion will also be introduced. Also chapter 2 provides an overview of the entire thesis.

The theory and mathematics of satellite and target motion for a specific case are developed in Chapter 3. The geometry of motion on a spherical surface is detailed in that chapter. Specifics such as geometric swath width, line-of-sight and precession are furnished. This leads into an in-depth examination of coordinate systems. Various attempts to find a suitable set of reference axes for analytic studies of the tracking problem are presented. It is desired to achieve a target and observation model that has a convenient basis for analysis such as either linear or

bilinear in state space. Several trial coordinate systems were developed mathematically but found unsuitable. One trial system is considered satisfactory under certain assumptions and is, therefore, completely developed.

Chapter 4 presents a discourse on observability in general, and non-linear observability in particular. The concept of connectedness and univalence is discussed. The chosen system is then analyzed for observability.

The topic of observers is presented in Chapter 5. A background on basic observers is provided. Finally an observer is designed and simulated by computer for the preferred system.

Chapter 6 offers conclusions and recommendations for further studies.

II. THE SATELLITE IN ORBIT

Before an understanding of satellite tracking can be achieved it is essential to have an understanding of basic satellite dynamics and satellite sensors. The concepts and equations that govern the motion of a satellite in orbit around the earth are based on the physical laws put forth by Kepler and Newton. These laws of motion apply to artificial satellites as well as planets and moons. The physical geometries and forces are the same. The following explanations and derivations form a basis for orbital motion of a satellite.

A. THE SHAPE OF THE EARTH

In reality the earth is neither exactly round nor exactly a rigid body. The constituents can be molded and deformed to a certain degree. The earth's rotation causes its own materials to feel a force that pulls tangentially into space. Fortunately the earth's materials also undergo a constant centripetal (center seeking) acceleration to keep them in place. This centripetal acceleration, which is directed towards the center of curvature, is provided by earth's gravity.

The gravitational force produced by the earth is directed towards the center of the earth. However, the momentum produced by the earth's rotation pulls at the

earth's materials. Each particle of earth has both these forces acting on it. The earth's surface at the equator is actually moving faster around the rotation axis than the surface material at or nearer the poles. Figure 2.1 illustrates this. Therefore the materials on the surface at the equator feel this tangential pull the most. Analysis shows that the result is an earth shaped like an oblate ellipsoid.

An oblate ellipsoid can be described as a sphere which has been compressed along the polar axis and therefore bulges at the equator. A cross sectional slice through the poles yields an ellipse. A slice along the equatorial plane yields a circle.

This oblateness (measure of the earth's flattening) of the earth is only slight. The equatorial diameter is calculated to be 12,757 km whereas the polar diameter is calculated to be 12,714 km. This is only a 43 km difference which is about 1 part in 297.

B. GREAT AND SMALL CIRCLES

The earth's equatorial bulge can be temporarily disregarded in order to consider the earth as a sphere turning beneath an orbiting satellite. The intersection of a plane passed through the center of the sphere and the sphere is the largest circle that can be drawn on the sphere's surface. This is known as a great circle. The shortest distance between any two points on the surface of

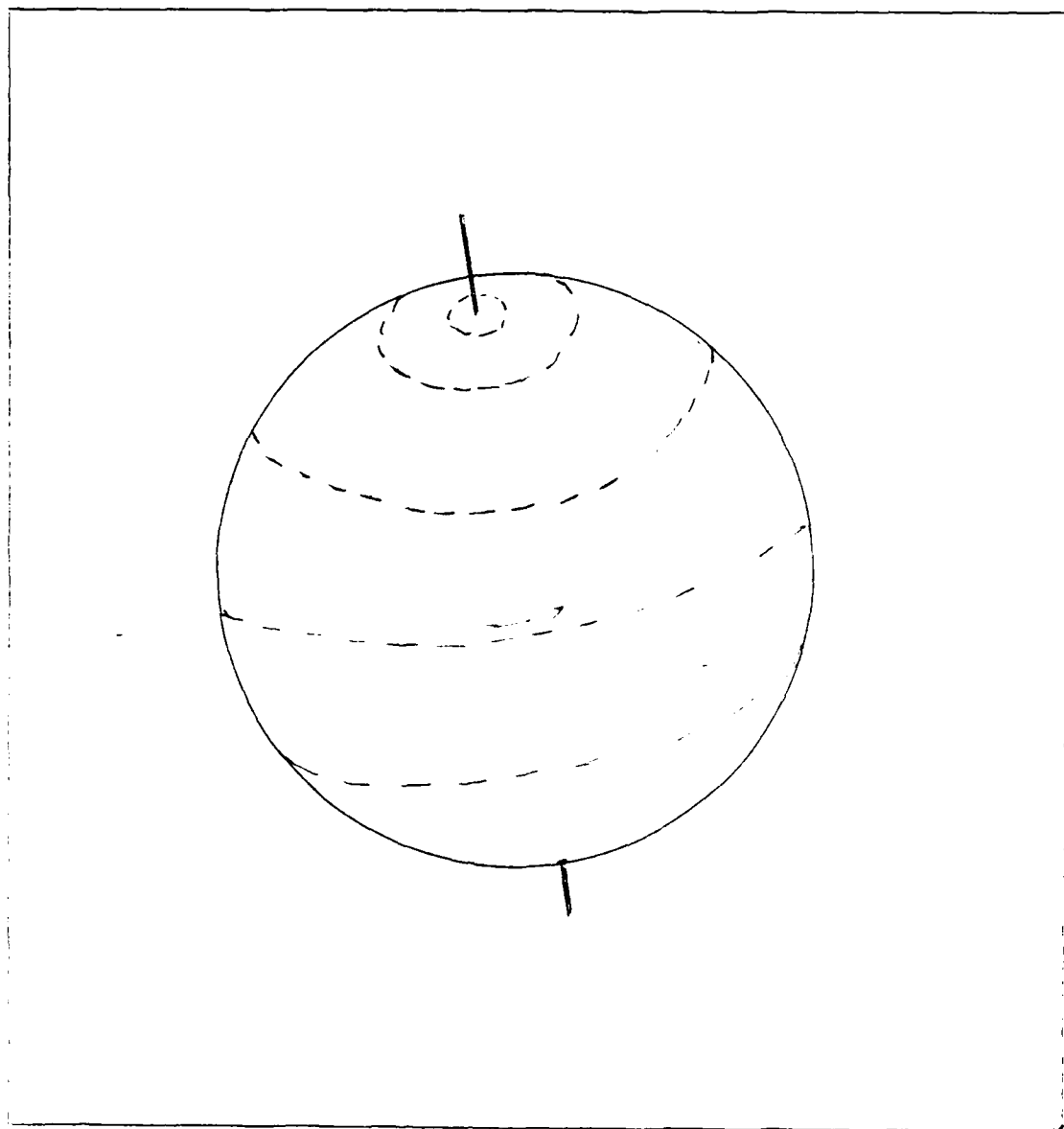


Figure 2.1 Rotating Earth

the earth is an arc of a great circle. The earth's equator is an example of a great circle. There are an infinite number of approximate great circles on the earth's surface since there are an infinite number of planes that can be passed through the earth's center.

There is a series of 24 special great circles that pass through the earth's poles and are evenly spaced from each other. These are called meridians and they intersect with the equator at right angles. Meridians join at both poles. Forming other right angles to the Meridians are parallels. Parallels are small circles created by passing planes through the earth parallel to the equatorial great circle. See Figure 2.2.

In order to determine precise locations on the earth's surface, latitudes and longitudes are utilized. The longitude of a specific place refers to the arc (measured in degrees) of a parallel between that place and the prime meridian (which passes through Greenwich, England for reasons of history). Longitudes run east and west. Latitudes, however, run north and south. The latitude of a specific place may be defined as the arc (in degrees) of a meridian between that place and the equator. Figure 2.3 shows an example. When the earth is considered as having an ellipse as a cross section (which it has) instead of a circular one, the length of a degree of latitude is slightly greater at the poles than at the equator.

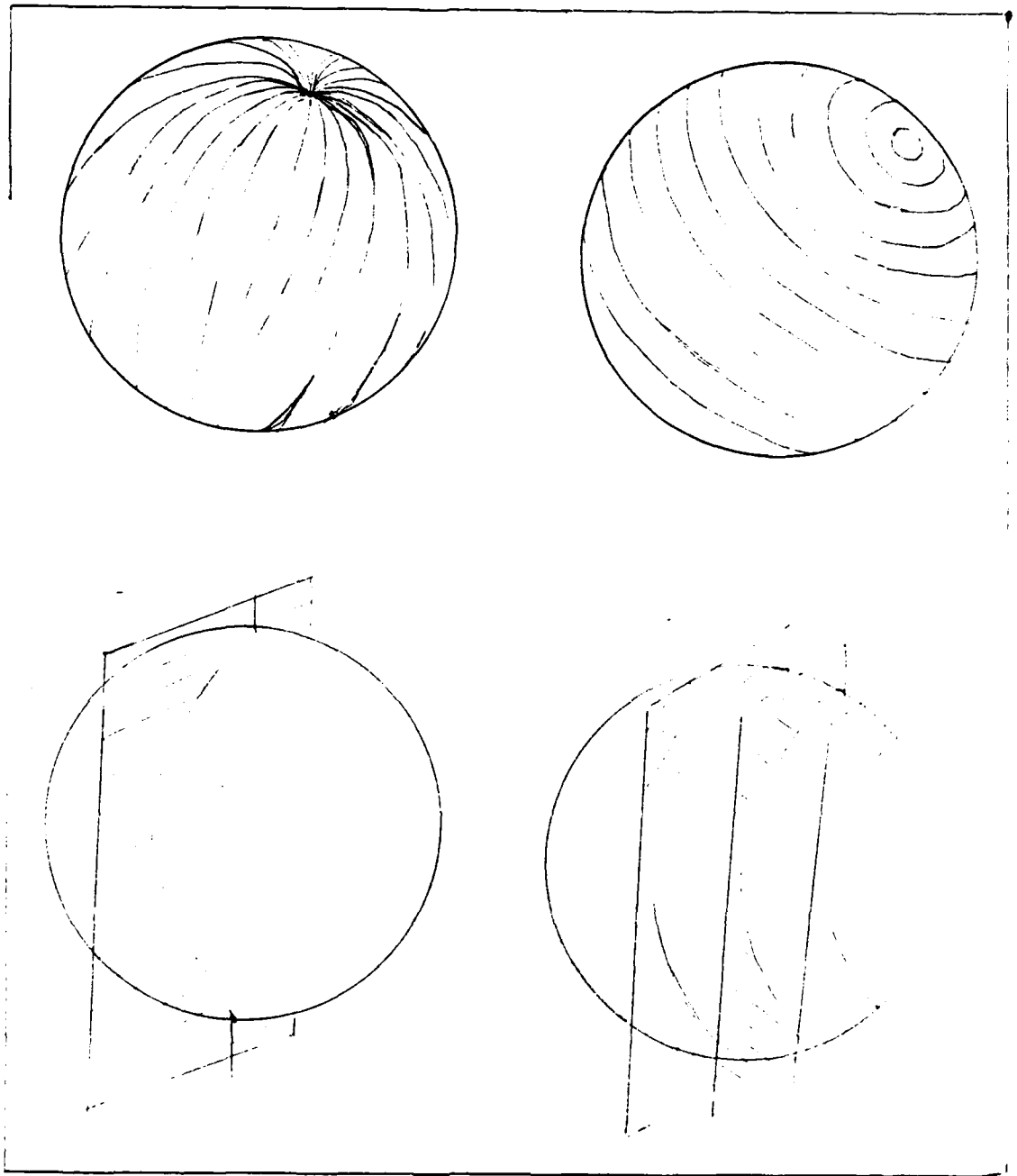


Figure 2.2 Meridians and Parallels

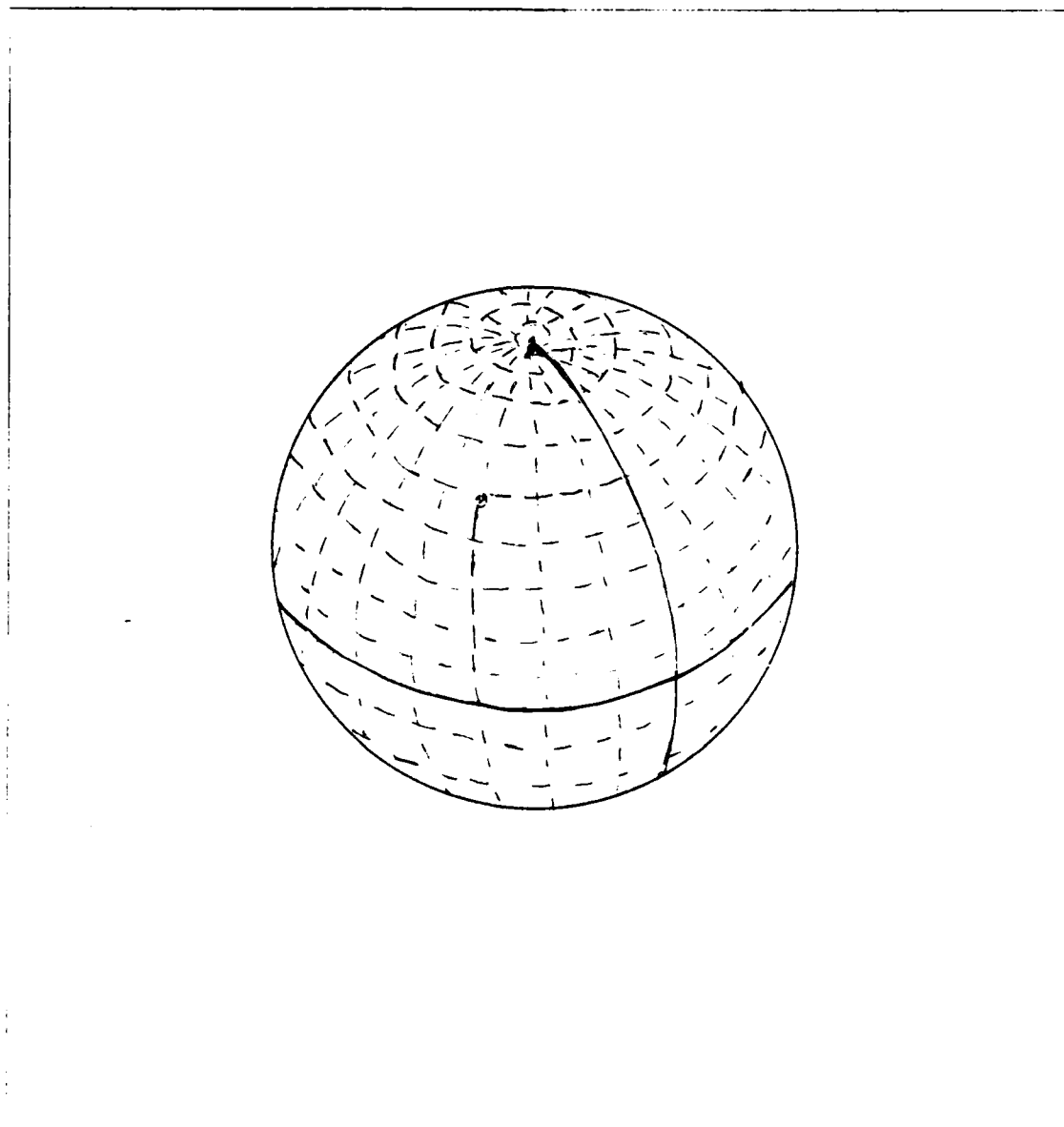


Figure 2.3 Longitude and Latitude

C. ORBITAL MOTION

A presentation concerning orbital motion is basic to satellite tracking. Gravitational attraction and momentum combine to keep a satellite in perpetual orbit above the earth (in the absence of friction and external celestial attractions).

1. Gravity

The understanding of gravity and orbital motion can be traced back to Johannes Kepler (1571-1630) and Issac Newton (1642-1727). Kepler is known predominantly for his three laws of planetary motion. The laws are as follows;

- (1) Each planet moves about the sun in an orbit that is an ellipse, with the sun at one of the foci of the ellipse.
- (2) The straight line joining a planet and the sun sweeps out equal areas in space in equal intervals of time.
- (3) The squares of the sidereal periods of the planets are in direct proportion to the cubes of the semimajor axes of their orbits.

The above three laws apply equally well for artificial satellites as they do for planets. Newton restated and clarified Kepler's laws. Newton was an advocate of rigorous proofs whereas Kepler preferred to state empirical laws based on observations.

Kepler's first law stated mathematically is

$$f = mv^2/r \quad (2.1)$$

where: f = centripetal force needed for circular orbit,
 m = mass of planet (or satellite) in orbit,
 v = velocity of orbiting body,
 r = distance between sun and planet (or satellite and earth),

Kepler's third law restated mathematically is

$$(m_1 + m_2)p^2 = 4\pi^2 a^3 / G \quad (2.2)$$

where m_1 and m_2 refer to the masses of two bodies that revolve mutually about each other.

p = period of revolution,

a = semimajor axis of relative orbit,

G = universal gravity constant ($6.67 \times 10^{-11} \text{ m}^3/\text{kg} \cdot \text{s}^2$)

Newton also explained the reasons behind Kepler's original observations. That is, Newton supplied the laws of motion which are at the root of classical mechanics.

These laws are as follows;

- (1) Every object remains at rest or in uniform motion unless an external force acts upon it.
- (2) The product of the mass of an object and its acceleration vary directly as the resultant force, and the change in motion takes place in the direction of that force.
- (3) For every action there is an equal (in magnitude) and opposite (in direction) reaction.

In the case of orbiting planets or satellites, gravity is the unseen force referred to in Newton's first law. Newton also postulated that every particle of matter in the universe attracts every other particle. The force of

this attraction is proportional to the product of their masses and inversely proportional to the square of the distance which separates them.

In equation form this is

$$F = Gm_1 m_2 / d^2 \quad (2.3)$$

where d is the distance between the center of mass 1 and mass 2.

Orbital motion can be understood in terms of Newton's laws previously stated. The critical factors in putting a satellite in orbit (by the traditional launch method) are speed and direction of movement at burnout. Burnout is when the rocket engine shuts off and the satellite behaves as an astronomical object.

As a satellite follows its orbital path it continuously falls toward the earth due to the earth's gravitational pull. However, the satellite's momentum prevents it from really being pulled any nearer to the earth. The satellite's orbit is the result of two main forces. The momentum of the satellite is a measure of its state of motion. The inertia of the satellite (recall Newton's first law) is that property that causes the satellite to resist acceleration and travel in a straight line. For the satellite to move in a circular path rather than in a straight line, it must continually suffer an acceleration toward the center of the circle. This acceleration is centripetal acceleration. The central force

that produces the centripetal acceleration is that gravitational attraction between the satellite and the earth. Figure 2.4 illustrates this in vector form.

The period of an artificial satellite is directly related to the size of it's orbit; i.e., the closer the satellite is to the earth the faster it travels.

2. The Center of Mass

The center of mass can be defined as that point within a system that either remains fixed or moves as if the entire mass of the system were concentrated at that point. For a number of particles the center of mass is defined as

$$\underline{r}_{cm} = (1/M_{Total}) \sum_{i=0}^{Total} m_i \underline{r}_i \quad (2.4)$$

An example of this for a two body system is

$$x_{cm} = \frac{m_1 x_1 + m_2 x_2}{m_1 + m_2} \quad (2.5)$$

Mass 1 is a distance $x(1)$ from an arbitrary origin, and mass 2 is a distance $x(2)$ from the origin. $x(cm)$ represents the location of the center of mass. A solid object can be thought of as a collection of a great many particles. In this case equation 2.4 applies.

Very often it is useful in certain calculations to treat a particular body as if its entire mass is concentrated at one point. That one point is the center of mass.

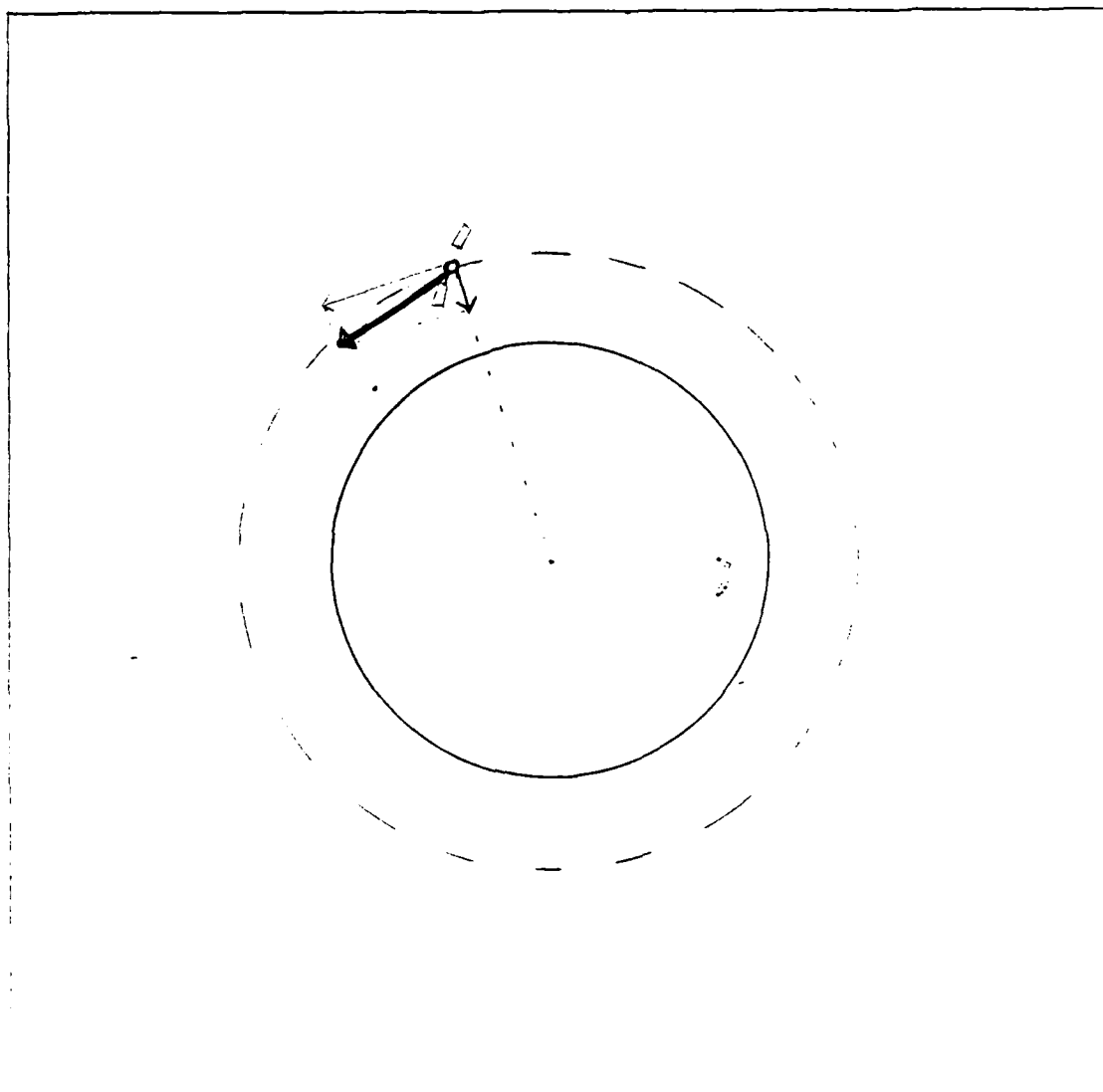


Figure 2.4 Centripetal Acceleration

It can be shown [Ref. 1] that a large sphere attracts other bodies as though the sphere's mass is all located at the center. This holds true as long as the sphere is of uniform density or is made up of concentric shells each being of uniform density. The earth is often approximated as being a sphere made up of uniformly dense shells [Ref. 2].

3. Equations of Motion

A satellite in orbit around the earth will feel by far the strongest gravitational pull from the earth itself. Other astronomical bodies, such as the moon or sun, do exert force disturbances but are too far away to exert a very strong pull on the satellite. Assuming the gravitational acceleration of the satellite is due only to the earth's gravitational attraction, g can be defined as

$$g = Gm_e/r^2 \quad (2.6)$$

The value of g does vary with respect to altitude and latitude (since the earth is not really an exact sphere). Tables 1 and 2 depict the variations of g . The values of g are close enough to allow an approximation of the earth's shape as spherical for most applications.

An orbiting satellite is considered to be in the earth's gravitational field. The vector symbol \mathbf{g} refers to this field and is defined as

TABLE 1

VARIATION OF g WITH LATITUDE AT SEALEVEL

Latitude	$g(m/s^2)$
0° (equator)	9.78039
10°	9.78195
20°	9.78641
30°	9.79329
40°	9.80171
50°	9.81071
60°	9.81918
70°	9.82608
80°	9.83059
90°	9.83217

TABLE 2

VARIATION OF g WITH ALTITUDE AT 45° LATITUDE

Altitude(km)	$g(m/s^2)$
0	9.806
1	9.803
4	9.794
8	9.782
16	9.757
32	9.710
100	9.600
500	8.530
1000	7.410
380000	0.003

$$\underline{g} = \underline{F}/m \quad (2.7)$$

When an object is a distance h above the earth's surface it has potential energy defined as

$$U = -(-mg)h = mgh \quad (2.8)$$

Gravity is a conservative force pointing to the earth's center and has the value $(-mg)$. The gravitational force exerted on an object in this field can be derived from the potential energy equation as

$$F = \frac{-du}{dr} = \frac{d}{dr} \left[\frac{-GMm}{r} \right] = \frac{-GMm}{r^2} \quad (2.9)$$

A more general form for potential energy invoking the universal constant G is

$$U = -GMm/r \quad (2.10)$$

Potential energy can be converted into kinetic energy [Ref. 3]. As an object falls to earth it loses its potential energy as its height decreases but gains kinetic energy as its velocity increases. Kinetic energy is mathematically defined as

$$K = GMm/2r = mv^2/2 \quad (2.11)$$

The total mechanical energy is

$$E = K + U \quad (2.12)$$

Orbital motion can be considered as motion in a plane. For one full revolution around the earth the satellite remains in a plane as it traces out an ellipse or circle.

The velocity, period and altitude of a satellite are all inter-related. The period of a satellite [Ref. 2] can be defined as

$$\tau = 2\pi(R + h)/v , \quad (2.13)$$

where v is the velocity of the satellite.

The centripetal force, is often defined as

$$F = m_3 v^2 / (R + h) \quad (2.14)$$

where m is the mass of the satellite.

It is obvious to the casual observer that the centripetal force is also in part a function of the satellite's altitude and velocity. Polar coordinates are used in figure 2.5 to illustrate the elliptical orbit variables.

4. Uniform Circular Motion

Sometimes a satellite's elliptical orbit is that perfect ellipse the circle. If the satellite's orbital velocity remains unchanged in a circular path then the satellite is moving with uniform circular motion.

Since the orbit of a two body system (earth and satellite) is often in a plane it is possible to use polar coordinates to develop basic equations. Figure 2.6 shows the relation between polar and rectangular coordinates. Velocity in polar coordinates for circular motion can be expressed as

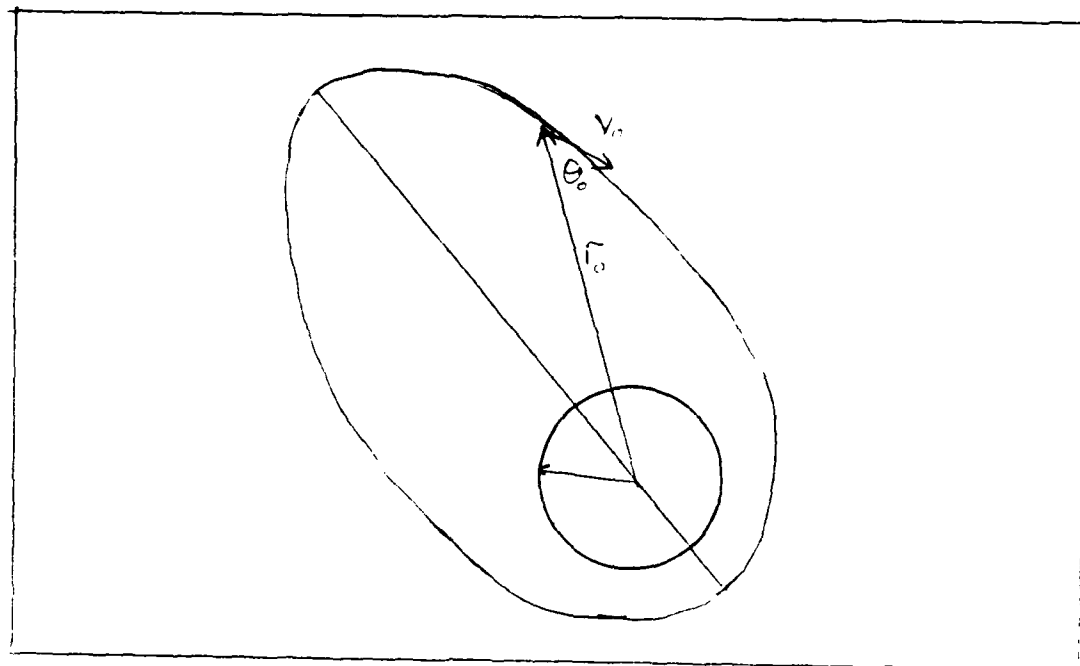


Figure 2.5 Elliptical Orbit

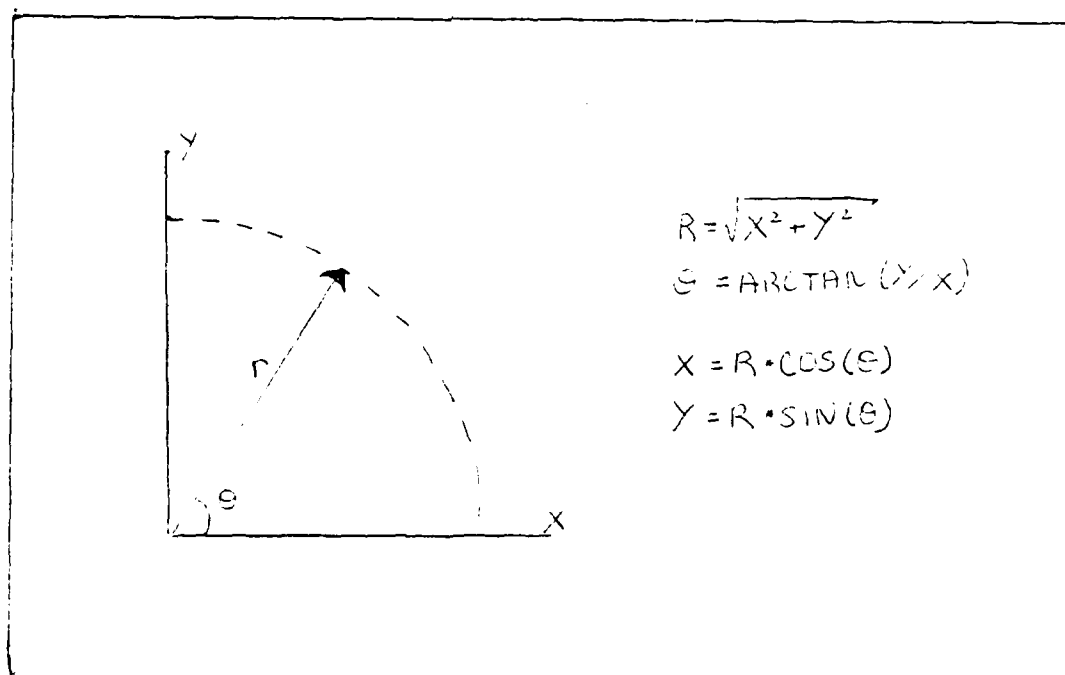


Figure 2.6 Polar and Rectangular Coordinates

$$V = r\dot{\theta}\hat{\theta} \quad (2.15)$$

where θ refers to motion in the theta (θ) direction. Acceleration is found by taking the derivative of the velocity

$$a = -r\dot{\theta}^2\hat{r} + r\ddot{\theta}\hat{\theta} \quad (2.16)$$

Energy can be expressed as

$$E = K + U = m(r'\dot{\theta}^2)/2 - GMm/r \quad (2.17)$$

and angular momentum as

$$L = mr'^2\theta \quad (2.18)$$

Uniform circular motion is easier to deal with than non-uniform circular motion. There is only an angular component of velocity present in the equation. It is often useful to simplify the satellite dynamics in order to more easily manipulate equations.

5. Equations of Motion in Polar Coordinates

Consider the special case of a satellite in a circular orbit. This can be treated as motion in a plane. Polar coordinates are especially useful for this case. The two variables that define motion and position are the radial coordinate, r , and the angular coordinate, θ , conversion between rectangular coordinates and polar coordinates is as follows.

$$\begin{aligned} r &= \sqrt{X^2 + Y^2} & X &= r\cos(\theta) \\ \theta &= \arctan(Y/X) & Y &= r\sin(\theta) \end{aligned}$$

Figure 2.7 illustrates this.

Polar coordinates are often used any time curvilinear motion occurs. In Figure 2.8 basic curvilinear motion is shown. The differential length dr has components in both the r and θ directions. The vector r can be expressed as rn where n is a unit vector in the radial direction.

Velocity can be defined as;

$$\underline{v} = \frac{d(r)}{dt} = \frac{d(rn_r)}{dt} = \frac{dr}{dt}n_r + r\frac{dn_r}{dt} \quad (2.19)$$

Rectangular coordinates are used once again to achieve an expression for the time derivative of the unit vector n and

\underline{n}_θ :

$$\begin{aligned} \underline{n}_r &= \cos(\theta)i + \sin(\theta)j & \underline{n}_\theta &= -\sin(\theta)i + \cos(\theta)j \\ \frac{d\underline{n}_r}{dt} &= -\sin(\theta)\dot{\theta}i + \cos(\theta)\dot{\theta}j = (-\sin(\theta)i + \cos(\theta)j)\dot{\theta} = \dot{\theta}\underline{n}_\theta \\ \frac{d\underline{n}_\theta}{dt} &= -\cos(\theta)\dot{\theta}i - \sin(\theta)\dot{\theta}j = -(\cos(\theta)i + \sin(\theta)j)\dot{\theta} = -\dot{\theta}\underline{n}_r \end{aligned}$$

Velocity can now be expressed as;

$$\underline{v} = \dot{r}\underline{n}_r + r\dot{\theta}\underline{n}_\theta$$

Following the same rules of differentiation acceleration can be derived.

$$\underline{a} = \dot{\underline{v}} = \dot{r}\underline{n}_r + \dot{r}\dot{\theta}\underline{n}_\theta + r\ddot{\theta}\underline{n}_\theta + r\dot{\theta}\frac{d\underline{n}_\theta}{dt} - r\dot{\theta}^2\underline{n}_r$$

Simplifying,

$$\underline{a} = (\ddot{r} - r\dot{\theta}^2)\underline{n}_r + (2r\dot{\theta} + r\ddot{\theta})\underline{n}_\theta \quad (2.20)$$

For circular motion the radial component, r , remains constant. Only θ varies. Therefore;

$$\underline{v} = r\dot{\theta}\underline{n}_\theta \quad (2.21)$$

$$\underline{a} = -r\dot{\theta}^2\underline{n}_r + r\ddot{\theta}\underline{n}_\theta \quad (2.22)$$

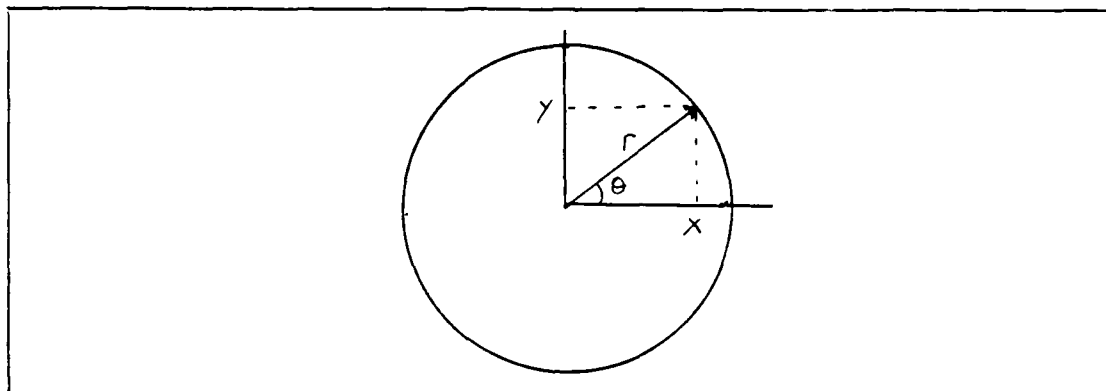


Figure 2.7 Coordinate Conversion

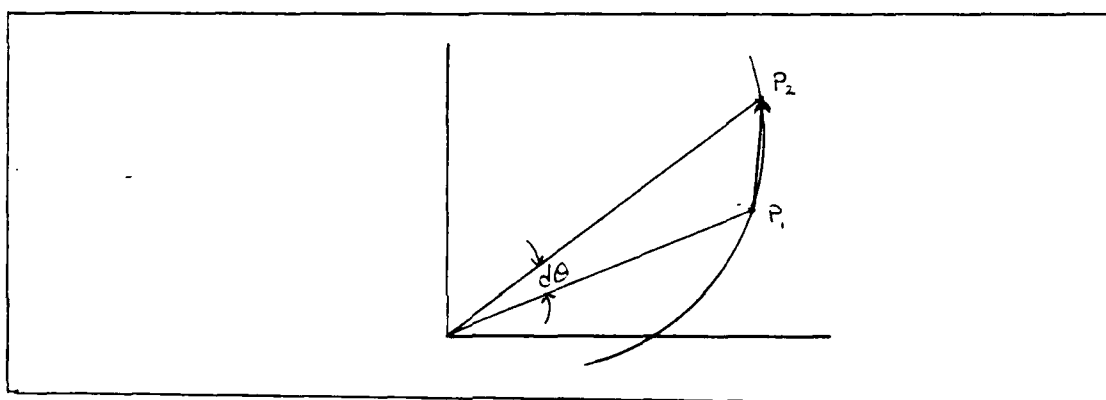


Figure 2.8 Curvilinear

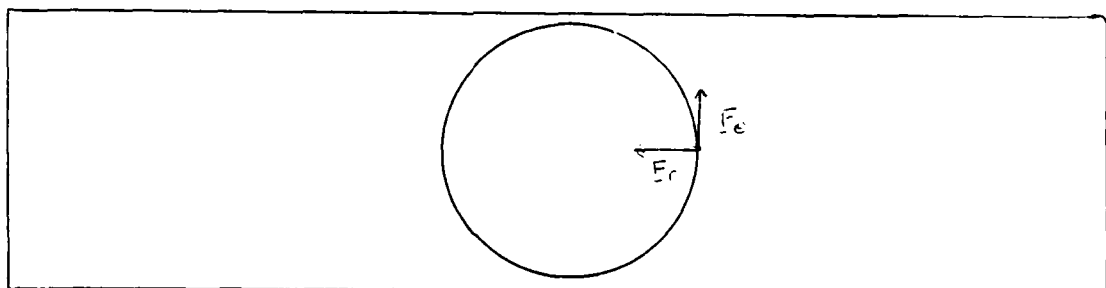


Figure 2.9 Vector Forces

The acceleration term directed in the negative radial direction is the center seeking acceleration.

Figure 2.9 depicts the directions for the force vectors. The sum of forces is calculated as follows;

$$\Sigma \underline{F}_r = m \underline{a}_r = m(\ddot{r} - r\dot{\theta}^2) \underline{n}_r \quad (2.23)$$

$$\Sigma \underline{F}_\theta = m \underline{a}_\theta = m(r\ddot{\theta} + 2\dot{r}\dot{\theta}) \underline{n}_\theta \quad (2.24)$$

Using differential equations and state form motion can be represented as in equations 2.27 and 2.28.

$$dr/dt = V_r \quad (2.25)$$

$$d\theta/dt = \omega \quad (2.26)$$

$$dV_r/dt = V_\theta^2/r - k/r + U - \delta_r \quad (2.27)$$

$$d\omega/dt = -2V_r\omega/r + (U_\theta - \delta_\theta)/r \quad (2.28)$$

where $U_r = F_r/m$ and $U_\theta = F_\theta/m$. Both variables represent thrusts. The symbols δ_r and δ_θ are used to represent disturbances which are assumed to be zero in this case.

D. SATELLITE SENSORS

Various sensors on board the satellite are employed to keep the satellite itself on track, and to detect and track a possible target. The satellite guidance system uses sensors for measuring certain vehicle dynamic variables. Such variables include satellite acceleration, velocity, position and angular velocity. Guidance systems generally determine these variables, compare the received information with desired parameters, and generate correction commands. Various types of sensors include inertial, optical and radio sensors. The satellite may make use of gyroscopes to

establish a set of reference axes on board. Active thrust control is used to align the body axes with the reference axes. Once the satellite has established the craft's position and attitude active control components are activated. These components respond either to a telecommand from a ground station or to the satellite's on-board computer in order to correct the satellites's status. In some applications where perturbations are likely, feedback control is added to the active control of a satellite. In some cases optical sensors are used in conjunction with inertial equipment. Optical sensors include such devices as sun finders, sun sensors, planet sensors, celestial trackers, and horizon scanners. The gyroscopes and accelerometers are examples of inertial sensors. In certain applications the inertial sensors provide short-term stability and optical sensors provide long-term stability.

The gyroscope is an inertial guidance system that is often used for ships, aircraft and spacecraft. A gyroscope is a device that possesses a high rate of spin about an axis of symmetry that has freedom of angular rotation. Examples of gyroscopes are the rate gyro and the integrating gyro.

Surveillance satellites normally have an entirely different set of sensors for target acquisition. Very often this type of satellite carries several types of information gathering devices. High resolution optical devices, radar scanners and infrared capacity can all be included in a

satellite payload. Passive systems are sensitive receivers which normally provide data on bearing and bearing rate. These systems have the advantage that they do not alert the target of their actions. Optical techniques normally involve lenses and cameras. This can be very precise, especially at low altitudes.

Radar is an example of an active sensor. It bounces radio waves off a chosen target. This is excellent for determining both bearing and range. Both optical and radar methods can be degraded by poor atmospheric conditions. For the radar tracking technique noise is always the main limitation.

Inverse scattering methods are being developed to enable polarimetric radar to obtain better target information. This procedure involves illuminating the target with polarized waves and observing the amplitudes and phases of a set scattered waves.

Another type of sensor is the synthetic aperture radar system. This is based on holography methods. Holography has the ability to record three dimensional pictures and focus sharply on both the near field and the far field at the same time. This involves recording a wave interference pattern. A microwave generator is used to provide a constant frequency microwave signal as well as a reference wave. This is considered to be a highly precise and accurate sensor.

Passive sensors are normally infrared sensors. There are two major techniques used in infrared detectors. The two main types are called photon detectors and thermal detectors.

In photon detectors, the technique used involves a photon of infrared radiation being absorbed by a semiconductor electron which raises its energy level into a conduction band. Photons with less energy than the band gap produce no signal and are thereby effectively filtered out.

Thermal detectors function by sensing the temperature change resulting from absorption of infrared radiation by a suitable element. Usually, this absorbing element has some temperature sensitive electrical property such as resistivity so that the temperature change is sensed electrically.

One device often used in passive detectors is the radiometer. This device is a broadband, dual frequency, low noise, solid state, remote controlled mechanism. Radiometers are used to obtain high resolution imagery from low altitude satellites.

A promising type of detector is the Silicide Schottky diode based infrared camera. These are easy to manufacture and have excellent performance. The camera focal plane consists of a two dimensional array of metal electrodes fabricated on a silicon substrate. The focal plane is back illuminated. When an infrared picture is observed, hot

carriers are emitted from the focal plane electrodes. An electronix image of the scene is formed by accumulation of these carriers on a pixel by pixel basis.

Another technique involves the Charge Injection Devices (CID). These devices are surface charge devices that collect photon generated charges and store them in MOS capacitors.

Other types of infrared detectors include the Lead Sulfide (PbS) Detectors, Lead Selenide Detectors (PbSe), Thermister Infrared Detectors and Indium Antimode Charge Injection Devices.

One tracking technique available to surveillance satellites involves the use of the doppler effect. The satellite emits a signal and then receives the signal's return after it reflects off a given target. The change in frequency as a result of the relative motion between satellite and target leads to a calculation of the targets velocity. Ref 3 defines the return frequency, ν , detected by the satellite as

$$\nu = \nu_0(1-u/c) / 1-(u/c)^2, \quad (2.29)$$

where

ν_0 = frequency detected if both were at rest,

u = relative separation speeds,

c = speed of light,

Artificial satellites are often subject to a variety of disturbing forces. These include atmospheric drag, variation of atmospheric density, solar radiation pressure, surface charge drag, meteorite impacts, lunar or solar gravity caused perturbations and possible encounters with hostile killer satellites. These potential disturbances can act seriously to impede the position as well as the attitude stability of a satellite. Fortunately, there are passive and active stabilization systems to enable recovery from most perturbations.

III. SATELLITE COVERAGE AND COORDINATE SYSTEMS

This chapter includes satellite coverage, spherical geometry and coordinate systems. A coordinate system which enables analytical calculations of satellite observer and tracker is desired for at least a single case. Several systems are explored in an attempt to find a suitable set of reference axes to establish a base for more complicated analysis by computer. A simple case is introduced and an appropriate coordinate system is presented.

A. GENERAL SATELLITE COVERAGE

Basic information on satellite coverage is discussed here. An understanding of geometric swath width and precession is required for a detailed study of satellite tracking.

1. Geometric Swath Width

As a satellite travels around the earth it covers a certain amount of surface area. This area is in the form of a spherical cap (figure 3.1). As the satellite's altitude above the earth increases the area of the spherical cap increases. The area of the spherical cap [Ref.5] can be calculated as

$$A = 2\pi R^2(1 - \sin(90^\circ - \theta)) \quad (3.1)$$

where R is the radius of the earth and θ is the angle shown in Figure 3.2.

It appears from this that a high altitude orbit is beneficial. However, it must be considered that as satellite altitude increases, satellite sensor accuracy decreases.

If a target is at point 'a' (as in Figure 3.2) it can be viewed by the satellite as long as the satellite is between points 1 and 2 on its orbit. This portion of the orbit keeps the satellite above the horizon with respect to the target. The amount of time the satellite is above the horizon is calculated [Ref. 5] to be

$$t = 2\theta/w \quad (3.2)$$

where w is the angular velocity of the satellite.

As the satellite progresses in its orbit the spherical cap of coverage moves with it. As it moves, the cap traces out a ribbon around the earth. The width of the ribbon (Figure 3.3) is the geometric swath width (GSW).

Figure 3.4 illustrates the GSW as the very dark arc on the earth's surface. The dotted line from point 1 to point 2 is tangent to the earth at the surface location directly beneath the satellite. R is the radius of the earth and h is the satellite altitude. The arc, $a(1)$, in Figure 3.5 is one half the dark arc in Figure 3.4. Simple geometry proves that $\text{arc } a(1) = R\theta$. Therefore the

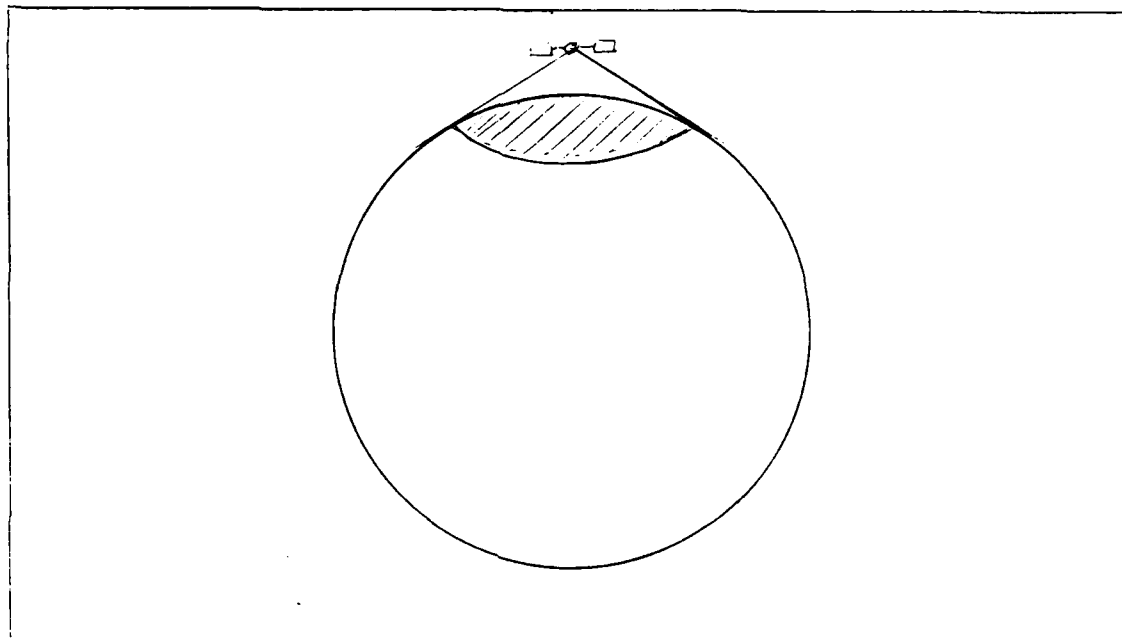


Figure 3.1 Spherical Cap

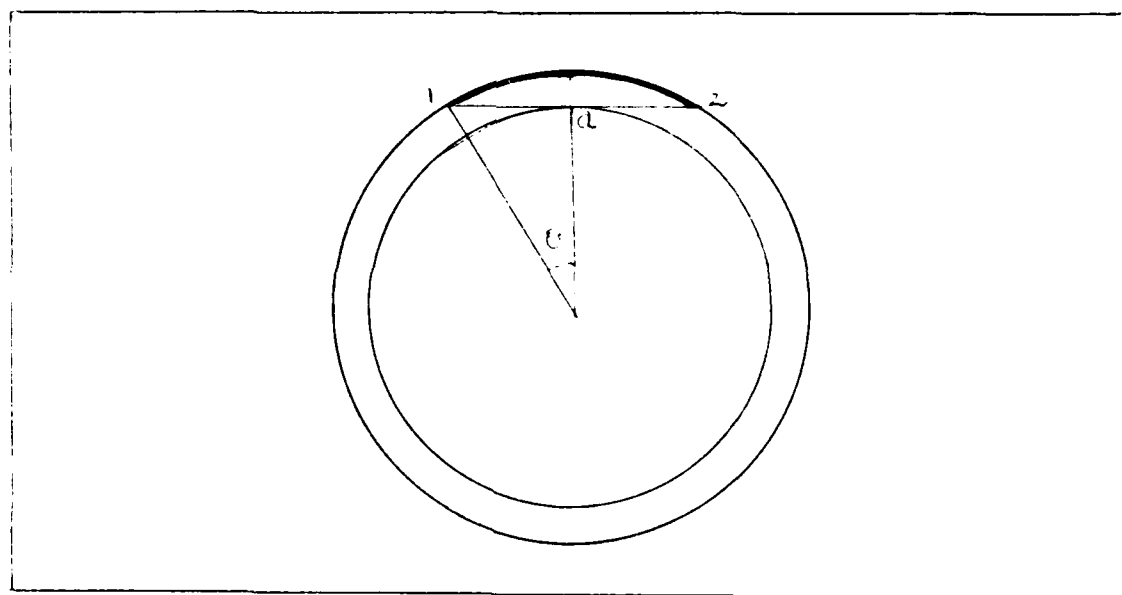


Figure 3.2 View of the Target

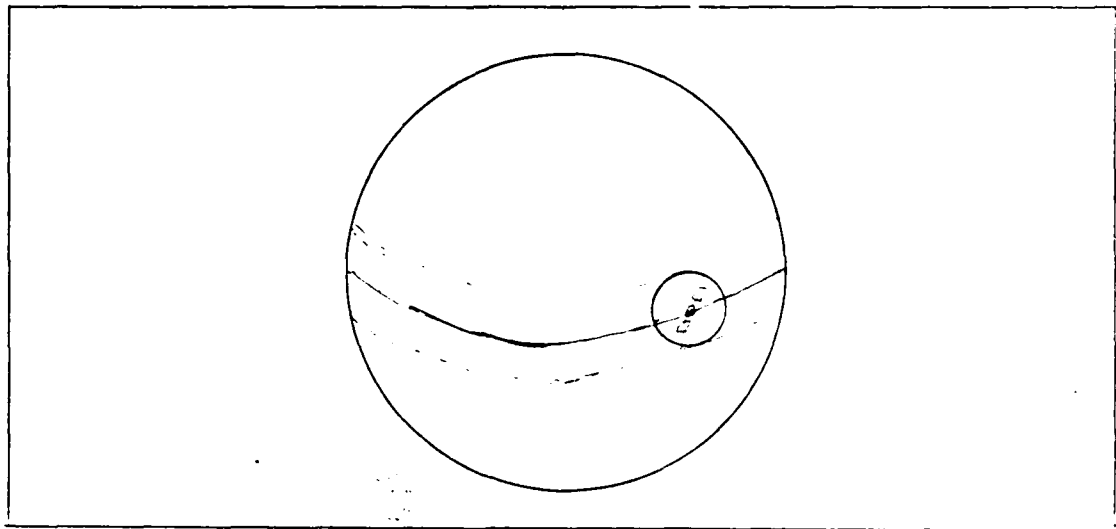


Figure 3.3 Geometric Swath Width Ribbon

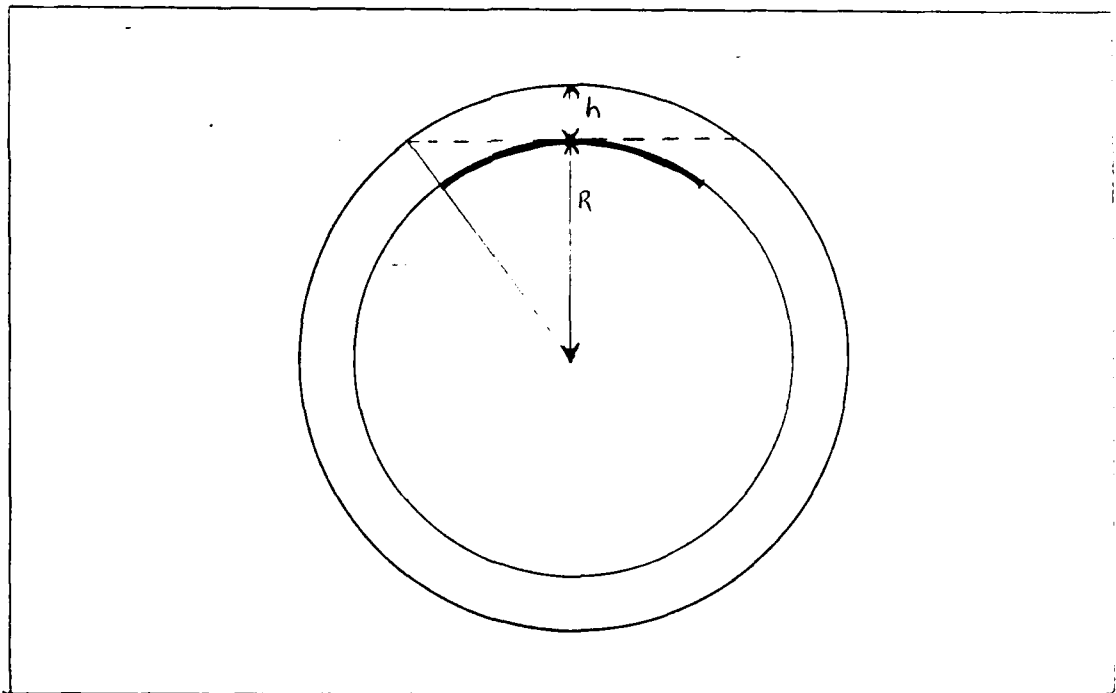


Figure 3.4 Geometric Swath Width

GSW = 2θR. Figure 3.6 depicts a right triangle. From the rules of trigonometry $\cos(\theta) = R/(R+h)$. Therefore,

$$\theta = \arccosine(R/(R+h))$$

It follows by substitution that

$$GSW = 2R(\arccosine(R/(R+h))) \quad (3.3)$$

2. Ground Track and Coverage

As a satellite travels in its orbit the distance it moves in one full trip around the earth is

$$D = 2\pi(R+h) \quad (3.4)$$

where R is the radius of the earth and h is the satellite's height above the surface. The orbital speed is calculated [Ref.5] to be

$$S_o = 4.2685(R/(R+h)) \text{ km/sec} \quad (3.5)$$

The satellite also has a ground speed and a ground track. The satellite's position can be projected on to the earth's surface. This point on the earth's surface directly below the satellite is called the sub-satellite point (SSP). As the satellite moves its SSP forms a ground track which can appear as simple as a circle about the earth or a mere point on the surface or they can appear very complicated. The ground speed due to the satellite's motion alone is

$$S_g = 7.9053(R/(R+h)) \text{ km/sec} \quad (3.6)$$

However, the earth does rotate at about 0.267472 km/sec at the equator. The actual ground speed depends on the inclination of the orbit plane to the equatorial plane.

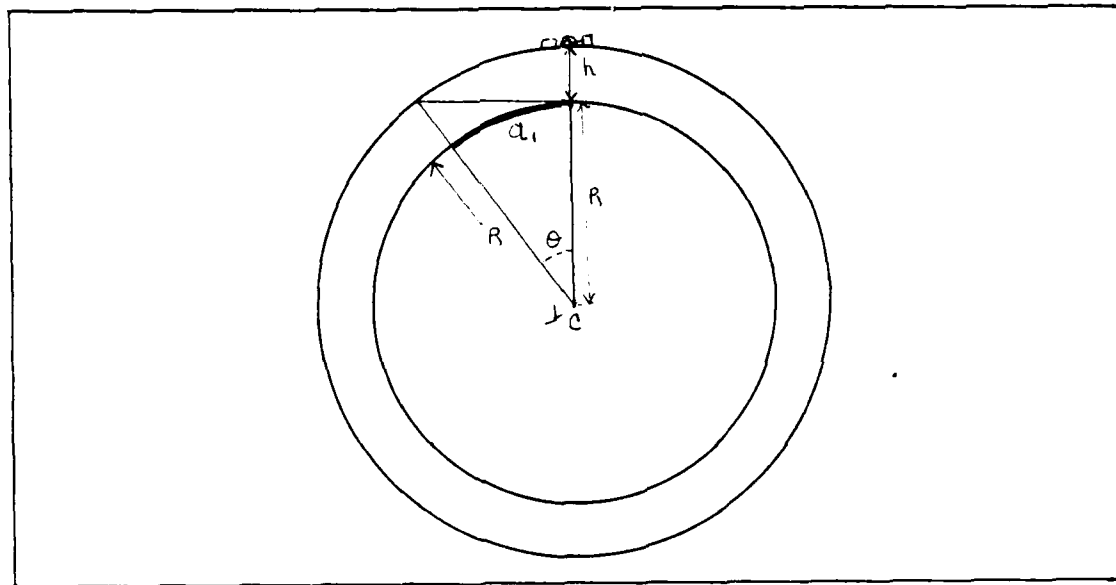


Figure 3.5 Arc

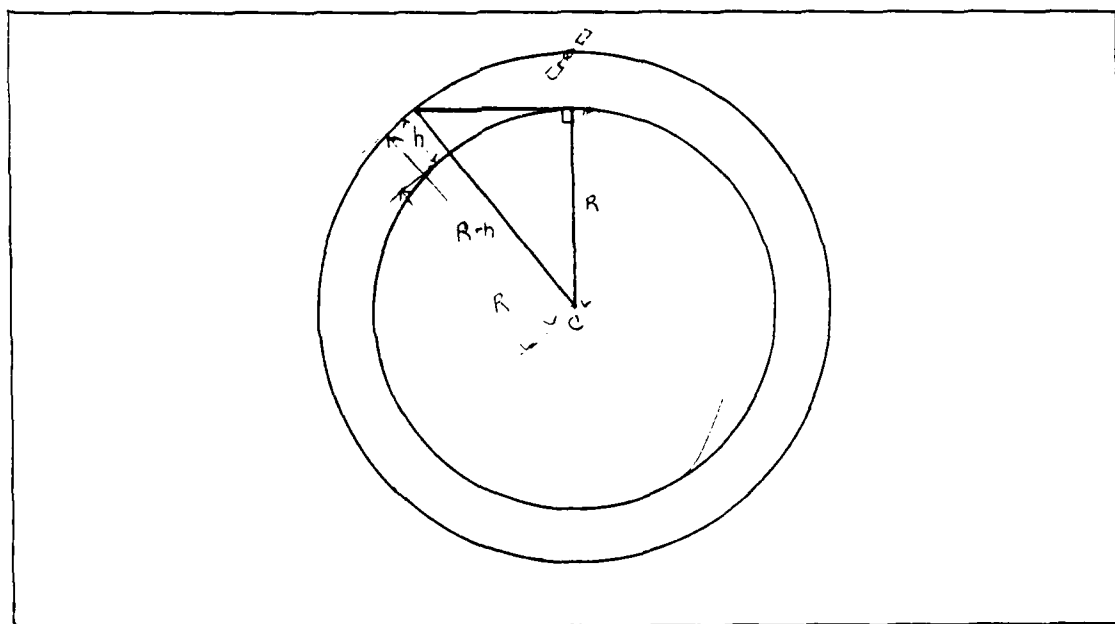


Figure 3.6 Right Triangle

For all cases the ground speed is less than the actual orbital speed. As the ground track is formed so is the ribbon whose width is the GSW. Because of the earth rotation beneath the satellite the swaths may overlap at some places yet never cover other places. If the earth's rotation is ignored and its shape is assumed spherical a satellite staying in one plane traces the same circular swath on every orbit.

If the earth's equatorial bulge is taken into account the plane of the orbit precesses about the earth's axis of rotation. This precession is caused by the non central gravity force field in which the satellite travels. It is measured by the rate of drift of longitude on the surface of the earth.

For an elliptical orbit the rate of precession is

$$\dot{\Omega} = 9.95(R/a) * (\cosine(i)/(1-e^2)) \quad (3.7)$$

where $\dot{\Omega}$ = orbital plane precession rate in degrees/day

R = mean radius of the earth

a = semimajor axis

e = eccentricity of ellipse

i = angle of inclination of orbit

For the special case of a circular orbit the precession rate is

$$\dot{\Omega} = 9.95(R/(R+h)) * cosine(i) \quad (3.8)$$

If the effect of this precession is ignored, the motion of a satellite lies in a plane passing through the

center of the earth. A satellite making one revolution per day at 0° inclination to the equator is stationary over a point on the equator. In this case a stationary spherical cap on the earth's surface is the only area covered.

Commercial communications satellites are usually geostationary. This is a special case of the synchronous orbit (24 hour orbit). If a synchronous orbit is inclined to the equator the ground track is a figure eight.

3. The Spherical Triangle

At this time all the simplifying assumptions are invoked to establish a base for further analysis. The satellite is traveling in a circular orbit above the equator. Obviously, transformations to other orbits are readily available. The SSP is always on the equator. There is a target traveling on a steady course at a constant velocity and therefore following a great circle heading. This is not an unreasonable assumption. It is normal for a ship or an aircraft to keep to a great circle heading at a most efficient cruising speed and altitude. The target is assumed to be on the earth's surface or very near to the surface. Figure 3.7 illustrates the paths for both the surveillance satellite and the target. The target track is inclined i° to the satellite track. It is assumed that both can be considered to be moving on the surface of the same sphere with transformations readily available to the actual

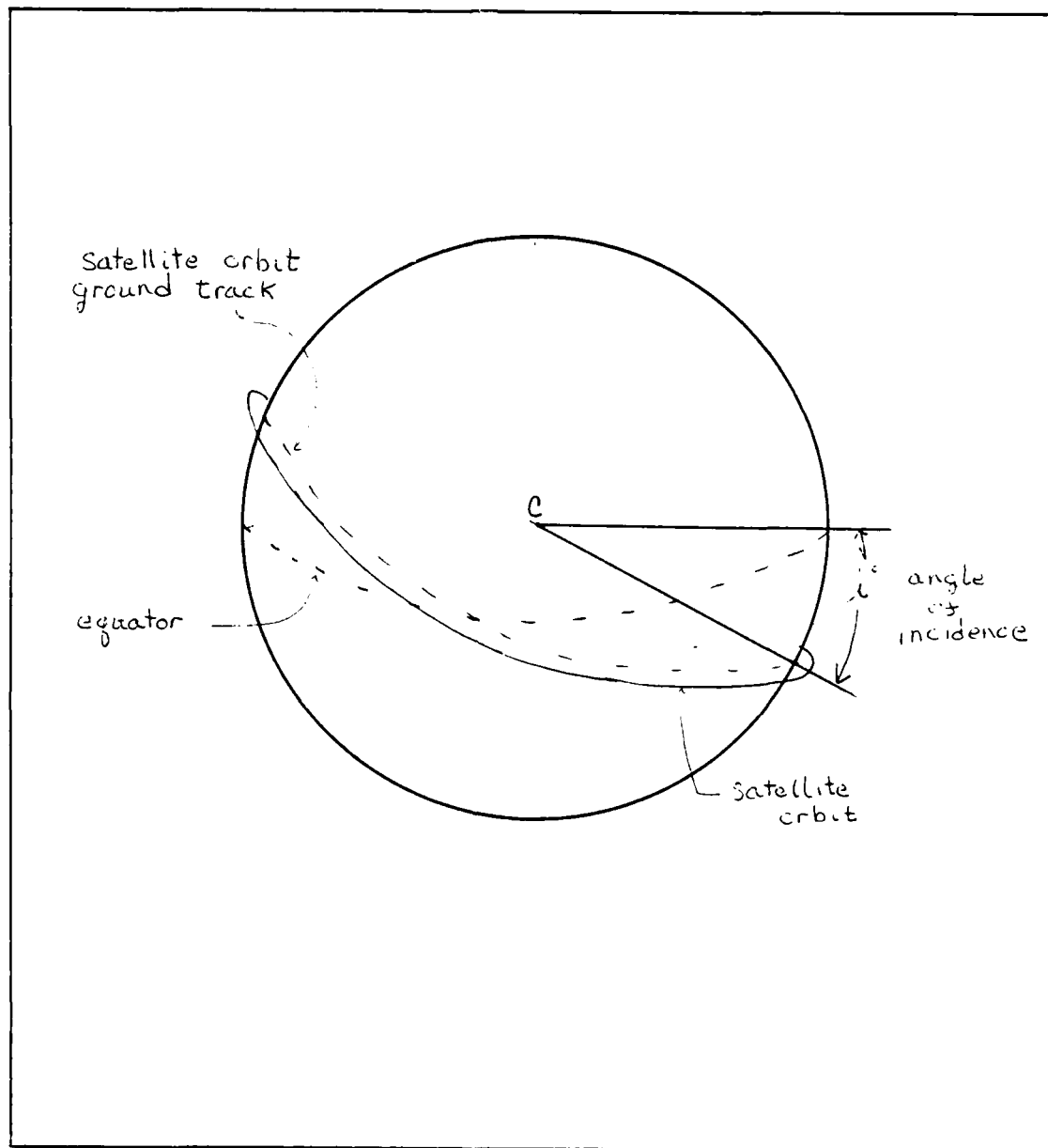


Figure 3.7 Satellite and Target Tracks

satellite position. The earth is assumed to be a perfect sphere and is approximated by a point mass at the center.

The two paths intersect in Figure 3.8 at point O. The letter S represents the present position of the satellite and the letter T represents the present position of the target. These three points (O, S and T) on the surface of the sphere define a spherical triangle. Spherical trigonometry is used to attempt to find a suitable coordinate system for the satellite tracking analysis.

B. COORDINATE SYSTEMS

Several coordinate systems are tested at this time. The set of reference axes is a relative one. It is assumed that the origin of the coordinate system is moving with the satellite relative to the earth. Appendix B explains.

1. Use Variables \bar{x} and δ

Supposedly any two independent variables from Figure 3.9 can form the basis for a state-space model for target tracking. The variables \bar{x} and δ are chosen for the first attempt to form a suitable coordinate system. The original four state variables $x(1)$ through $x(4)$ are defined below. Derivatives are found for the four state variables. In an attempt to establish a least-complicated structure, however, these lead to other state variables and other derivatives; i.e.,

$$x(1) = \cosine(\bar{x})$$

$$x(2) = \text{sine}(\bar{x})$$

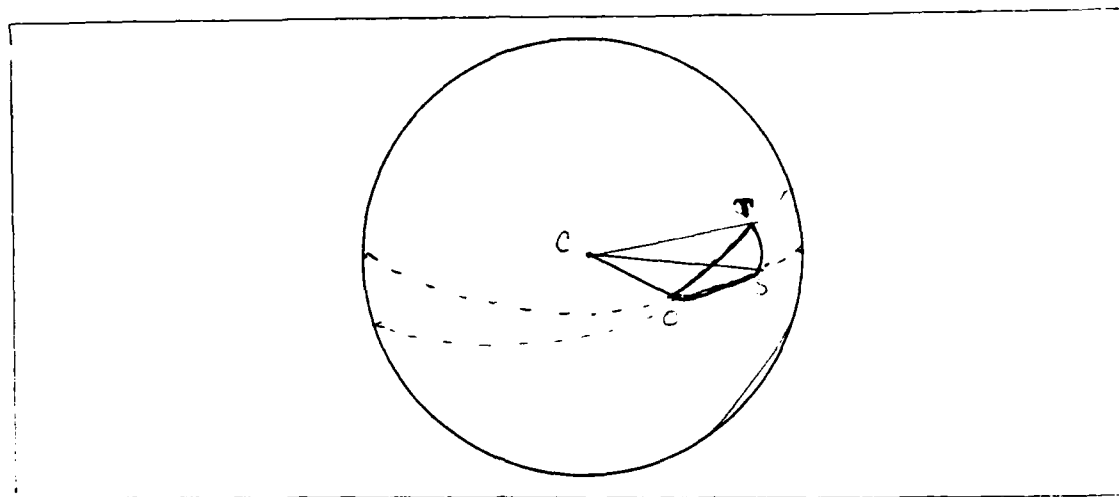


Figure 3.8 Intersecting Paths

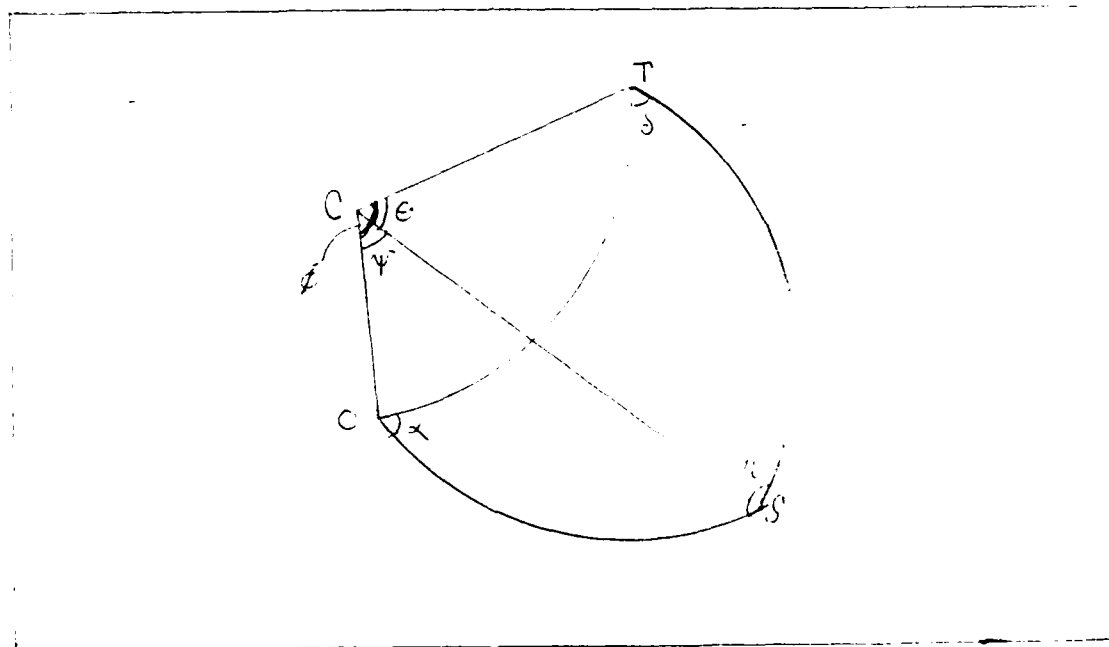


Figure 3.9 Spherical Triangle

$$x(3) = \cosine(\delta)$$

$$x(4) = \text{sine}(\delta)$$

Taking derivatives of two of the above variables yields

$$\dot{x}(1) = -x(2)$$

$$\dot{x}(3) = -x(4)$$

Using the trigonometric law of sines $X(2)$ can be defined as

$$x(2) = \left[\frac{\text{sine}(\eta)\text{sine}(\tau)}{\text{sine}(\delta)} \right] = \frac{\text{sine}(\eta)\text{sine}(\delta)}{\text{sine}(\alpha)}$$

Since in this case α and $\text{sine}(\alpha)$ are constants the second identity is easier to use. $\text{Sine}(\alpha)$ is replaced by the letter A and $\text{sine}(\delta)$ is replaced by $x(4)$. This yields

$$X(2) = \text{sine}(\eta)X(4)/A$$

The same procedure is used for $X(4)$. The law of sines provides an easy alternate form. $X(4)$ can be defined as

$$x(4) = \text{sine}(\tau)A/\text{sine}(\theta)$$

Table 3 summarizes the mathematics of expanding the state space. It is soon obvious that this state space is not readily reducible to a single structure by increased dimension. It therefore is abandoned.

2. Use of Variables θ and Ξ

Two new independent variables are now used in an attempt to generate a state-space model. As before the sine and cosine functions are employed.

$$X(1) = \text{sine}(\Xi)$$

TABLE 3. STATE SPACE FOR VARIABLES ξ and δ

$$X(1) = \cos(\xi) \quad X(2) = \sin(\xi)$$

$$X(3) = \cos(\delta) \quad X(4) = \sin(\delta)$$

$$\dot{X}(1) = -X(2) \quad \text{and} \quad \dot{X}(4) = -X(3)$$

$$X(2) = \sin(\eta) \sin(\delta) / \sin(\alpha) = \sin(\eta) X(4) / A$$

$$\dot{X}(2) = \cos(\eta) \dot{\eta} X(4) / A + \sin(\eta) \dot{X}(4) / A$$

$$\text{Let } X(5) = \cos(\eta) \dot{\eta} X(4) \text{ and } X(6) = \sin(\eta) \dot{X}(4)$$

$$\dot{X}(5) = -\sin(\eta) (\dot{\eta})^2 X(4) + \cos(\eta) \ddot{\eta} X(4) + \cos(\eta) (\dot{\eta}) (\ddot{\eta}) X(4)$$

$$\text{Let } X(7) = \sin(\eta) (\dot{\eta})^2 X(4) \text{ and } X(8) = \cos(\eta) \ddot{\eta} X(4)$$

$$\text{and } X(9) = \cos(\eta) (\dot{\eta}) (\ddot{\eta}) X(4)$$

$$\dot{X}(7) = \cos(\eta) (\dot{\eta})^3 X(4) + \sin(\eta) (2\dot{\eta} \ddot{\eta}) X(4) + \sin(\eta) (\dot{\eta})^2 \ddot{\eta} X(4)$$

$$\text{Let } X(10) = \cos(\eta) (\dot{\eta})^3 X(4) \text{ and } X(11) = \sin(\eta) (2\dot{\eta} \ddot{\eta}) X(4)$$

$$\text{and } X(12) = \sin(\eta) (\dot{\eta})^2 \ddot{\eta} X(4)$$

$$X(2) = \cosine(\Xi)$$

$$X(3) = \text{sine}(\theta)$$

$$X(4) = \cosine(\theta)$$

The derivatives for two of the above are

$$\dot{X}(2) = -x(1)$$

$$\dot{X}(4) = -x(3)$$

As before $\text{sine}(\alpha)$ is represented by the constant A. The law of sines is also used again. Table 4 summarizes the mathematics of the expanding state space. As before these variables as a basis for a coordinate system do not seem suitable for tracking purposes.

3. The Projected-Orbit Technique

This technique involves projecting the circle which is the target track onto the equator which is the satellite's ground track. Figure 3.10 illustrates the technique. The target position T is projected down onto the satellite's orbit at position T'.

Let $\dot{\tau} = w(s)$ (the angular velocity of the satellite) and let $\dot{\Xi} = w(t)$ (the angular velocity of the target).

For convenience let $Y = ST'$ (see Figure 3.11) and $X = \widehat{ST'}$ the arc length (see Figure 3.12). The arc length $OT' = \widehat{OT}$ and angle $\Xi = \text{angle } \Xi'$. It follows that

$$\Xi = \tau + \theta$$

and

$$\theta = \Xi - \tau.$$

TABLE 4. STATE SPACE FOR VARIABLES Φ and θ

$$X(1) = \sin(\Phi)$$

$$X(2) = \cosine(\Phi)$$

$$X(3) = \sin(\theta)$$

$$X(4) = \cosine(\theta)$$

$$\dot{X}(2) = -X(1)$$

$$\dot{X}(4) = -X(3)$$

$$X(1) = \sin(\eta) \left(\frac{\sin(\theta)}{\sin(\alpha)} \right) \quad X(3) = \sin(\alpha) \left(\frac{\sin(\Phi)}{\sin(\eta)} \right)$$

$$\dot{X}(1) = \dot{X}(3) \sin(\eta) / A + \cos(\eta) \dot{\eta} X(3) / A$$

$$\text{Let } X(5) = \dot{X}(3) \sin(\eta) \text{ and } X(6) = \cos(\eta) \dot{\eta} X(3)$$

$$\dot{X}(5) = \ddot{X}(3) \sin(\eta) + \cos(\eta) \dot{\eta} X(3)$$

$$\text{Let } X(7) = \ddot{X}(3) \sin(\eta) \text{ and } X(8) = \cos(\eta) \ddot{\eta} X(3)$$

$$\dot{X}(7) = \ddot{X}(3) \sin(\eta) + \ddot{X}(3) \cos(\eta) \eta = X(3) \cos(\eta) \eta; \quad (\ddot{X}(3) = 0)$$

$$\text{Let } X(9) = \ddot{X}(3) \cos(\eta) \eta$$

$$\dot{X}(9) = \ddot{X}(3) \sin(\eta) (\dot{\eta})^2 + \ddot{X}(3) \cos(\eta) \ddot{\eta}$$

$$\text{Let } X(10) = \ddot{X}(3) \sin(\eta) (\dot{\eta})^2 \text{ and } X(11) = \ddot{X}(3) \cos(\eta) \ddot{\eta}$$

$$\dot{X}(10) = \ddot{X}(3) \cos(\eta) (\dot{\eta})^3 + X(3) \sin(\eta) (2\dot{\eta} \ddot{\eta})$$

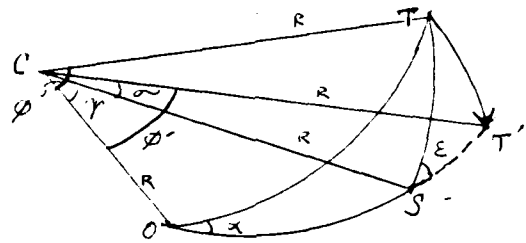


Figure 3.10 Projected Track

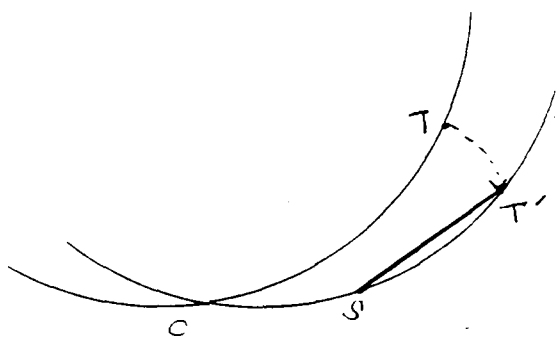


Figure 3.11 The Line Segment ST'

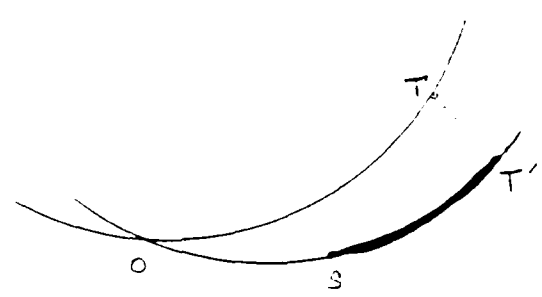


Figure 3.12 The Arc \widehat{ST}

Taking time derivatives we find

$$\dot{\theta} = \dot{x} - \dot{\tau} = \dot{w}(t) - \dot{w}(s)$$

To obtain a state space interpretation Y and X and their derivatives are defined. Figure 3.13 shows an angle bisector which splits θ and ST' . This forms two right triangles. Using geometry and trigonometry it follows that

$$\text{sine}(\theta/2) = T'A/R$$

$$AT' = ST'/2$$

$$ST' = 2R\text{sine}(\theta/2) = Y$$

$$Y = 2R\text{cosine}(\theta/2)\theta/2 = R\text{cosine}(\theta/2)\theta =$$

$$R\text{cosine}(\theta-\tau)(w(t)-w(s))$$

$$X = ST' = \theta R$$

$$\dot{X} = \theta R + R\dot{\theta},$$

$$\text{but } \dot{R} = 0;$$

therefore,

$$\dot{X} = R\dot{\theta} = R(\dot{w}(t)-\dot{w}(s))$$

Recall R is a constant for this case and therefore R is zero.

With Y and X defined above a logical state space is originated. The measurement equation is also important.

In order to define a measurement equation Figure 3.14 is constructed. Note that points O, S and T' do not form a straight line.

$$OT' \neq OS + ST'$$

However, in terms of arc lengths the following applies;

$$\widehat{OT'} = \widehat{OS} + \widehat{ST'}$$

The dotted line bisects angle α and therefore

$$BT = TT'/2$$

Using geometry and trigonometry it can be shown that

$$TT' = 2OT'\text{sine}(\alpha/2)$$

and

$$BT/OT = \text{sine}(\alpha/2)$$

From Figure 3.10 it follows that

$$OT' = 2R\text{sine}((\sigma+\tau)/2)$$

A new triangle is defined in Figure 3.15. Using simple geometry it is obvious that

$$\beta = \pi/2 - \alpha/2,$$

and by simple trigonometry

$$DT = TT'\text{sine}(\beta)$$

and

$$DT' = TT'\text{cosine}(\beta)$$

$$\text{tangent}(\epsilon) = TD/SD$$

therefore

$$SD = TD/\text{tangent}(\epsilon)$$

The line segment ST' is solved for

$$ST' = SD + DT' = TD/\text{tangent}(\epsilon) + TT'\text{cosine}(\beta)$$

It is essential to express ST' in terms of usable variables.

$$ST' = TT'(\text{sine}(\beta)/\text{tangent}(\epsilon) + \text{cosine}(\beta))$$

is achieved by substitution for segment length SD .

$$TT' = 2OT'\text{sine}(\alpha/2) = 2(2R\text{sine}((\sigma+\tau)/2))\text{sine}(\alpha/2)$$

therefore

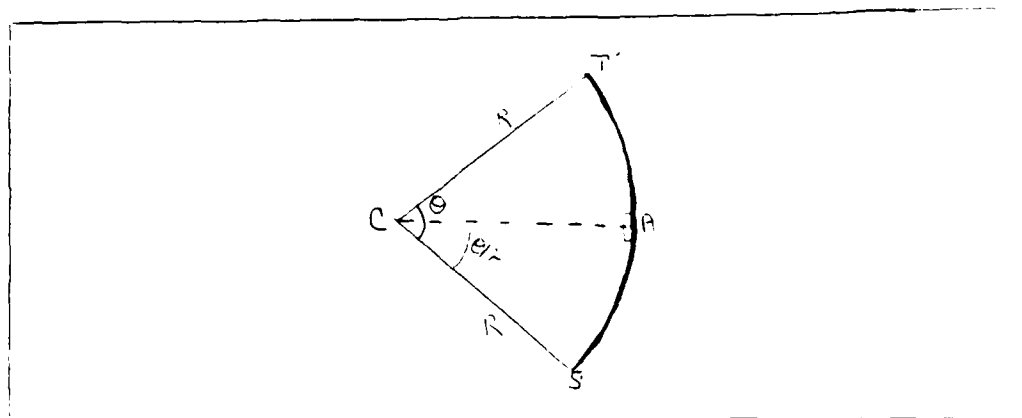


Figure 3.13 Angle Bisector

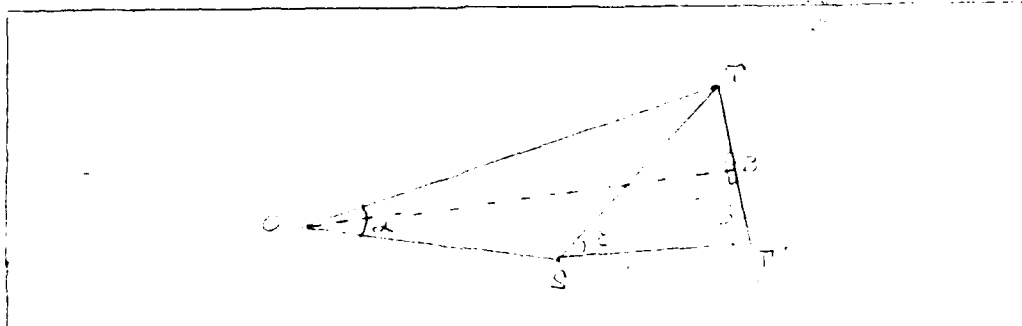


Figure 3.14 The Line Segment ST

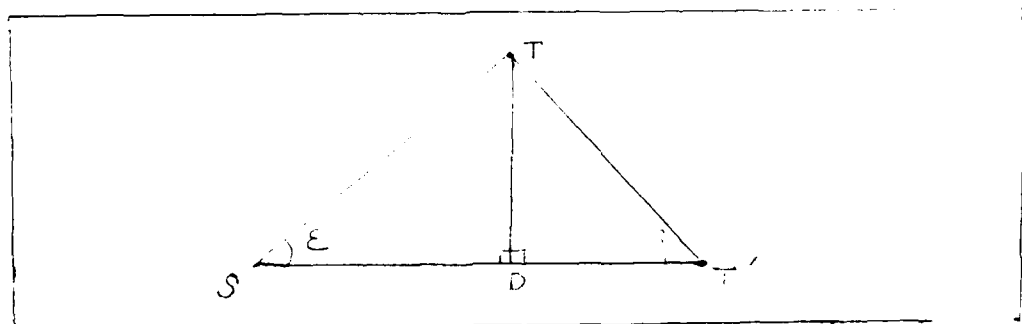


Figure 3.15 New Triangle

$$ST' = 4R \sin\left(\frac{\sigma+\tau}{2}\right) \sin(\alpha/2) \left[\frac{\sin(\beta)}{\tan(\epsilon)} + \cos(\beta) \right]$$

Let $4R \sin((\sigma+\tau)/2) \sin(\alpha/2) = Q$ for convenience.

Then $ST' = Q \left(\sin(\beta)/\tan(\epsilon) + \cos(\beta) \right)$. Also,

recall that $\beta = \pi/2 - \alpha/2$

$$ST' = Q \left[\frac{\sin(\pi/2 - \alpha/2)}{\tan(\epsilon)} + \cos(\pi/2 - \alpha/2) \right]$$

It is important to relate X and Y.

$$X = ST' = \theta R \quad \text{and} \quad Y = ST' = 2R \sin(\theta/2)$$

For convenience use $\sigma = X/R$

$$Y = 2R \sin(\sigma/2) \quad \text{and} \quad R = X/\sigma = Y/2 \sin(\sigma/2)$$

therefore

$$X = \sigma Y / 2 \sin(\sigma/2)$$

It is now necessary to solve for ϵ which indicates bearing.

$$Y = ST' = Q \cos(\alpha/2) \cot(\epsilon) + Q \sin(\alpha/2)$$

$$\cot(\epsilon) = \frac{Y}{Q \cos(\alpha/2)} - \frac{\sin(\alpha/2)}{\cos(\alpha/2)}$$

Taking the arccotangent of each side, substituting back in for Q and then simplifying leads to

$$\epsilon = \text{arccotangent} \frac{\sin(X/2R)}{\sin(\sigma/2) \sin(\alpha)} - \tan(\alpha/2)$$

This is the measurement equation. The final result is a two-variable state space and a measurement equation. From the measurement equation an observer can be modeled. Table 5 summarizes the results.

TABLE 5. STATE SPACE IN X AND Φ .

State Space	
$\dot{\Phi} = w_{\phi}(t)$	(3.9)
$X = R(w_{\phi}(t) - w_{\phi}())$	(3.10)
Bearing information (measurement)	
$\epsilon = \text{arccotangent} \left[\frac{\text{sine}(x/2R)}{\text{sine}(\Phi/2)\text{sine}(\alpha)} - \text{tangent}(\alpha/2) \right]$	(3.11)

Table 6 summarizes the results for an alternate coordinate system.

TABLE 6. STATE SPACE IN Y AND Φ .

State Space	
$Y = R(1 - Y^2)(w - w)$	(3.12)
$\dot{\Phi} = w$	(3.13)
Bearing information	
$\epsilon = \text{arccot} \frac{Y}{2R\text{sine}(\Phi/2)\text{cos}(\alpha)} - \text{tan}(\alpha/2)$	(3.14)

A previously researched thesis [Ref 6] provides a useful coordinate system based on latitudes and longitudes. Table 3.4 summarizes this coordinate system.

IV. OBSERVABILITY

At this time it is important to determine observability of the target. Assuming the satellite's detectors yield only the bearing information (as developed in Chapter 3), it is necessary to obtain the target's position defined with X and Ξ . Since this cannot be measured directly it must be estimated in some way. Analyzing the state equations from chapter three it appears that if ω_x and ω_z are given the knowledge of $X(0)$ and $\Xi(0)$ (the initialed states) are sufficient to determine $X(t)$ and $\Xi(t)$ all along the trajectory.

$$\begin{aligned} X(t) &= X(0) + R \int_0^t [\omega_x(\tau) - \omega_z(\tau)] d\tau \\ \Xi(t) &= \Xi(0) + \int_0^t \omega_z(\tau) d\tau \end{aligned}$$

The possibility of estimating the state from the output measurement under the assumption that the system dynamics is completely known is defined as observability. Therefore the observability of the system must be determined.

All changes in a given system must be reflected in the output for the system to be observable. Figure 4.1 shows a simple example. The states X and \dot{X} are estimated from knowledge of the output. If all states are observable for all times then the system is completely observable. This is defined in detail in [Ref. 6].

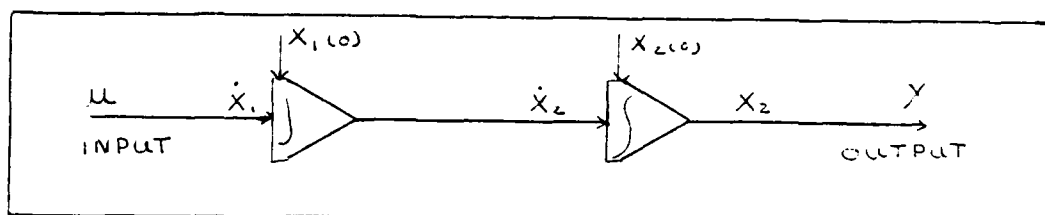


Figure 4.1 A Simple System

The test for observability on linear systems is fairly straight forward. In general the observability of linear systems is established by examining the linear independencies of the columns in the matrix function $C(t)\Phi(t, t_0)$, where $C(t)$ is the measurement matrix and $\Phi(t, t_0)$ is the state transition matrix. For the linear time invariant system this leads to a simple rank test on the appropriate observability matrix. To illustrate this approach we may consider the following linear system,

$$\dot{X} = AX$$

$$Y = CX$$

where A is a square matrix, X is an n -dimensional state vector and Y is an m -dimensional measurement vector. Assuming that $Y(t)$ is differentiable up to the $(n-1)$ th order, we have

$$Y' = CX = CAX$$

$$Y'' = CAX' = CA^2X$$

$$\vdots$$

$$Y^{(n)} = CA^{n-1}X$$

A matrix is set up as shown:

$$\begin{bmatrix} Y \\ Y' \\ \vdots \\ Y^{n-1} \end{bmatrix} = \begin{bmatrix} C \\ CA \\ \vdots \\ CA^{n-1} \end{bmatrix} X \Rightarrow \hat{Y} = Q_0 X$$

where Y is the extended measurement vector of dimension mn .

The matrix Q_0 is the observability matrix and has dimension $m \times n$. Clearly if $\text{rank } Q_0 = n$, X can be uniquely solved in terms of the measurement \hat{Y} . It should be noted that differentiability of $Y(t)$ is not required for observability of linear systems and that the above result can be derived in a different way. The presented procedure, however offers the possibility of extending this result to the observability of non-linear systems; namely in the equation, $\hat{Y} = Q_0 X$, any subset of n linearly independent equations can be considered $\hat{Y} = QX$, Q can be regarded as the Jacobian J of Y with respect to X . Hence if $\text{rank } J = n$ the linear time invariant system is observable.

A. OBSERVABILITY OF NON-LINEAR SYSTEMS

In the past it has been very difficult to determine observability of non-linear systems. Recently, however, a number of new methods for observability testing have been developed.

A fairly simple test that determines observability in non-linear systems is developed in [Ref. 6]. This new method tests observability and identifies any unobservable states that may exist. If the system is unobservable then the measurement doesn't provide enough information for state

estimation. System observability and state estimation are directly related.

A non-linear system can be represented as follows:

$$\dot{X}(t) = f(X(t), u(t), t) \quad (4.1)$$

where $f()$ is an n -function, $X \in R^n$, $U \in R^r$.

The measurement equation is:

$$Y(t) = h(X(t), t) \quad (4.2)$$

where $h()$ is an m -function, $Y \in R^m$.

$Y(t)$ must be differentiable up to the $(n-1)$ order and $U(t)$ must be differentiable up to the $(n-2)$ order. A state $X_0(t_0)$ is observable at t if knowledge of the input $U(t)$ and the output $Y(t)$ from time t_0 to t , enables $X_0(t_0)$ to be determined.

Equation 4.2 is differentiated to provide a necessary system of non-linear measurement equations.

$$Y = h(x)$$

$$Y' = \frac{\partial h}{\partial t} + \frac{\partial h}{\partial x} \frac{\partial x}{\partial t} = h_t + h_x f = h_1(x, u)$$

$$Y'' = \frac{\partial h'}{\partial t} + \frac{\partial h'}{\partial x} \frac{\partial x}{\partial t} + \frac{\partial h'}{\partial u} \frac{\partial u}{\partial t} =$$

$$h_{1t} + h_{1x} f + h_{1u} u' = h_2(x, u, u')$$

$$Y^{(n-1)} = h_{(n-2)t} + h_{(n-2)x} \dot{x} + h_{(n-2)u} \ddot{u} + \dots$$

$$+ h_{(n-2)u^{(n-3)}} u^{(n-2)} = h_{n-1}(x, u, u', \dots, u^{(n-2)})$$

Define an mn measurement vector \underline{Y} by

$$\underline{Y} = \begin{bmatrix} y \\ \vdots \\ y^{(n)} \end{bmatrix}$$

and an $m \times n$ function $H(\cdot)$ to be

$$H(\cdot) = \begin{bmatrix} h \\ \vdots \\ h_{m \times n} \end{bmatrix}$$

The functional relation in vector form is

$$Y = H(x, v) \quad (4.3)$$

where $v(t)$ is a function of $U^{(i)}$, $i = 1, \dots, (n-2)$.

With respect to equation 4.3 the question of observability can be developed as the existence of an inverse of this function. Clearly, this is related to the Jacobians of H . However, for the case of linear systems an inverse, if it exists, has to be unique. It will be shown later that here this need not be the case.

Two conditions must be met for this non-linear system to be observable in the strict sense. These two conditions are connectedness and univalence. Connectivity is a necessary condition for observability in the strict sense and a necessary and sufficient condition for observability in the wide sense. Connectedness is satisfied if every state is connected to the output in some way. Univalence is satisfied if every state is uniquely determined in terms of the measured output. A one-to-one mapping is considered

univalent. Both conditions together are necessary and sufficient to establish observability in the strict sense.

To explain this consider $Y(t)$ as expanded in a Taylor series.

$$Y(t) = y(t_c) + y'(t_c)(t-t_c) + \frac{1}{2}y''(t_c)(t-t_c)^2 + \dots + \frac{1}{(n-1)!}y^{(n-1)}(t_c)(t-t_c)^{n-1} + r(t)$$

Knowledge of the measurement trajectory $Y(t)$ is equivalent to knowing the coefficients and remainder in this equation. This Taylor series expansion is considered unique and therefore the coefficients are also unique. The coefficients are the elements of the measurement vector Y . Therefore, any state $X_i(t)$ is observable as long as it is connected in a one-to-one manner to an element of Y . If the connection is not one-to-one the system is observable only in the wide sense. An example of this follows.

$$X^2 = Y$$

$$X = \pm \sqrt{Y}$$

In this example X can equal either the positive or negative square root of Y . This is a multiple valued function. Therefore the mapping is not one-to-one. Hence the system cannot be observable in the strict sense.

As mentioned earlier the connectedness condition is satisfied if the existence of an inverse of the function can be established. According to [Ref. 6] the inverse function is considered established if the determinant of the $n \times n$ Jacobian of H does not equal zero for all x and v . If

$J = 0$ then one or more states are unobservable. If H has more than one right inverse then univalence is not satisfied and the system is only observable in the wide sense. However this will suffice for this case.

B. JACOBIANS AND NON-LINEAR ANALYSIS

Recall from chapter three that two possible bearing-only measurements have been found. These are illustrated in Tables 5 and 6. Both the measurement equations (bearing-only) are highly non-linear. The Jacobian matrices in Tables 7 and 8 are defined using the measurement equations.

These Jacobians are necessary for observability analysis. It is essential to ascertain whether or not their determinants are equal to zero. The Jacobians in Tables 7 and 8 are based on the state space and measurement information available in Tables 5 and 6 respectively.

The calculations for $\dot{\eta}$, $\partial\eta/\partial x$, $\partial\eta/\partial y$, $\partial\eta/\partial \dot{x}$ and $\partial\eta/\partial \dot{y}$ concerning the variable X are in Tables 9 through 11. The result of the calculations for $\dot{\eta}$, $\partial\eta/\partial x$, $\partial\eta/\partial y$, $\partial\eta/\partial \dot{x}$ and $\partial\eta/\partial \dot{y}$ concerning the variable Y proved very complicated and are therefore not used.

It is obvious that the determinants of these Jacobians are going to be difficult to analyze. Table 12 illustrates the determinant solution. To discover whether or not a zero value is achieved two separate methods are invoked. First, a simplification is utilized. Recall from chapter one that a satellite is restricted regarding the amount of area it

can cover. Therefore the numerical value of the angles $\bar{\theta}$ and τ are restricted. The variable X is composed of $\bar{\theta}$ and τ ($X=R(\bar{\theta}-\tau)$). The development of the spherical triangle in

TABLE 7 JACOBIAN UTILIZING X

$$J = \begin{bmatrix} \sin/sx & \sin/s\phi \\ \dot{\sin}/sx & \dot{\sin}/s\phi \end{bmatrix}$$

TABLE 8 JACOBIAN UTILIZING Y

$$J = \begin{bmatrix} \sin/sy & \sin/s\phi \\ \dot{\sin}/sy & \dot{\sin}/s\phi \end{bmatrix}$$

TABLE 9 JACOBIAN - X - PART 1

$$\dot{\eta} = - \frac{1}{1 + \left(\frac{\sin(X/2R)}{\sin(\alpha)\sin(\phi/2)} - \tan(\alpha/2) \right)^2} \left[\frac{\cos(X/2R) \left(\frac{\dot{X}}{2R} \right) \sin(\phi/2) - \cos(\phi/2) \left(\frac{\dot{\phi}}{2} \right) \sin(X/2R)}{\sin(\alpha)\sin^2(\phi/2)} \right]$$

$$\frac{\partial \eta}{\partial X} = \frac{-\cos(X/2R)}{2R} \frac{1}{\left\{ 1 + \left(\frac{\sin(X/2R)}{\sin(\alpha)\sin(\phi/2)} - \tan(\alpha/2) \right)^2 \right\} \sin(\alpha)\sin(\phi/2)}$$

$$\frac{\partial \eta}{\partial \phi} = \frac{\sin(X/2R) \cos(\phi/2)}{2 \sin(\phi/2)} \frac{1}{\left\{ 1 + \left(\frac{\sin(X/2R)}{\sin(\alpha)\sin(\phi/2)} - \tan(\alpha/2) \right)^2 \right\} \sin(\alpha)\sin(\phi/2)}$$

TABLE 10 JACOBIAN - X- PART 2

$$\dot{S}\eta / S_X =$$

$$\left\{ 1 + \left[\frac{\sin(X/2R)}{\sin(\alpha)\sin(\phi/2)} - \tan(\alpha/2) \right]^2 \right\} 2R \sin(\alpha) \sin^2(\phi/2)$$

$$\left\{ \left[\frac{\sin(X/2R)}{\sin(\alpha)\sin(\phi/2)} - \tan(\alpha/2) \right] \left[\frac{\dot{X}}{2R} \cos\left(\frac{X}{2R}\right) \sin\left(\frac{\phi}{2}\right) - \frac{\dot{\phi}}{2} \sin\left(\frac{X}{2R}\right) \cos\left(\frac{\phi}{2}\right) \right] \cos(X/2R) \right.$$

$$\left. \left\{ 1 + \left[\frac{\sin(X/2R)}{\sin(\alpha)\sin(\phi/2)} - \tan(\alpha/2) \right]^2 \right\} \sin(\alpha) \sin(\phi/2) \right.$$

$$\left. + \frac{\dot{X}}{2R} \sin\left(\frac{X}{2R}\right) \sin\left(\frac{\phi}{2}\right) + \cos\left(\frac{X}{2R}\right) \cos\left(\frac{\phi}{2}\right) \frac{\dot{\phi}}{2} \right\}$$

TABLE 11 JACOBIAN - X - PART 3

$$\dot{\eta}/\dot{\phi} =$$

$$\left\{ 1 + \left[\frac{\sin(X/2R)}{\sin(\alpha)\sin(\phi/2)} - \tan(\psi/2) \right]^2 \right\} \sin(\alpha)\sin^2(\phi/2) \quad *$$

$$\frac{\left[\frac{\sin(X/2R)}{\sin(\alpha)\sin(\phi/2)} - \tan(\psi/2) \right] \sin\left(\frac{X}{2R}\right) \cos\left(\frac{\phi}{2}\right) \left[\frac{\dot{X}}{2R} \cos\left(\frac{X}{2R}\right) \sin\left(\frac{\phi}{2}\right) - \frac{\dot{\phi}}{2} \sin\left(\frac{X}{2R}\right) \cos\left(\frac{\phi}{2}\right) \right]}{\left\{ 1 + \left[\frac{\sin(X/2R)}{\sin(\alpha)\sin(\phi/2)} - \tan(\psi/2) \right]^2 \right\} \sin(\alpha)\sin^2(\phi/2)}$$

$$- \left[\frac{\dot{X}}{2R} \cos\left(\frac{X}{2R}\right) \cos\left(\frac{\phi}{2}\right) + \frac{\dot{\phi}}{2} \sin\left(\frac{X}{2R}\right) \sin\left(\frac{\phi}{2}\right) \right] \frac{1}{2} +$$

$$\left[\frac{\dot{X}}{2R} \cos\left(\frac{X}{2R}\right) \sin\left(\frac{\phi}{2}\right) - \frac{\dot{\phi}}{2} \sin\left(\frac{X}{2R}\right) \cos\left(\frac{\phi}{2}\right) \right] \frac{\cos(\phi/2)}{\sin(\phi/2)}$$

TABLE 12 DETERMINANT OF JACOBIAN

$$\begin{aligned}
 & \left[\frac{1}{\left\{ 1 + \left[\frac{\sin(X/2R)}{\sin(\alpha) \sin(\phi/2)} - \tan(\alpha/2) \right]^2 \right\}^2 2R \sin^2(\alpha) \sin^3(\phi/2)} \right]^* \\
 & \left[\frac{\left(\frac{\sin(X/2R)}{\sin(\alpha) \sin(\phi/2)} - \tan(\alpha/2) \right) \sin\left(\frac{X}{2R}\right) \cos\left(\frac{\phi}{2}\right) \left(\frac{\dot{X}}{2R} \cos\left(\frac{X}{2R}\right) \sin\left(\frac{\phi}{2}\right) - \frac{\dot{\phi}}{2} \sin\left(\frac{X}{2R}\right) \cos\left(\frac{\phi}{2}\right) \right)}{\left\{ 1 + \left[\frac{\sin(X/2R)}{\sin(\alpha) \sin(\phi/2)} - \tan(\alpha/2) \right]^2 \right\} \sin(\alpha) \sin^2(\phi/2)} \right. \\
 & \quad \left. - \left(\frac{\dot{X}}{2R} \cos\left(\frac{X}{2R}\right) \cos\left(\frac{\phi}{2}\right) + \frac{\dot{\phi}}{2} \sin\left(\frac{X}{2R}\right) \sin\left(\frac{\phi}{2}\right) \right) \frac{1}{2} + \right. \\
 & \quad \left. \left(\frac{\dot{X}}{2R} \cos\left(\frac{X}{2R}\right) \sin\left(\frac{\phi}{2}\right) - \frac{\dot{\phi}}{2} \sin\left(\frac{X}{2R}\right) \cos\left(\frac{\phi}{2}\right) \right) \frac{\cos(\phi/2)}{\sin(\phi/2)} \right) \left(\frac{-\cos(X/2R)}{2R} \right) - \\
 & \quad \left(\frac{2 \left(\frac{\sin(X/2R)}{\sin(\alpha) \sin(\phi/2)} - \tan(\alpha/2) \right) \left(\frac{\dot{X}}{2R} \cos\left(\frac{X}{2R}\right) \sin\left(\frac{\phi}{2}\right) - \frac{\dot{\phi}}{2} \sin\left(\frac{X}{2R}\right) \cos\left(\frac{\phi}{2}\right) \right) \cos\left(\frac{X}{2R}\right)}{\left\{ 1 + \left[\frac{\sin(X/2R)}{\sin(\alpha) \sin(\phi/2)} - \tan(\alpha/2) \right]^2 \right\} \sin(\alpha) \sin(\phi/2)} \right. \\
 & \quad \left. + \left(\frac{\dot{X}}{2R} \sin\left(\frac{X}{2R}\right) + \cos\left(\frac{X}{2R}\right) \cos\left(\frac{\phi}{2}\right) \frac{\dot{\phi}}{2} \right) \left(\frac{\sin(X/2R) \cos(\phi/2)}{2 \sin(\phi/2)} \right) \right]
 \end{aligned}$$

chapter three assumes a limit to angles Ξ , τ and α . For the purposes of this work the range of possible values for these angles are confined as follows;

Ξ : 0 (plus epsilon) radians - $\pi/4$ radians

τ : 0 (plus epsilon) radians - $\pi/4$ radians

α : 0 (plus epsilon) radians - $\pi/2$ radians

These limitations are reasonable for this particular case and they enable a useful simplification. For small angles the sine of that angle can be approximated as the angle value itself (in radians). Table 13 verifies the assumptions made here.

TABLE 13. SIMPLIFICATIONS

$$\pi/8 = \Xi/2 \text{ at } \Xi\text{'s maximum}$$

$$\pi/8 = .3926991 \text{ radians}$$

$$\sin(\pi/8) = .326834$$

For this case the angle α is held constant. Using all the above assumptions and approximations the Jacobians and their determinants are greatly reduced in complexity. Tables 14 and 15 summarizes the development of the simplified Jacobian and determinant for the measurement equation containing the variable X . This Jacobian is chosen because it is the least complicated of the two.

TABLE 14

SIMPLIFIED VERSION

Measurements:

$$\eta = \operatorname{arccot}\left(\frac{X-2R\Phi S}{R\Phi a}\right)$$

$$S = \sin^2(\alpha/2)$$

$$a = \sin(\alpha)$$

$$\dot{\eta} = -aR \left(\frac{\dot{X}\Phi - \Phi\dot{X}}{X^2 - 4R\Phi SX + 4R^2\Phi^2 S} \right)$$

Jacobian:

$$J_{11} = - \frac{aR}{X^2 - 4R\Phi SX + 4R^2\Phi^2 S} \Phi = \partial\eta/\partial X$$

$$J_{12} = \partial\eta/\partial\Phi = \frac{aR}{X^2 - 4R\Phi SX + 4R^2\Phi^2 S} (X)$$

$$J_{21} = \partial\eta/\partial X = \frac{aR}{X^2 - 4R\Phi SX + 4R^2\Phi^2 S} \left(\frac{2X\Phi(X-2R\Phi S) + \Phi(4R^2\Phi^2 S - X^2)}{X^2 - 4R\Phi SX + 4R^2\Phi^2 S} \right)$$

$$J_{22} = \partial\eta/\partial\Phi = \frac{aR}{X^2 - 4R\Phi SX + 4R^2\Phi^2 S} \left(\frac{X(4R^2\Phi^2 S - X^2) + 4RSX\Phi(X-2R\Phi)}{X^2 - 4R\Phi SX + 4R^2\Phi^2 S} \right)$$

TABLE 15
LINEAR DEPENDENCE

$$|J| = J_{11} J_{22} - J_{12} J_{21} = \frac{a^2 R^2}{X^2 - 4R\Phi SX + 4R^2\Phi^2 S} (X\Phi - \Phi X)$$

since $X^2 - 4R\Phi SX + 4R^2\Phi^2 S = R^2\Phi^2 a^2 \left(1 + \frac{X}{R\Phi a} - b^2 \right) > 0$

This holds for every X and Φ where $a = \sin(\alpha)$ and $b = 2S/a = \tan(\alpha/2)$.

$$|J| = 0 \text{ if } X\Phi - \Phi X = 0 \quad \frac{X}{\Phi} = \frac{\Phi}{X}$$

$$\ln X + \frac{X}{\Phi} = \ln \Phi + \frac{\Phi}{X} \quad \ln X - \frac{\Phi}{X} = \ln \Phi - \frac{X}{\Phi} = C$$

$$\frac{X}{\Phi} = e^C = \text{constant} \quad X = C_1 \Phi$$

Therefore $|J| = 0$ if X and Φ are linearly dependent.

The second method involves the use of computer simulation. The determinant (with the variable X as before) is calculated using no assumptions. The angles Φ and τ are incremented in small steps from 0 radians to $\pi/4$ radians. The angle α (that is actually constant) has been given five different values for test purposes. The value of the determinant approaches zero but never actually achieves zero.

Note from table 15 that,

$$|J| = \frac{a'R'}{X' - 4R\Phi SX + 4R'\Phi'S} (X\Phi - \Phi X) \quad (4.4)$$

If $X\Phi = \Phi X$ the determinant of the Jacobian is zero and the system is not observable. From Table 15 it is apparent that the system is not observable if X and Φ are linearly dependent.

The various calculations and computer simulations indicate that the system initially developed in chapter three (Table 5) is observable under general conditions. According to the results of the computer simulation the determinant never actually reached zero for the particular test values (50 test values) chosen. However there are certain conditions dependent upon the initial values Φ and τ , when the system is not observable. Equation 4.1 defines these circumstances. Since the system is observable for most cases it is possible to design an adaptive observer. This is the goal of Chapter 5.

V. OBSERVERS

At this point in the satellite tracking project it is necessary to approach the state estimation problem. In general, a process can be characterized by the state and measurement equations;

$$\dot{X}(t) = AX(t) \quad (5.1)$$

$$Z(t) = CX(t) \quad (5.2)$$

where $X(t)$ is an n -element column vector representing the states, $Z(t)$ is a q -element vector of measurements, A and C are $n \times n$ and $q \times n$ matrices respectively. The order of n is greater than or equal to the order of q . It is desired to obtain knowledge of the states of $X(t)$. However, it is $Z(t)$ that is measurable and therefore known. For this reason it is necessary to estimate $X(t)$. The device for estimating the state $X(t)$ is the observer.

A. LINEAR LUENBERGER OBSERVERS

A model of an open loop observer can be constructed as follows;

$$\dot{Y}(t) = AY(t) \quad (5.3)$$

This model operates as does the process or plant. The estimation error is

$$e(t) = Y(t) - X(t) \quad (5.4)$$

This is differentiated with respect to time(t).

$$\begin{aligned} \dot{e}(t) &= \dot{Y}(t) - \dot{X}(t) \\ &= AY(t) - AX(t) \\ &= Ae(t) \end{aligned} \quad (5.5)$$

Therefore,

$$e(t) = e^{At} e(0) = \theta(t)e(0) \quad (5.6)$$

If the eigenvalues of A all have negative real parts then $e(t)$ approaches zero as t approaches infinity. The error signal $e(t)$ decays at a rate determined by the location of the eigenvalues of A. The rate of response of the process is also determined by the eigenvalues of A.

To make the decay rate independent of the dynamic process, often a state model is 'driven' by an error signal. In this case the observer is characterized by;

$$\dot{Y}(t) = AY(t) + G(Z(t) - CY(t)) \quad (5.7)$$

and the error equation is

$$\dot{e}(t) = \dot{Y}(t) - \dot{X}(t)$$

The matrix G is an $n \times q$ gain matrix which can be selected to determine the rate at which $y(t)$ approaches $X(t)$. The observer equation can be written as;

$$\dot{Y} = AY(t) + G((X(t) - CY(t))) = AY(t) + GCe(t) \quad (5.8)$$

The driving term is $GCe(t)$ and its purpose is to drive the estimate Y towards X . The error equation is differentiated with respect to time.

$$\begin{aligned} \dot{e}(t) &= \dot{Y}(t) - \dot{X}(t) \\ \dot{e}(t) &= AY(t) + G(CX(t) - CX(t)) - AX(t) \end{aligned}$$

$$\dot{e}(t) = (A-GC)(Y(t)-X(t)) \quad (5.9)$$

$$\dot{e}(t) = Fe(t) \quad (5.10)$$

where

$$F = A-GC$$

$$e(t) = e^{Ft} e(0) \quad (5.11)$$

As expected, the results depend on the initial conditions. The gain matrix G must be chosen to place the eigenvalues of F at suitable locations. In designing an observer it is usual to place the eigenvalues of F where desired and then determine G .

If the process has an input signal, u , then the appropriate equations are;

$$\dot{X}(t) = AX(t) + BU(t) \quad (5.12)$$

$$Z(t) = CX(t)$$

The observer for this system is characterized by the following equation.

$$\dot{Y}(t) = AY(t) + BU(t) + G(Z(t) - CY(t)) \quad (5.13)$$

The error response is the same as in the above and is given by equation 5.11. A block diagram of the observer is shown in Figure 5.1.

When designing a linear or non-linear observer it is desirable that the observer error become small rapidly and that the observer not be very responsive to noise. It is very difficult to meet both these goals since they seem to conflict. The observer must also be supplied with a set of initial conditions.

If some of the states of a given system can be measured there is no reason to estimate them. An observer of reduced dimension can be designed to estimate only those states that cannot be directly measured. For example, if there are n states in a system and q of them can be measured, the observer only requires $(n-q)$ states. Figure 5.2 illustrates the reduced order observer.

B. NON-LINEAR OBSERVER

For the design of the non-linear observer the techniques developed in [Ref. 7] can be applied.

Declare two given n -dimensional vector valued functions of time to be $Y(t)$ and $\theta(t)$. Let these two functions be related by $H(\theta)$ as $Y(t) = H(\theta)$. The vector $H(\theta)$ is considered known.

Assume that each i th row $H(\theta)$ is differentiable at least once on all parameters θ . Therefore an $n \times n$ Jacobian matrix is defined as

$$J(\theta) = \frac{\partial H(\theta)}{\partial \theta} = \left[J_{ij}(\theta) \right] \quad (5.14)$$

$$J_{ij}(\theta) = \frac{\partial H_i(\theta)}{\partial \theta_j} \quad (5.15)$$

Also;

$$Y(t) = H(\theta) + \frac{\partial H(\theta)}{\partial \theta} \frac{\partial \theta}{\partial t} = J(\theta) \dot{\theta}(t) \quad (5.16)$$

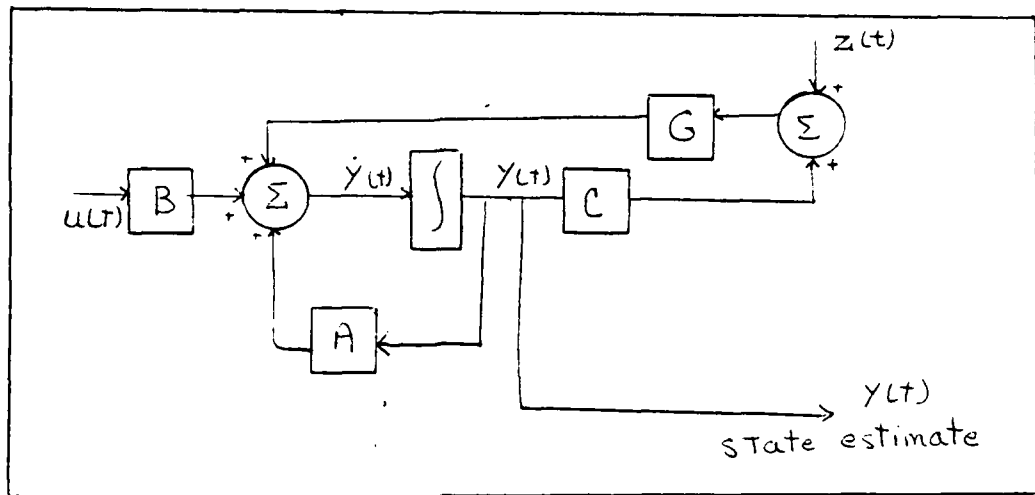


Figure 5.1 Basic Observer

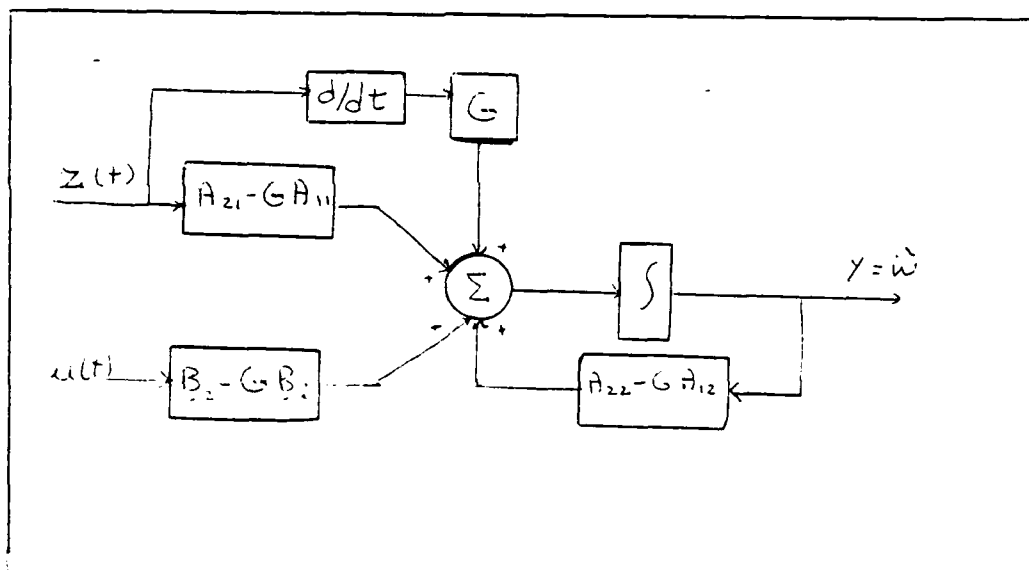


Figure 5.2 Reduced Order Observer

Figure 5.3 is the general non-linear observer referred to in [Ref. 7]. The transpose of the Jacobian is represented as $J^T(\theta)$. A string of parallel integrators are denoted as \int_n and $\theta_d(t)$ represents a solution of $Y(t) = H(\theta)$ for any given trajectory $Y_d(t)$. In regards to this figure there exists a positive scalar s and a time $T > 0$ such that for time $t > T$

$\|\theta_s(t) - \theta_d(t)\| \leq s$ if the following three conditions are met.

1. K is positive definite
2. The magnitude of the determinant of the Jacobian is bounded both from above and away from zero from below for the particular trajectory $Y_d(t)$.
3. The magnitude of $Y_d(t)$ is bounded from above.

In addition, by increasing the minimum eigenvalue of K the scalar s is made arbitrarily small.

An estimation error signal is defined as:

$$e(t) = \theta_s(t) - \theta_d(t) \quad (5.17)$$

Rearranging provides:

$$\theta_s(t) = e(t) + \theta_d(t)$$

Referring to Figure 5.3 the following relation is stated;

$$\dot{\theta}_s = -KJ^T(\theta_s) (H(\theta_s) - H(\theta_d)) \quad (5.18)$$

For notational convenience the following is defined;

$$\Sigma(e, \theta_d) = H(e + \theta_d) - H(\theta_d) = H(\theta_s) - H(\theta_d) \quad (5.19)$$

In this case sigma (Σ) does not refer to a summation.

It is simply a variable.

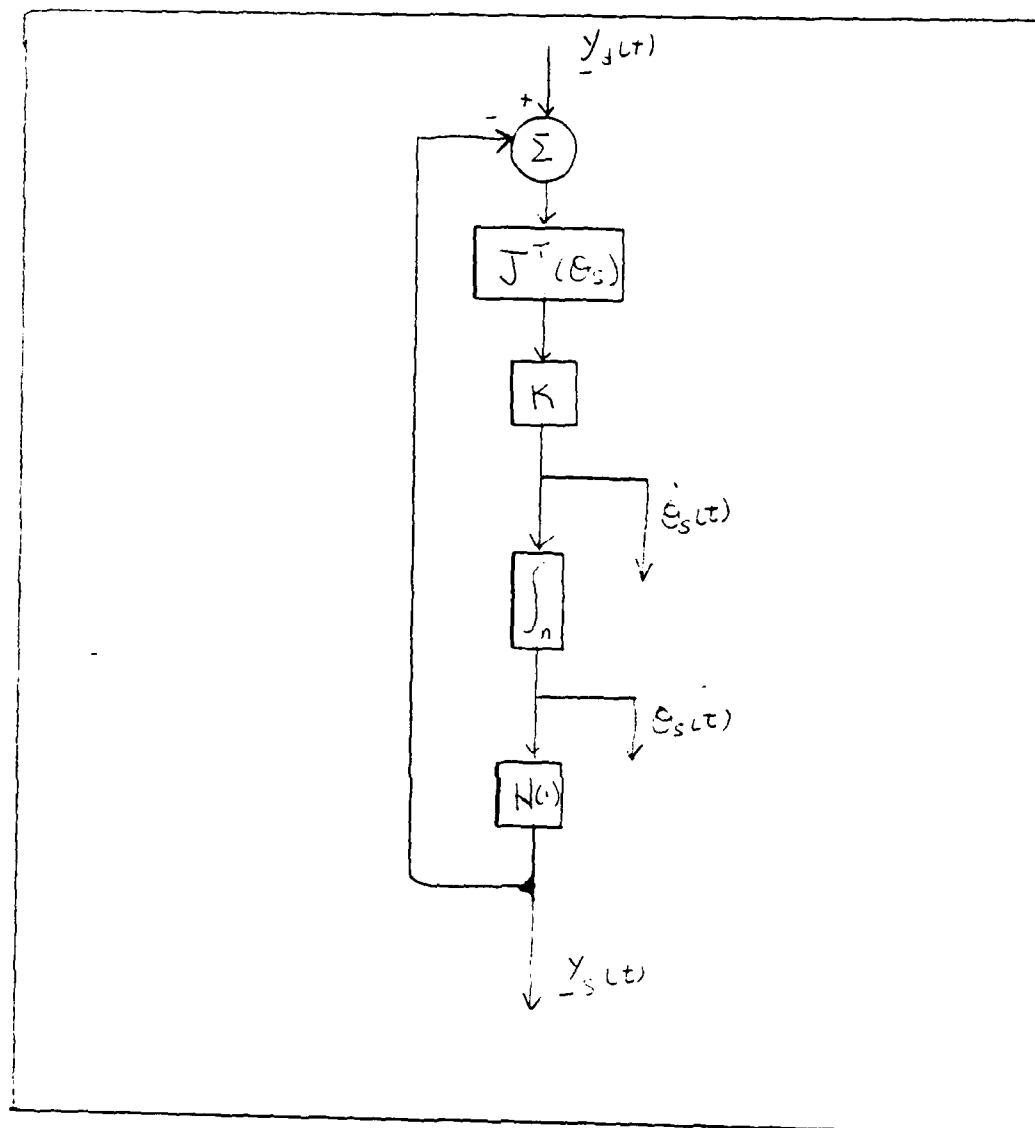


Figure 5.3 Non-Linear Observer

It follows from the above calculations that:

$$\dot{e} = \dot{\theta}_j - \dot{\theta}_d = -KJ^T(\theta_j) \Sigma(e, \theta_d) - \theta_j \quad (5.20)$$

The time-varying Lyapunov functions of the error signal are defined as:

$$V(e, t) = \frac{1}{2} \Sigma^T(e, \theta_d) \Sigma(e, \theta_d) \quad (5.21)$$

Since the determinant of the Jacobian is bounded $\Sigma(e, \theta_d) = 0$ if $e = 0$ then it follows that $V(e, t) > 0$ if $e \neq 0$. Further calculations are summarized in Table 16.

The minimum eigenvalue of $J(e + \theta_d) J^T(e + \theta_d)$ is denoted by λ_f which is always greater than zero. The minimum eigenvalue of K is denoted by λ_K which is also greater than zero so both eigenvalues are positive. It follows that;

$$\dot{V} \leq -\lambda_f \lambda_K \|\Sigma(e, \theta_d)\|^2 - \dot{\theta}_d^T J^T(\theta_d) \Sigma(e, \theta_d) \quad (5.24)$$

$$\dot{Y}_j = J(\theta_d) \dot{\theta}_d \quad (5.25)$$

$$\dot{\theta}_d = J(\theta_d)^T \dot{Y}_j \quad (5.26)$$

Since Y and $J(\theta)$ are both bounded $J(\theta_d)^T$ and $\dot{\theta}_d$ are also bounded for all $t > 0$. Therefore $\|\dot{\theta}_d\| \leq C_1$ and $\|J(\theta_d)\| \leq C_2$.

$$\begin{aligned} \dot{V} &\leq -\lambda_f \lambda_K \|\Sigma(e, \theta_d)\|^2 + C_1 C_2 \|\Sigma(e, \theta_d)\| \\ \dot{V} &\leq -(\lambda_f \lambda_K) \|\Sigma(e, \theta_d)\| - C_1 C_2 / \sqrt{2 \lambda_f \lambda_K} + C_1 C_2 / 2 \lambda_f \lambda_K \quad (5.27) \end{aligned}$$

C. DEVELOPMENT OF SATELLITE OBSERVER

For the design of the satellite observer (the system initially presented in Table 5) the state θ as described above now represents both X and \dot{X} as equation 5.28 shows:

$$\theta = \begin{bmatrix} X_1 \\ X_2 \end{bmatrix} = \begin{bmatrix} X \\ \dot{X} \end{bmatrix} \quad (5.28)$$

TABLE 16 LYAPUNOV FUNCTION OF THE ERROR SIGNAL

$$\dot{V}(t) = \left[\frac{\partial V(e, t)}{\partial e} \right]^T \frac{\partial e}{\partial t} + \frac{\partial V(e, t)}{\partial t}$$

$$\frac{\partial V(e, t)}{\partial e} = \left[\frac{\partial \Sigma(e, \theta_d)}{\partial e} \right]^T \Sigma(e, \theta_d)$$

$$= \frac{\partial H^T(e, \theta_d)}{\partial e} \Sigma(e, \theta_d) = J^T(e, \theta_d) \Sigma(e, \theta_d)$$

$$\left[\frac{\partial V(e, t)}{\partial e} \right]^T \frac{\partial e}{\partial t} = -\Sigma^T(e, \theta_d) J(e, \theta_d) K J^T(e, \theta_d) \Sigma(e, \theta_d)$$

$$\frac{\partial V(e, t)}{\partial t} = \left[\frac{\partial \Sigma^T}{\partial \theta_d} \cdot \frac{\partial V}{\partial \Sigma} \right]^T \frac{d\theta_d}{dt}$$

$$= -\left[J^T(\theta_d) \Sigma(e, \theta_d) \right]^T \dot{\theta}_d = -\Sigma^T(e, \theta_d) J(\theta_d) \dot{\theta}_d = -\dot{\theta}_d^T J^T(\theta_d) \Sigma^T(e, \theta_d)$$

$$\dot{V} = -\Sigma^T(e, \theta_d) J(e, \theta_d) K J^T(e, \theta_d) \Sigma(e, \theta_d) - \dot{\theta}_d^T J^T(\theta_d) \Sigma(e, \theta_d)$$

$$U = \begin{bmatrix} u_1 \\ u_2 \\ u_3 \end{bmatrix}$$

$$Y = \begin{bmatrix} y_1 \\ y_2 \\ y_3 \end{bmatrix}$$

The results developed earlier in this chapter (part B) are now applied to the particular problem of the satellite tracker. The Jacobian of Table 7 is redefined in equation 5.31.

It is intuitively obvious that;

$$Y = H(X, \theta, U) = H(\theta)$$

The further development of both $H(\theta)$ and θ is presented in table 17. The information in Table 17 leads to the design of an observer for the satellite. This design is depicted in Figure 5.3. Figure 5.4 shows the model used to check observer results. Both the observer and model are simulated using the FORTRAN programming language. The results are discussed in the next chapter.

TABLE 17 CALCULATIONS FOR OBSERVER DESIGN

$$H(e) = \left[\begin{array}{c} \text{arccot} \left(\frac{\sin(X/2R)}{\sin(\alpha) \sin(\phi/2)} - \tan(\alpha/2) \right) \\ \hline \frac{-1}{\left(\frac{\sin(X/2R)}{\sin(\alpha) \sin(\phi/2)} - \tan(\alpha/2) \right)^2} \left(\frac{1}{2R} \cos\left(\frac{X}{2R}\right) \sin\left(\frac{\phi}{2}\right) - \frac{1}{2} \left(\sin\left(\frac{X}{2R}\right) \cos\left(\frac{\phi}{2}\right) \right) \right) \\ \sin(\alpha) \sin^2(\phi/2) \end{array} \right]$$

$$H(e) = \begin{bmatrix} h_1(e_s) \\ h_2(e_s) \end{bmatrix} = Y_s \quad ; \quad \text{The calculated values}$$

$$J^T(e_s) = \begin{bmatrix} J_{11} & J_{12} \\ J_{21} & J_{22} \end{bmatrix} ; \quad K = \begin{bmatrix} K_1 & 0 \\ 0 & K_2 \end{bmatrix}, \quad K_1, K_2 > 0,$$

$$\dot{\Theta}_s = K J^T(e_s) [y_d(t) - y_s(t)]$$

$$y_d(t) = \begin{bmatrix} \eta \\ \dot{\eta} \end{bmatrix} ; \quad \text{the measured values}$$

Let $y_d(t) - y_s(t) = y_e$; The error signal

$$\dot{\Theta}_s = \begin{bmatrix} K_1 J_{11} y_{e1} + K_1 J_{21} y_{e2} \\ K_2 J_{12} y_{e1} + K_2 J_{22} y_{e2} \end{bmatrix} \quad \text{final result for observer}$$

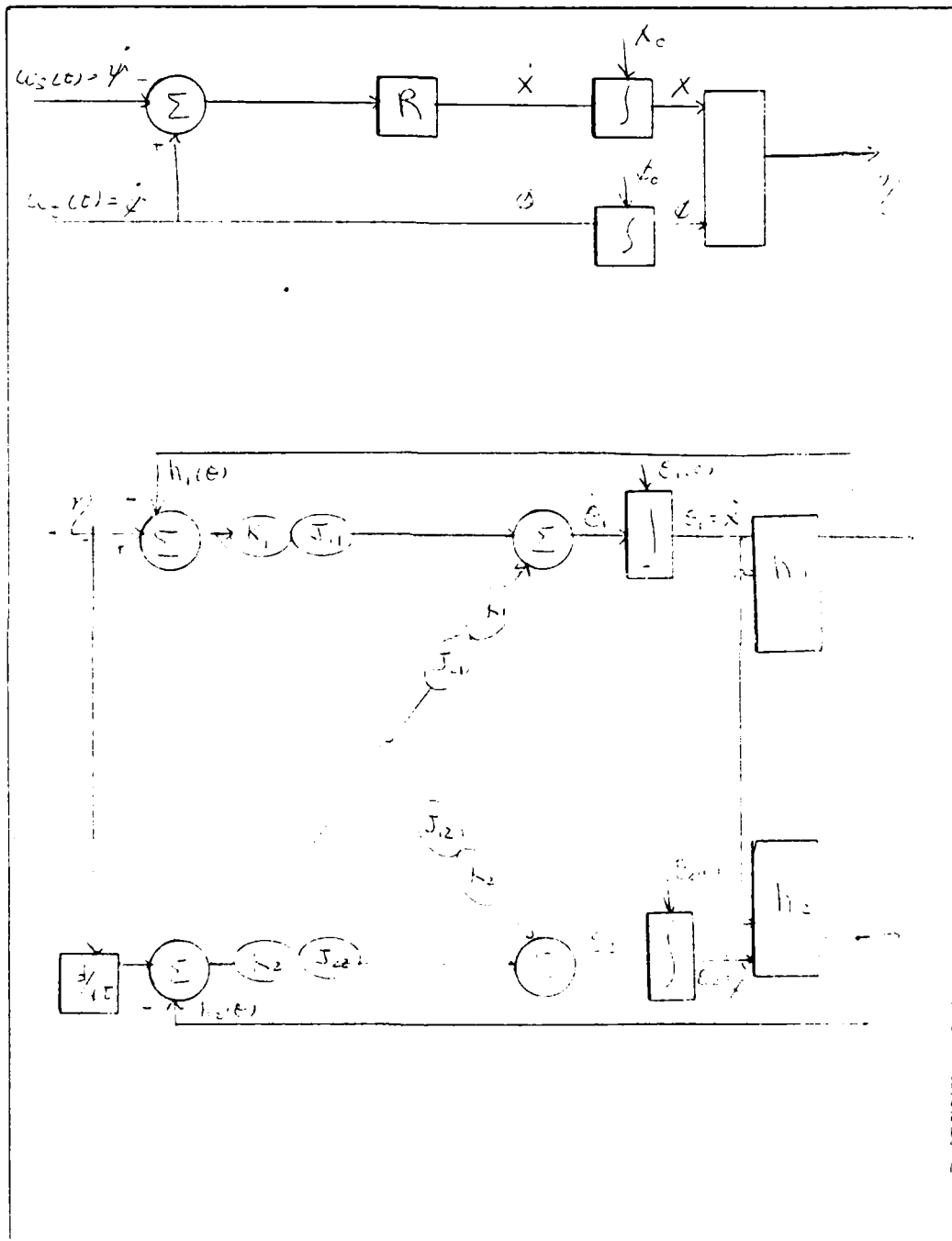


Figure 5.4 Satellite Observer

VI. SIMULATION RESULTS

The basic observer designed in Chapter 5 is simulated to prove authenticity. Recall that the original state and measurement equations were developed in Chapter 3. Due to the satellite's limited GSW, several parameters (including angles $\bar{\theta}$ and τ) are confined in their maximum attainable values. Therefore, these parameters were kept within specific ranges. The angle alpha (α) is taken to be a constant 30° . This value is selected for convenience.

The angular velocity of the target ($\dot{\theta}$) is chosen to be 0.0005 rad/sec. This sets the target speed at about 2 mi/sec. The angular velocity ($\dot{\phi}$) of the satellite is chosen to be 0.00045 rad/sec which yields a speed of about 1.8 mi/sec. These are arbitrary but not unrealistic values.

A. THE BASIC CONTINUOUS OBSERVER

Figure 6.1 depicts the basic simulation block diagram. The initial conditions $\bar{\theta}$ and X are 0.2 radians and 1000km (621.5 mi) respectively. These values are arbitrary but within the acceptable range. Recall that $X = R(\bar{\theta} - \tau)$.

Figure 6.2 is a block diagram depicting the basic observer design that is simulated. Note that Figure 6.2 is virtually identical to Figure 5.5.

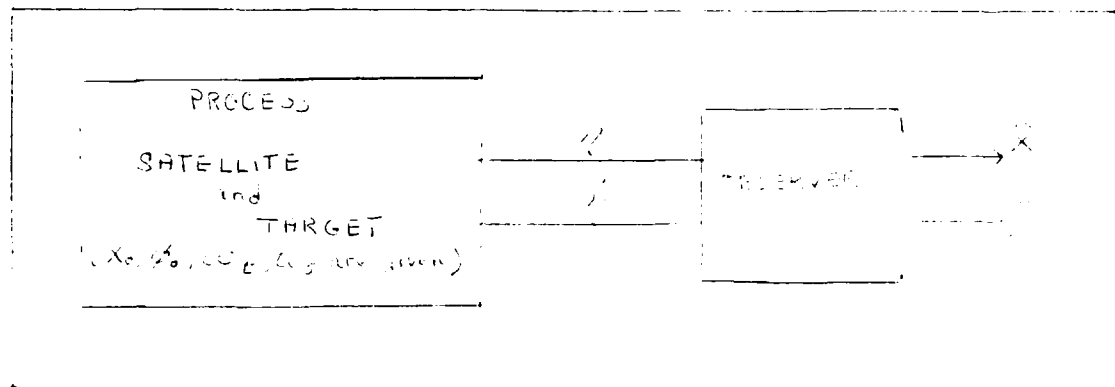


Figure 6.1 Basic Simulation Block Diagram

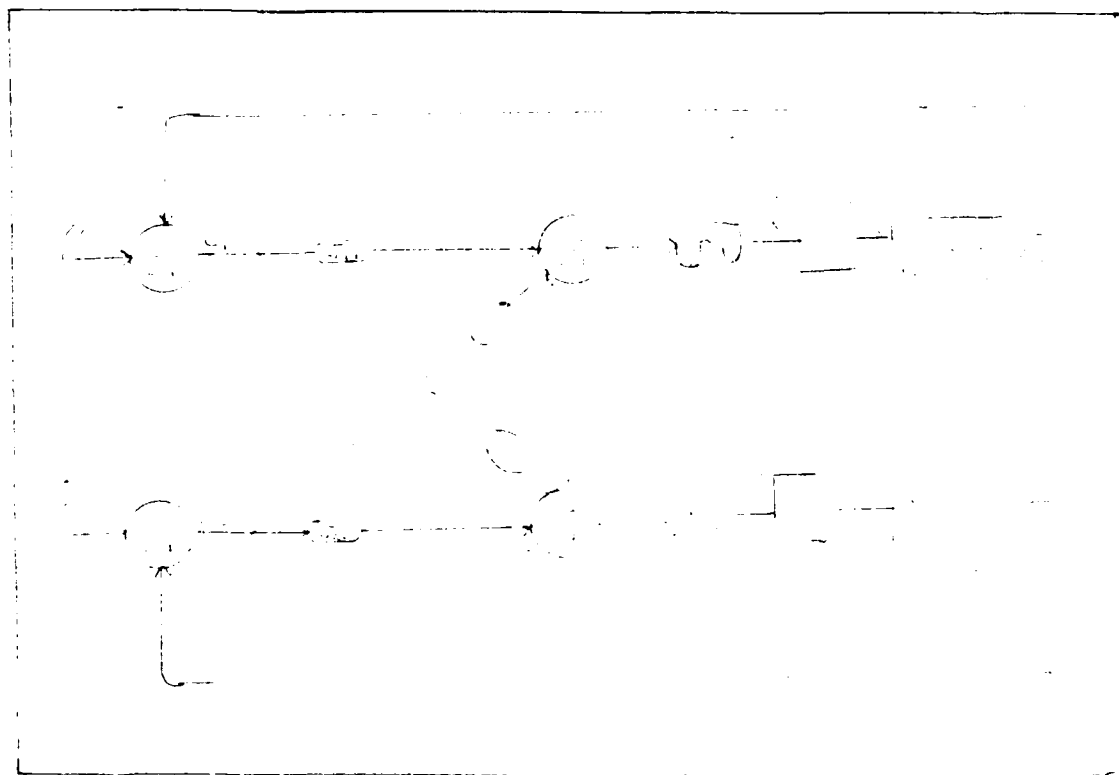


Figure 6.2 Observer Block Diagram

The equations representing the various elements in Figure 6.2 were initially developed in Chapters 3,4 and 5. Table 18 summarizes these equations.

The gain matrix (as developed in Table 17) is chosen to be a diagonal matrix of the form:

$$K = \begin{bmatrix} k_1 & 0 \\ 0 & k_2 \end{bmatrix}$$

The elements k_1 and k_2 both must be greater than zero. A diagonal matrix was chosen because it is fairly easy to work with and it allows the error changes to be monitored.

There are two ways to describe the observer to be simulated. It can be described in the continuous domain or in the discrete domain.

The observer was initially represented as a continuous model. A forth-order Runge-Kutta method is used for integration. The continuous model was used in order to eliminate any possible errors that could be introduced as a result of discretization. However, simulations for both versions produce no real differences.

B. THE DISCRETE OBSERVER

With the advent of micro-computers a discrete observer acting as a one-step predictor is a more realistic choice. In this model the forward difference approximation is employed.

The basic definition is:

$$X(t_{n+1}) = X(t_n) + \Delta t \dot{X}(t_n)$$

TABLE 18 OBSERVER EQUATIONS

OBSERVER:

$$e_1 = \eta - h_1$$

$$e_2 = \dot{\eta} - \dot{h}_2$$

$$\hat{X} = \int \hat{X} dt = \left(K_1 \int e_1 dt + \int e_2 dt \right) ; \hat{Y} = \hat{Y}_1 + \hat{Y}_2$$

MEASUREMENTS:

$$\eta = \arccos \left(\frac{\sin \theta \sin \phi}{\sin \theta \sin \phi} \right) - \tan^{-1} \left(\frac{\sin \theta \sin \phi}{\sin \theta \sin \phi} \right)$$

$$\dot{\eta} = \frac{-1}{1 + \left(\frac{\sin \theta \sin \phi}{\sin \theta \sin \phi} \right) - \tan^{-1} \left(\frac{\sin \theta \sin \phi}{\sin \theta \sin \phi} \right)} \cdot \frac{\sin \theta \sin \phi}{\sin \theta \sin \phi}$$

$$h_1 = \arccos \left(\frac{\sin \theta \sin \phi}{\sin \theta \sin \phi} \right) - \tan^{-1} \left(\frac{\sin \theta \sin \phi}{\sin \theta \sin \phi} \right)$$

$$h_2 = \frac{-1}{1 + \left(\frac{\sin \theta \sin \phi}{\sin \theta \sin \phi} \right) - \tan^{-1} \left(\frac{\sin \theta \sin \phi}{\sin \theta \sin \phi} \right)} \cdot \frac{\sin \theta \sin \phi}{\sin \theta \sin \phi}$$

INITIALS:

$$\hat{X}_0 = \eta_0, \quad \hat{Y}_0 = \eta_0$$

$$\hat{X}_1 = \eta_1, \quad \hat{Y}_1 = \eta_1$$

1. Full Non-Linear Observer

First the original, highly non-linear observer (figure 5.5) was simulated using a FORTRAN program on the IBM 370 system. All attempts to find values of gains and integration step for which observed states converge were unsuccessful. Typically the observer enters steady state with very small errors e_1 and e_2 ; however, the estimated states were far from actual values. It is possible that this behavior is the consequence of the sinusoidal periodic functions ($\sin(x/2R)$ and $\sin(\tilde{x}/2)$) in \hat{x} and $\hat{\tilde{x}}$. Recall from Chapter 4 that this observer is not shown to be observable in the strict sense. Univalence may not exist due to the reiterative nature of the sine function. In order to avoid periodicity an approximation of a non-linear observer is considered.

The simplified observer has the same form as the full observer (see Table 18), but the measurement equations and the corresponding Jacobian are approximated as developed in Chapter 4 (and repeated in Table 19).

The simplified observer simulated was being very insensitive to changes in X and \tilde{x} . The observer stabilized with a small error (e_1 and e_2) while \hat{X} and $\hat{\tilde{x}}$ remained significantly different from X and \tilde{x} respectively. The exact reason for this behavior is unknown. However it is theorized that the relative smoothness of the arccotangent curve ($\text{arccot } \cdot$) is responsible for this behavior.

TABLE 19 SIMPLIFIED OBSERVER

Measurement equations:

$$\text{set } s = \sin^2(\alpha/2) \text{ and } a = \sin(\alpha)$$

$$h_1(X, \Phi) = \text{arccot} \left(\frac{x - 2R\Phi S}{R\Phi a} \right)$$

$$h_2(X, \Phi) = -aR \left(\frac{X\Phi - \Phi X}{X^2 - 4R\Phi SX + 4R^2\Phi^2 S} \right)$$

Jacobian:

$$J_{11} = \frac{\partial h_1}{\partial X} = \frac{-aR}{X^2 - 4R\Phi SX + 4R^2\Phi^2 S} \Phi$$

$$J_{12} = \frac{\partial h_1}{\partial \Phi} = \frac{aR}{X^2 - 4R\Phi SX + 4R^2\Phi^2 S} X$$

$$J_{21} = \frac{\partial h_2}{\partial X} = \frac{aR}{X^2 - 4R\Phi SX + 4R^2\Phi^2 S} \cdot \frac{2X\Phi(X-2R\Phi S) + \Phi(4R^2\Phi^2 S - X^2)}{X^2 - 4R\Phi SX + 4R^2\Phi^2 S}$$

$$J_{22} = \frac{\partial h_2}{\partial \Phi} = \frac{aR}{X^2 - 4R\Phi SX + 4R^2\Phi^2 S} \cdot \frac{X(4R^2\Phi^2 S - X^2) + 4ESX\Phi(X-2R\Phi)}{X^2 - 4R\Phi SX + 4R^2\Phi^2 S}$$

In order to circumvent this problem the measurement signal is redefined.

2. Redefined Non-Linear Model

A new measurement variable is defined as:

$$u(t) = x(t)/\bar{x}(t) = R \sin(\alpha) (\cot(\gamma(t)) + \tan(\alpha/2))$$

If the value of α is known and $\gamma(t)$ is measured; then $u(t)$ can be calculated. Taking into account the assumed range for $\bar{x}(t)$ and $x(t)$ and the values for parameters R and α , the expression $X/(R\bar{x}\sin(\alpha)) - \tan(\alpha/2)$ never achieves a very large value. Therefore $\gamma(t)$ is bounded away from zero. This implies that $\cotan(\gamma(t))$ has a bounded value.

The derivative of $u(t)$ is:

$$\dot{u}(t) = R \sin(\alpha) (-\dot{\gamma}(t) / \sin^2(\gamma(t)))$$

where $\dot{\gamma}(t)$ and $\gamma(t)$ are measured values and $u(t)$ is evaluated.

The redefined non-linear model and observer are presented in Figure 6.3. It is noted that this observer has the same form as the observer given on the block diagram in Figure 6.2. Observer equations are shown in Table 20.

All attempts to find the power K_1 , K_2 and Δt (the time increment) that would force the states to converge failed. A satisfactory theoretical explanation for this behavior was not established. However, one possible explanation is that e_1 and e_2 are extremely sensitive to

TABLE 20

MEASUREMENT EQUATIONS - REDEFINED NON-LINEAR MODEL

Measurement equations:

$$h_1(X, \Phi) = \mu(X, \Phi) = \frac{X}{\Phi}$$

$$h_2(X, \Phi) = \mu'(X, \Phi) = \frac{X\Phi - \Phi X}{\Phi^2} = \frac{1}{\Phi} \left(X - \frac{\Phi X}{\Phi} \right)$$

Jacobian:

$$J_{11} = \frac{\partial h_1}{\partial X} = \frac{1}{\Phi} ; \quad J_{12} = \frac{\partial h_1}{\partial \Phi} = -\frac{X}{\Phi^2} = -\frac{1}{\Phi} \frac{X}{\Phi}$$

$$J_{21} = \frac{\partial h_2}{\partial X} = -\frac{1}{\Phi^2} \left(\frac{\Phi}{\Phi} \right)$$

$$J_{22} = \frac{\partial h_2}{\partial \Phi} = \frac{X(\Phi)^2 - 2\Phi(X\Phi - \Phi X)}{\Phi^4} = -\frac{1}{\Phi^3} (X\Phi + 2\Phi X)$$

$$= \frac{1}{\Phi^2} \left(\frac{2\Phi X}{\Phi} - X \right)$$

Observability;

$$|J| = J_{11} J_{22} - J_{12} J_{21} = \frac{1}{\Phi} \frac{2\Phi X - X}{\Phi} - \frac{1}{\Phi} \frac{\Phi X}{\Phi} = \frac{1}{\Phi} \frac{\Phi X}{\Phi} - X$$

$$|J| = 0 \text{ if } \frac{\Phi X}{\Phi} - X = 0 \quad X = \frac{\Phi}{X} \frac{\Phi}{\Phi}$$

Note that these conditions were defined previously.

change in states which results in an extremely slow convergence with a highly oscillatory transient response.

3. Redefinition of State Variables

Analysis of the model with redefined measurements reveals that the form of the equations allow redefinition of state variables. This may reduce the sensitivity of the model.

A new state vector $[U, V]^T$ is defined as:

$$U = X/\bar{\omega} \text{ and } V = 1/\bar{\omega}$$

Table 21 illustrates further development.

The block diagram in figure 6.4 shows the discrete observer. A simulation of the discrete observer was run with $\omega_t = 0.0005$ and $\omega_s = 0.00045$. Several different gains were used to test convergence. Convergence is obtained for the following ranges:

$$0 < K, \Delta t < 2 \text{ and } 0 < K, \Delta t / |J_{\omega}| < 2$$

Arbitrary initial values for \hat{U} and \hat{V} were employed. It seemed natural to assume $\hat{U}_0 = 0$, $X = 0$ and $\hat{V} = 1$ ($\bar{\omega} = 1$ is within the allowable value for $\bar{\omega}$).

To examine the observer's ability to track varying angular speeds it is assumed that ω_t and ω_s are sine waves.

$$\omega_t = \hat{A} \sin(Dt)$$

$$\omega_s = \hat{B} \sin(Dt)$$

Different amplitudes and periods are tested and successful tracking is achieved. Appendix C contains the resulting computer graphs.

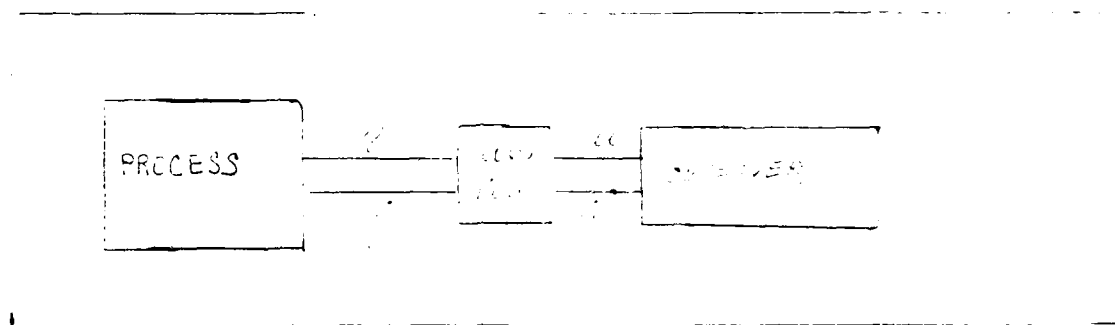


Figure 6.3 Redefined Model

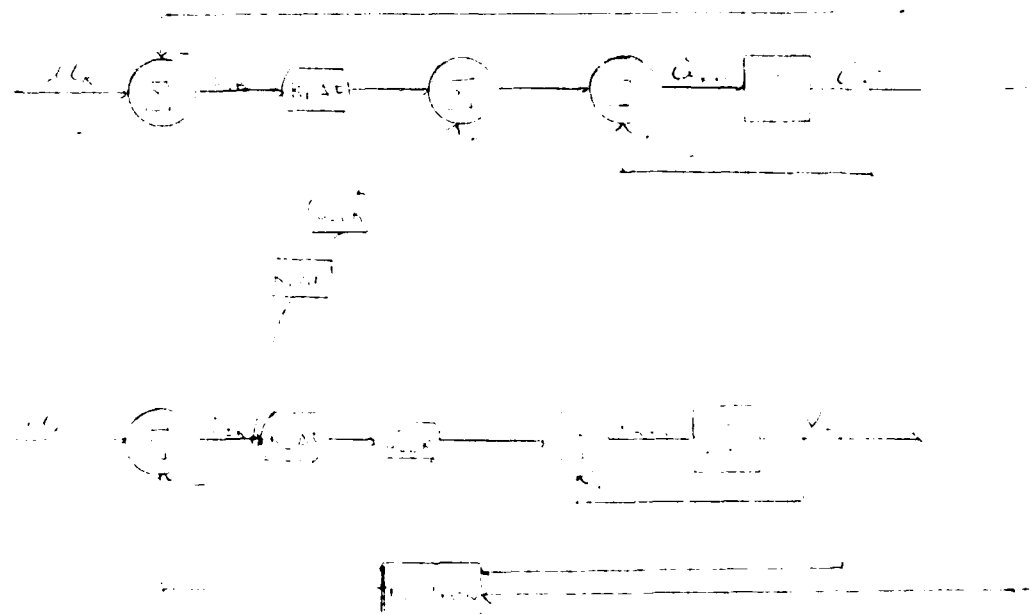


Figure 6.4 Discrete Observer

TABLE 21

OBSERVABILITY CONDITIONS AND DISCRETIZED OBSERVER

Measurement equations:

$$f_1(U, V) = h_1(U, V) = U$$

$$f_2(U, V) = h_2(U, V) = V(\dot{X} - \Phi U)$$

Jacobian:

$$J_{11} = \frac{\partial h_1}{\partial U} = 1 \quad ; \quad J_{12} = \frac{\partial h_1}{\partial V} = 0$$

$$J_{21} = \frac{\partial h_2}{\partial U} = -\Phi V \quad ; \quad J_{22} = \frac{\partial h_2}{\partial V} = X - \Phi U$$

Observability conditions are the same:

$$|J| = X - \Phi U \neq 0 \quad \dot{X} - \Phi X \neq 0 \quad \dot{X} \neq \Phi X$$

Continuous observer:

$$\dot{\hat{U}} = K_1 J_{11} e_1 + K_2 J_{12} e_2$$

$$\dot{\hat{V}} = K_2 J_{21} e_1 + K_2 J_{22} e_2$$

The discretized observer becomes:

$$e_{1k} = f_1(U_k, V_k) - h_1(\hat{U}_k, \hat{V}_k) = y_k - \hat{U}_k$$

$$e_{2k} = f_2(U_k, V_k) - h_2(\hat{U}_k, \hat{V}_k) = y_k - \hat{V}_k(\dot{X} - \Phi \hat{U}_k)$$

$$\hat{U}_{k+1} = U_k + K_1 \Delta t e_{1k} + K_2 \Delta t \cdot J_{12}(\hat{U}_k, \hat{V}_k) e_{2k}$$

$$\hat{V}_{k+1} = \hat{V}_k + K_2 \Delta t J_{22}(\hat{U}_k, \hat{V}_k) e_{2k}$$

As expected the amplitude of the sine wave representing state (A/D;B/D) which can be tracked is inversely related to the period of oscillation.

4. Model Decoupling

Analysis of the error equations provide;

$$\begin{aligned} e_1 &= f_1(U,V) - h_1(\hat{U},\hat{V}) = U - \hat{U} \\ e_2 &= f_2(U,V) - h_2(\hat{U},\hat{V}) = V(\dot{X} - \Phi U) - \hat{V}(\dot{X} - \Phi U) \\ &= \dot{X}(\hat{V} - V) - \Phi(UV - \hat{U}\hat{V}) \end{aligned}$$

The block diagram in Figure 6.4 indicates the possibility of decoupling the observer into two first order models by letting J_{11} equal zero (J_{12} is already zero).

Figure 6.5 shows a block diagram of the discrete subsystem. The discrete system of Figure 6.6 is certainly stable if it's eigenvalue lies within the unit circle.

$$|1-a| < 1 \Rightarrow 0 < a < 2 \Rightarrow 0 < K_{at} < 2$$

Under this condition the system has a steady-state error of zero for a constant input u .

Hence the system acts as positioning servo-mechanism and is capable of tracking the relatively slow varying inputs with very small errors.

5. Subsystem Two

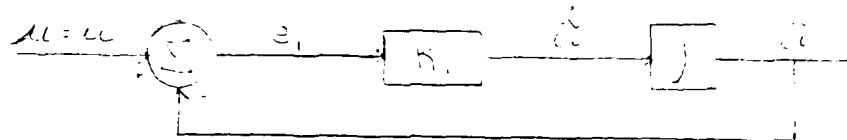
Assuming that subsystem 1 is tracking u ($\hat{u}(t) = u(t)$) the error e_2 can be approximated as:

$$e_2 \approx (\dot{X} - \Phi U)(V - \hat{V})$$

The observer is reduced to the gradient algorithm where the gradient is:

SUBSYSTEM 1

$$\dot{\hat{u}} = k_1 e_1 = k_1 (u - \hat{u})$$



CORRESPONDING DISCRETE MODEL

$$\begin{aligned}\hat{u}_{k+1} &= (1 + T k_1 \Delta t) \hat{u}_k + T k_1 \Delta t u_k \\ &= (1 + T k_1 \Delta t) \hat{u}_k + T k_1 \Delta t u_k = \hat{u}_k + T e_{1k}\end{aligned}$$

$$T k_1 \Delta t = K$$

Figure 6.5 Subsystem 1

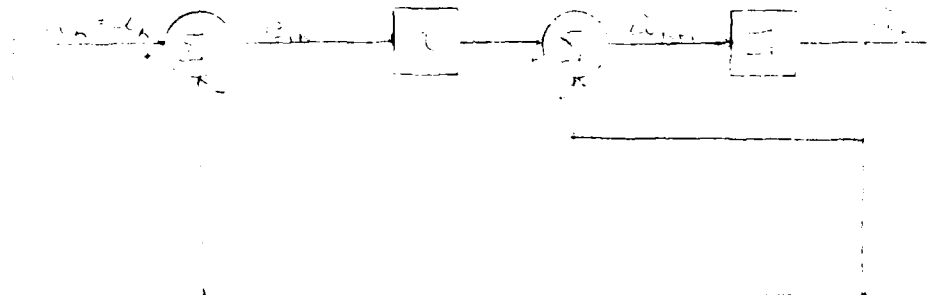


Figure 6.6 Discretized Block Diagram

AD-A168 394

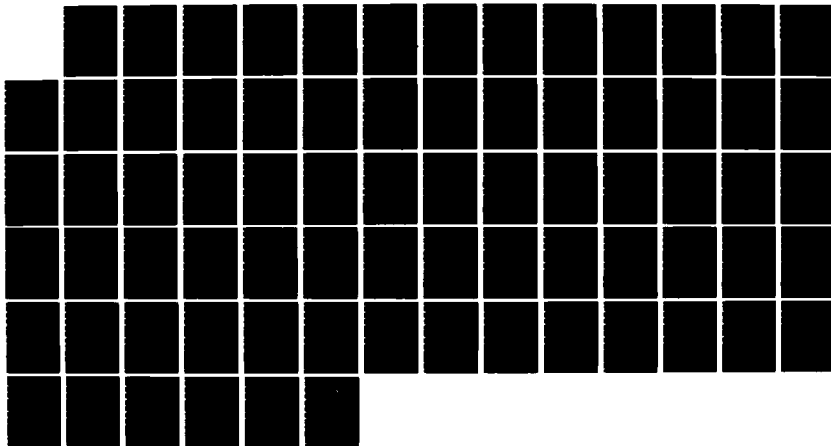
SATELLITE TRACKING AND OBSERVABILITY(U) NAVAL
POSTGRADUATE SCHOOL MONTEREY CA M G MORT MAR 86

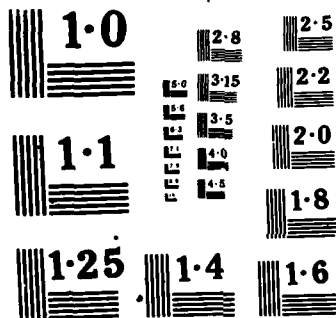
2/2

UNCLASSIFIED

F/G 22/3

NL





NATIONAL BUREAU OF S
MICROCOPY RESOLUTION TEST

$$\frac{\partial(e_z)}{\partial(V-\hat{V})} = \dot{\hat{X}} - \hat{X}\hat{U} = J$$

Figure 6.7 illustrates the observer. This result is also in accordance with the method proposed in [Ref. 6].

Defining $V = (\dot{\hat{X}} - \hat{X}\hat{U})V$ as a new measurement the corresponding function h is $h = (\dot{\hat{X}} - \hat{X}\hat{U})V$. The Jacobian is $J = \partial h / \partial V = \dot{\hat{X}} - \hat{X}\hat{U}$.

In order to simplify the stability analysis the Jacobian, J , is replaced with the signum function, $\text{signum}(J)$. This is sufficient to guarantee the negative feedback of subsystem 2. Subsystem 2 is analogous to subsystem 1 and will be stable if $0 < K_2 \Delta t < 2$. Consequently this system also performs as positioning servo-mechanism and will track relatively slow varying inputs $V(t)$ with very small error.

The presented analysis leads to a definition of the decoupled observer. This observer is depicted in Table 22. Appendix D contains the computer simulation results.

Figure 6.8 is essentially the same as Figure 6.4 with $J_{11} = 0$ and $J_{12} = \text{signum}(J_{12})$. Therefore it is possible to consider this algorithm a simplification of the algorithm developed in [Ref. 7]. However, it should be pointed out that the decoupled observer can be derived directly through analysis of the two linear subsystems presented above.

TABLE 22
DISCRETIZATION

$$e_1 = \mathcal{L} - \hat{U} = -h_1(\hat{U}, \hat{V})$$

$$e_2 = -\hat{V}(X - \mathcal{E}U) = -h_2(\hat{U}, \hat{V})$$

$$\hat{U} = K_1 e_1$$

$$\hat{V} = K_2 \text{Sygn}(J_{22}) e_2$$

After discretization this becomes

$$\hat{U}_{n+1} = \hat{U}_n + K_1 \Delta t e_{1n}$$

$$\hat{V}_{n+1} = \hat{V}_n + K_2 \Delta t \text{sygn}(J_{22}) e_{2n}$$

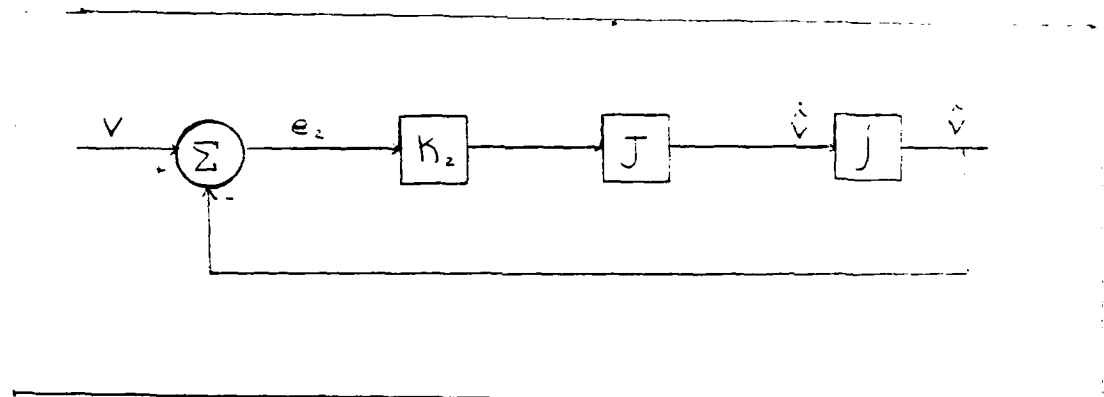


Figure 6.7 Subsystem 2

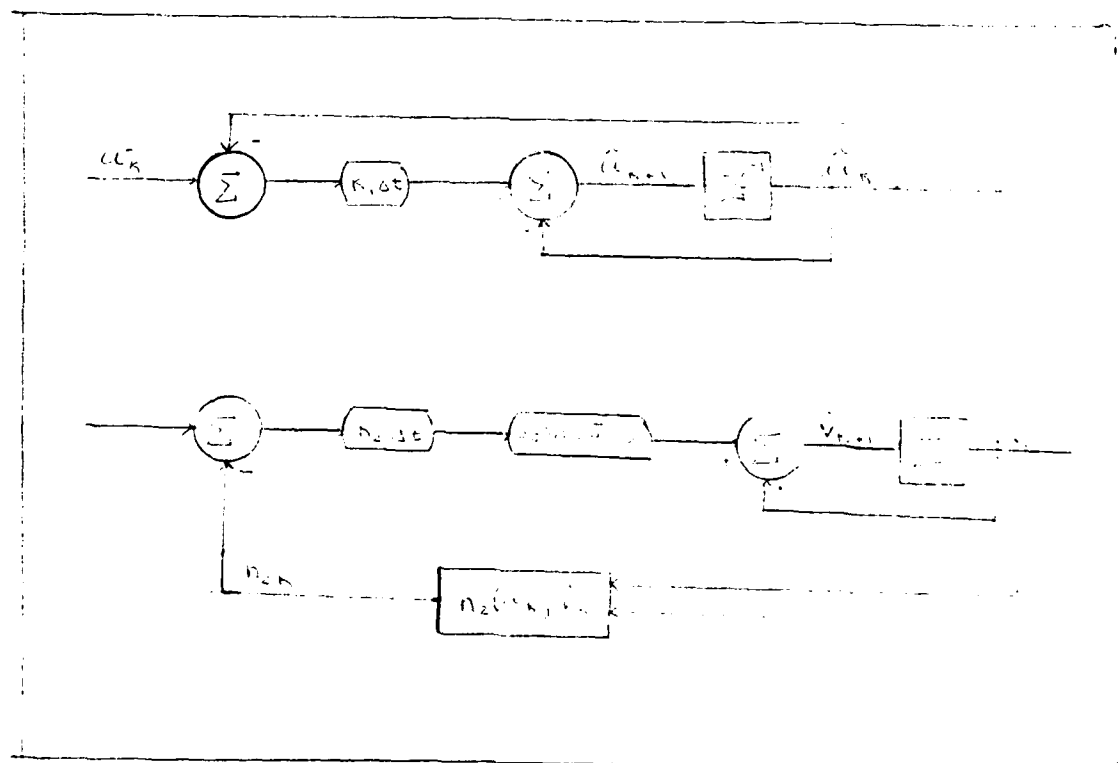


Figure 6.8 Decoupled Observer

In the decoupled model it is easier to control gains since the J_{12} element does not affect stability. It is noted that slightly more oscillatory behavior is present at the beginning of the simulation. This is not unusual for gradient type algorithms.

Satisfactory results for the product $K\Delta t = 0.1$ are expected if the observer is analyzed from the sampling theorem point of view. This presupposes that both continuous subsystems possess only one time constant $\tau = 1/K$. The sampling theorem requires that $\tau < T/2$ and $\Delta t K < 0.5$.

Experience has shown that the best results for the one-step integration are obtained if the integration step (sampling time) is ten times less than the smaller time constant in the system. This means $\Delta t = 0.1(1/K)$ and $\Delta t K = 0.1$.

The sampling theorem is violated if $\Delta t K = 1$. As a consequence the observer requires much more time to extract sufficient information from the measurement and to start state tracking. The simulation results demonstrate that when the product $\Delta t K$ equals unity convergence starts after fifty seconds. This is approximately ten times slower from previous experiments where the sampling theorem is satisfied.

In the case of $\Delta t K = 0.01$ the system pole is very close to the unit circle. Therefore, convergence is relatively slow.

As demonstrated by the various computer generated graphs, the simulation results for this system are satisfactory. Therefore the selected coordinate system is proven acceptable.

VI. SIMULATION RESULTS

The basic observer designed in Chapter 5 is simulated to prove authenticity. Recall that the original state and measurement equations were developed in Chapter 3. Due to the satellite's limited GSW, several parameters (including angles \bar{x} and γ) are confined in their maximum attainable values. Therefore, these parameters were kept within specific ranges. The angle alpha (α) is taken to be a constant 30° . This value is selected for convenience.

The angular velocity of the target (ω_t) is chosen to be 0.0005 rad/sec. This sets the target speed at about 2 mi/sec. The angular velocity (ω_s) of the satellite is chosen to be 0.00045 rad/sec which yields a speed of about 1.8 mi/sec. These are arbitrary but not unrealistic values.

A. THE BASIC CONTINUOUS OBSERVER

Figure 6.1 depicts the basic simulation block diagram. The initial conditions \bar{x} and X are 0.2 radians and 1000km (621.5 mi) respectively. These values are arbitrary but within the acceptable range. Recall that $X = R(\bar{x} - \gamma)$.

Figure 6.2 is a block diagram depicting the basic observer design that is simulated. Note that Figure 6.2 is virtually identical to Figure 5.5.

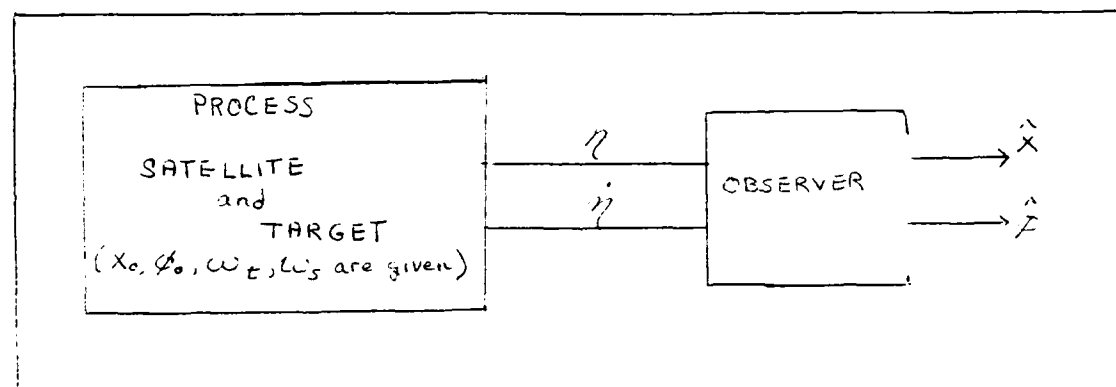


Figure 6.1 Basic Simulation Block Diagram

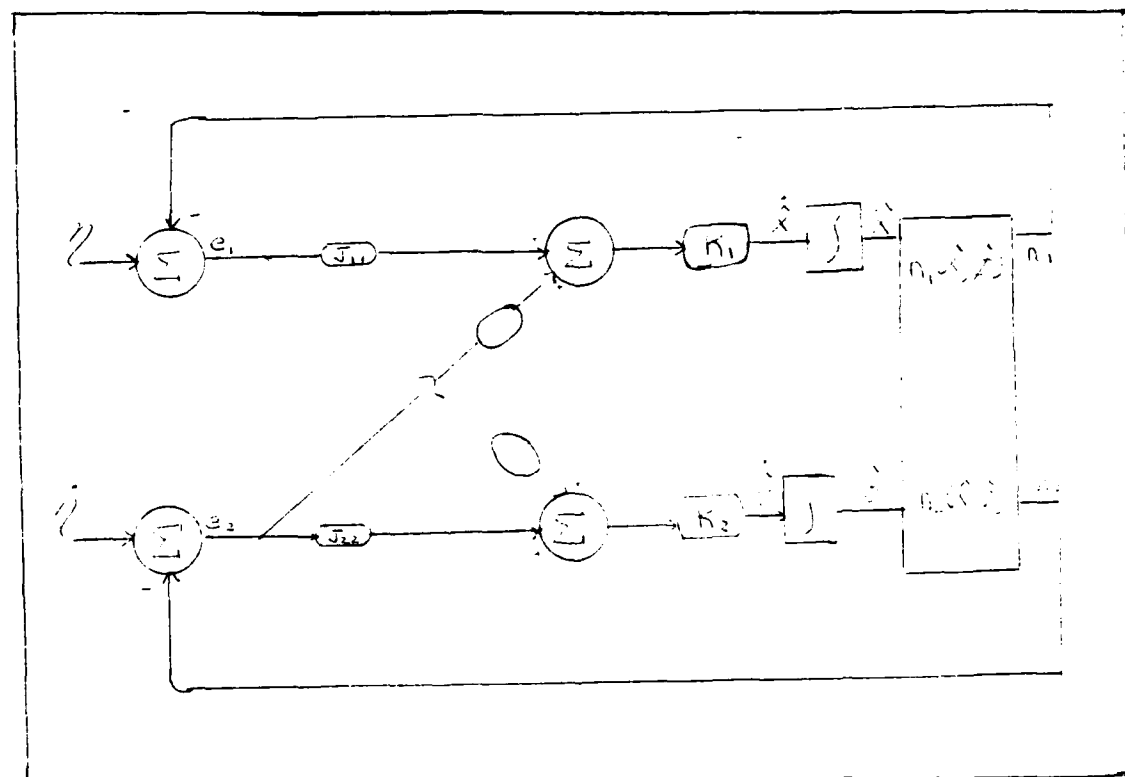


Figure 6.2 Observer Block Diagram

The equations representing the various elements in Figure 6.2 were initially developed in Chapters 3,4 and 5. Table 18 summarizes these equations.

The gain matrix (as developed in Table 17) is chosen to be a diagonal matrix of the form:

$$K = \begin{bmatrix} k_1 & 0 \\ 0 & k_2 \end{bmatrix}$$

The elements k_1 and k_2 both must be greater than zero. A diagonal matrix was chosen because it is fairly easy to work with and it allows the error changes to be monitored.

There are two ways to describe the observer to be simulated. It can be described in the continuous domain or in the discrete domain.

The observer was initially represented as a continuous model. A forth-order Runge-Kutta method is used for integration. The continuous model was used in order to eliminate any possible errors that could be introduced as a result of discretization. However, simulations for both versions produce no real differences.

B. THE DISCRETE OBSERVER

With the advent of micro-computers a discrete observer acting as a one-step predictor is a more realistic choice. In this model the forward difference approximation is employed.

The basic definition is;

$$X(t_{k+1}) = X(t_k) + \Delta t \dot{X}(t_k)$$

TABLE 18 OBSERVER EQUATIONS

OBSERVER:

$$e_1 = \eta - h_1$$

$$e_2 = \dot{\eta} - h_2$$

$$\hat{x} = \int \dot{\hat{x}} dt = \int (k_1 [J_{21} e_2 + J_{11} e_1]) dt ; \hat{\phi} = \int \dot{\hat{\phi}} dt = \int (k_2 [J_{22} e_2 + J_{12} e_1]) dt$$

MEASUREMENTS:

$$\eta = \arccot \left(\frac{\sin(x/2R)}{\sin(\alpha) \sin(\phi/2)} - \tan(\alpha/2) \right)$$

$$\dot{\eta} = \frac{-1}{1 + \left(\frac{\sin(x/2R)}{\sin(\alpha) \sin(\phi/2)} - \tan(\alpha/2) \right)} \left[\frac{\cos(\frac{x}{2R}) \left(\frac{\dot{x}}{2R} \right) \sin(\frac{\phi}{2}) - \cos(\frac{\phi}{2}) \left(\frac{\dot{\phi}}{2} \right) \sin(\frac{x}{2R})}{\sin(\alpha) \sin^2(\phi/2)} \right]$$

$$h_1 = \arccot \left(\frac{\sin(\hat{x}/2R)}{\sin(\alpha) \sin(\hat{\phi}/2)} - \tan(\alpha/2) \right)$$

$$h_2 = \frac{-1}{1 + \left(\frac{\sin(\hat{x}/2R)}{\sin(\alpha) \sin(\hat{\phi}/2)} - \tan(\alpha/2) \right)^2} \left(\frac{\frac{1}{2R} \cos(\frac{\hat{x}}{2R}) \sin(\frac{\hat{\phi}}{2}) - \frac{1}{2} \sin(\frac{\hat{x}}{2R}) \cos(\frac{\hat{\phi}}{2})}{\sin(\alpha) \sin^2(\hat{\phi}/2)} \right)$$

JACOBIAN:

$$J_{11} = \partial \eta / \partial x$$

$$J_{12} = \partial \eta / \partial \phi$$

AS DEVELOPED

IN CHAPTER 4.

$$J_{21} = \partial \dot{\eta} / \partial x$$

$$J_{22} = \partial \dot{\eta} / \partial \phi$$

1. Full Non-Linear Observer

First the original, highly non-linear observer (figure 5.5) was simulated using a FORTRAN program on the IBM 370 system. All attempts to find values of gains and integration step for which observed states converge were unsuccessful. Typically the observer enters steady state with very small errors e_1 and e_2 ; however, the estimated states were far from actual values. It is possible that this behavior is the consequence of the sinusoidal periodic functions ($\sin(x/2R)$ and $\sin(\bar{x}/2)$) in η and $\bar{\eta}$. Recall from Chapter 4 that this observer is not shown to be observable in the strict sense. Univalence may not exist due to the reiterative nature of the sine function. In order to avoid periodicity an approximation of a non-linear observer is considered.

The simplified observer has the same form as the full observer (see Table 18), but the measurement equations and the corresponding Jacobian are approximated as developed in Chapter 4 (and repeated in Table 19).

The simplified observer simulated was being very insensitive to changes in X and \bar{x} . The observer stabilized with a small error (e_1 and e_2) while \hat{X} and $\hat{\bar{x}}$ remained significantly different from X and \bar{x} respectively. The exact reason for this behavior is unknown. However it is theorized that the relative smoothness of the arccotangent curve ($\text{arccot } \eta$) is responsible for this behavior.

TABLE 19 SIMPLIFIED OBSERVER

Measurement equations:

$$\text{set } s = \sin^2(\alpha/2) \text{ and } a = \sin(\alpha)$$

$$h_1(X, \bar{x}) = \text{arccot} \left(\frac{x - 2R\bar{x}S}{R\bar{x}a} \right)$$

$$h_2(X, \bar{x}) = -aR \left(\frac{\dot{X}\bar{x} - \bar{x}\dot{X}}{X^2 - 4R\bar{x}SX + 4R^2\bar{x}^2S} \right)$$

Jacobian:

$$J_{11} = \partial h_1 / \partial X = \frac{-aR}{X^2 - 4R\bar{x}SX + 4R^2\bar{x}^2S} \bar{x}$$

$$J_{12} = \partial h_1 / \partial \bar{x} = \frac{aR}{X^2 - 4R\bar{x}SX + 4R^2\bar{x}^2S} X$$

$$J_{21} = \partial h_2 / \partial X = \frac{aR}{X^2 - 4R\bar{x}SX + 4R^2\bar{x}^2S} \cdot \frac{2\dot{X}\bar{x}(X-2R\bar{x}S) + \bar{x}(4R^2\bar{x}^2S-X^2)}{X^2 - 4R\bar{x}SX + 4R^2\bar{x}^2S}$$

$$J_{22} = \partial h_2 / \partial \bar{x} = \frac{aR}{X^2 - 4R\bar{x}SX + 4R^2\bar{x}^2S} \cdot \frac{X(4R^2\bar{x}^2S-X^2) + 4R\dot{S}\bar{x}(X-2R\bar{x})}{X^2 - 4R\bar{x}SX + 4R^2\bar{x}^2S}$$

In order to circumvent this problem the measurement signal is redefined.

2. Redefined Non-Linear Model

A new measurement variable is defined as:

$$\mu(t) = x(t)/\xi(t) = R\sin(\alpha)(\cot(\eta(t)) + \tan(\alpha/2))$$

If the value of α is known and $\eta(t)$ is measured; then $u(t)$ can be calculated. Taking into account the assumed range for $\xi(t)$ and $X(t)$ and the values for parameters R and α , the expression $X/(R\xi\sin(\alpha)) - \tan(\alpha/2)$ never achieves a very large value. Therefore $\eta'(t)$ is bounded away from zero. This implies that $\cotan(\eta(t))$ has a bounded value.

The derivative of $\mu(t)$ is:

$$\dot{\mu}(t) = R\sin(\alpha)(-\eta'(t)/\sin^2(\eta(t)))$$

where $\eta(t)$ and $\eta'(t)$ are measured values and $\mu(t)$ is evaluated.

The redefined non-linear model and observer are presented in Figure 6.3. It is noted that this observer has the same form as the observer given on the block diagram in Figure 6.2. Observer equations are shown in Table 20.

All attempts to find the power K_1 , K_2 and Δt (the time increment) that would force the states to converge failed. A satisfactory theoretical explanation for this behavior was not established. However, one possible explanation is that e and e are extremely sensitive to

TABLE 20

MEASUREMENT EQUATIONS - REDEFINED NON-LINEAR MODEL

Measurement equations:

$$h_1(X, \vartheta) = \mu(X, \vartheta) = \frac{X}{\vartheta}$$

$$h_2(X, \vartheta) = \dot{\mu}(X, \vartheta) = \frac{\dot{X}\vartheta - \dot{\vartheta}X}{\vartheta^2} = \frac{1}{\vartheta} \left(\frac{\dot{X}}{\vartheta} - \frac{\dot{\vartheta}X}{\vartheta^2} \right)$$

Jacobian:

$$J_{11} = \frac{\partial h_1}{\partial X} = \frac{1}{\vartheta} ; \quad J_{12} = \frac{\partial h_1}{\partial \vartheta} = \frac{-X}{\vartheta^2} = -\frac{1}{\vartheta} \frac{X}{\vartheta}$$

$$J_{21} = \frac{\partial h_2}{\partial X} = \frac{-1(\dot{\vartheta})}{\vartheta^2}$$

$$J_{22} = \frac{\partial h_2}{\partial \vartheta} = \frac{\dot{X}(\dot{\vartheta})^2 - 2\dot{\vartheta}(\dot{X}\dot{\vartheta} - \dot{\vartheta}^2 X)}{\vartheta^4} = \frac{-1}{\vartheta^3} (\dot{X}\dot{\vartheta} + 2\dot{\vartheta}^2 X)$$

$$= \frac{1}{\vartheta^2} \left(\frac{2\dot{\vartheta}X}{\vartheta} - \frac{\dot{X}}{\vartheta} \right)$$

Observability;

$$|J| = J_{11} J_{22} - J_{12} J_{21} = \frac{1}{\vartheta^3} \left(\frac{2\dot{\vartheta}X}{\vartheta} - \frac{\dot{X}}{\vartheta} \right) - \frac{1}{\vartheta^2} \frac{\dot{\vartheta}X}{\vartheta} = \frac{1}{\vartheta^3} \left(\frac{\dot{\vartheta}X}{\vartheta} - \dot{X} \right)$$

$$|J| = 0 \text{ if } \frac{\dot{\vartheta}X}{\vartheta} - \dot{X} = 0 \quad \frac{\dot{X}}{X} = \frac{\dot{\vartheta}}{\vartheta}$$

Note that these conditions were defined previously.

change in states which results in an extremely slow convergence with a highly oscillatory transient response.

3. Redefinition of State Variables

Analysis of the model with redefined measurements reveals that the form of the equations allow redefinition of state variables. This may reduce the sensitivity of the model.

A new state vector $[U, V]^T$ is defined as:

$$U = X/\bar{\omega} \text{ and } V = 1/\bar{\omega}$$

Table 21 illustrates further development.

The block diagram in figure 6.4 shows the discrete observer. A simulation of the discrete observer was run with $\omega_t = 0.0005$ and $\omega_s = 0.00045$. Several different gains were used to test convergence. Convergence is obtained for the following ranges:

$$0 < K_1 \Delta t < 2 \text{ and } 0 < K_2 \Delta t / |J_{22}| < 2$$

Arbitrary initial values for \hat{U} and \hat{V} were employed. It seemed natural to assume $\hat{U}_0 = 0$, $X = 0$ and $\hat{V} = 1$ ($\bar{\omega} = 1$ is within the allowable value for $\bar{\omega}$).

To examine the observer's ability to track varying angular speeds it is assumed that ω_t and ω_s are sine waves.

$$\omega_t = \hat{A} \sin(Dt)$$

$$\omega_s = \hat{B} \sin(Dt)$$

Different amplitudes and periods are tested and successful tracking is achieved. Appendix C contains the resulting computer graphs.

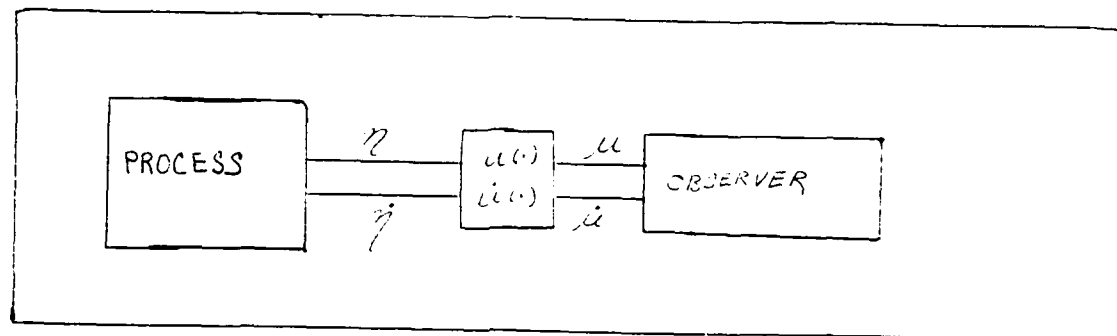


Figure 6.3 Redefined Model

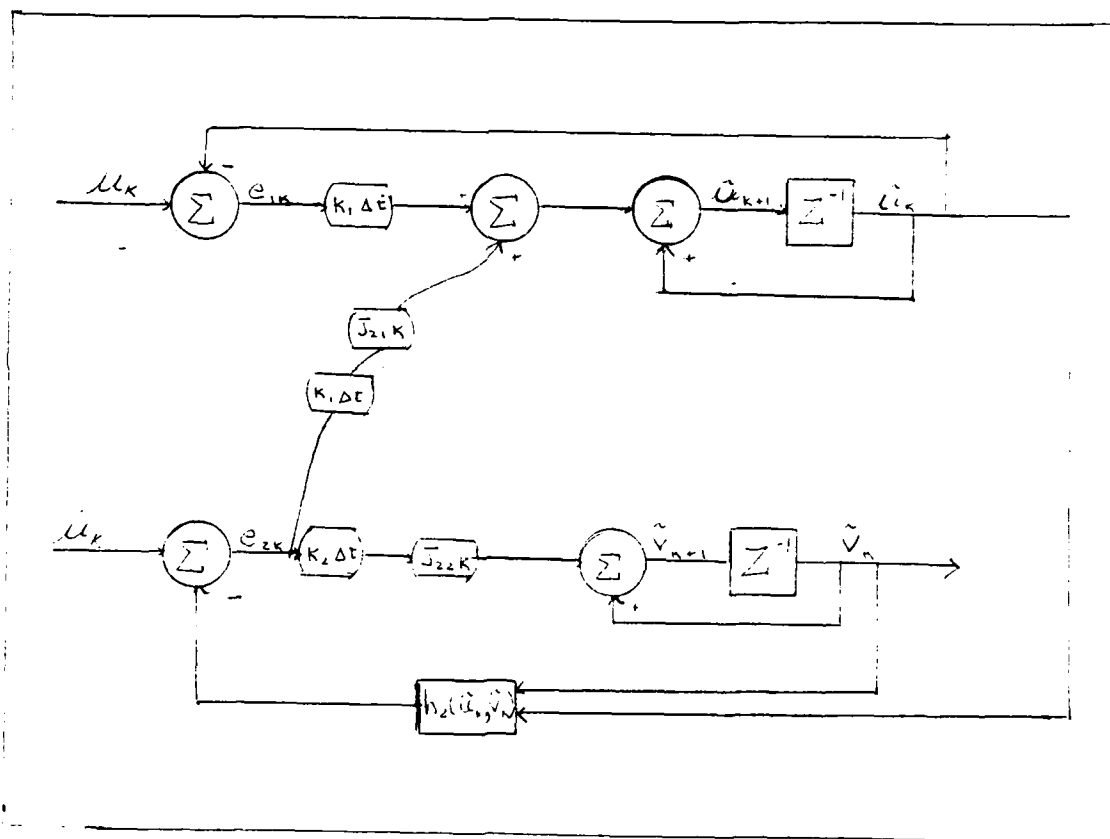


Figure 6.4 Discrete Observer

TABLE 21

OBSERVABILITY CONDITIONS AND DISCRETIZED OBSERVER

Measurement equations:

$$\mu(U, V) = h_1(U, V) = U$$

$$\dot{\mu}(U, V) = h_2(U, V) = V(\dot{X} - \dot{\Phi}U)$$

Jacobian:

$$J_{11} = \frac{\partial h_1}{\partial U} = 1 \quad ; \quad J_{12} = \frac{\partial h_1}{\partial V} = 0$$

$$J_{21} = \frac{\partial h_2}{\partial U} = -\dot{\Phi}V \quad ; \quad J_{22} = \frac{\partial h_2}{\partial V} = \dot{X} - \dot{\Phi}U$$

Observability conditions are the same:

$$|J| = \dot{X} - \dot{\Phi}U \neq 0 \quad \dot{X} - \frac{\dot{\Phi}X}{\dot{\Phi}} \neq 0 \quad \frac{\dot{X}}{X} \neq \frac{\dot{\Phi}}{\Phi}$$

Continuous observer:

$$\dot{\hat{U}} = K_1 J_{11} e_1 + K_1 J_{21} e_2$$

$$\dot{\hat{V}} = K_2 J_{12} e_1 + K_2 J_{22} e_2$$

The discretized observer becomes;

$$e_{1K} = \mu(U_K, V_K) - h_1(\hat{U}_K, \hat{V}_K) = \mu_K - \hat{U}_K$$

$$e_{2K} = \dot{\mu}(U_K, V_K) - h_2(\hat{U}_K, \hat{V}_K) = \dot{\mu}_K - \hat{V}_K(\dot{X} - \dot{\Phi}\hat{U}_K)$$

$$\hat{U}_{K+1} = \hat{U}_K + K_1 \Delta t e_{1K} + K_1 \Delta t \cdot J_{21}(\hat{U}_K, \hat{V}_K) e_{2K}$$

$$\hat{V}_{K+1} = \hat{V}_K + K_2 \Delta t J_{22}(\hat{U}_K, \hat{V}_K) e_{2K}$$

As expected the amplitude of the sine wave representing state (A/D;B/D) which can be tracked is inversely related to the period of oscillation.

4. Model Decoupling

Analysis of the error equations provide;

$$\begin{aligned} e_1 &= \mu(U,V) - h_1(\hat{U},\hat{V}) = U - \hat{U} \\ e_2 &= \mu(U,V) - h_2(\hat{U},\hat{V}) = V(\dot{X} - \hat{X}) - \hat{V}(\dot{X} - \hat{X}) \\ &= \dot{X}(V - \hat{V}) - \hat{X}(UV - \hat{U}\hat{V}) \end{aligned}$$

The block diagram in Figure 6.4 indicates the possibility of decoupling the observer into two first order models by letting J_{21} equal zero (J_{12} is already zero).

Figure 6.5 shows a block diagram of the discrete subsystem. The discrete system of Figure 6.6 is certainly stable if it's eigenvalue lies within the unit circle.

$$|1-a| < 1 \Rightarrow 0 < a < 2 \Rightarrow 0 < K \Delta t < 2$$

Under this condition the system has a steady-state error of zero for a constant input u .

Hence the system acts as positioning servo-mechanism and is capable of tracking the relatively slow varying inputs with very small errors.

5. Subsystem Two

Assuming that subsystem 1 is tracking u ($\hat{u}(t) = u(t)$) the error e_2 can be approximated as:

$$e_2 = (\dot{X} - \hat{X})\hat{U}(V - \hat{V})$$

The observer is reduced to the gradient algorithm where the gradient is:

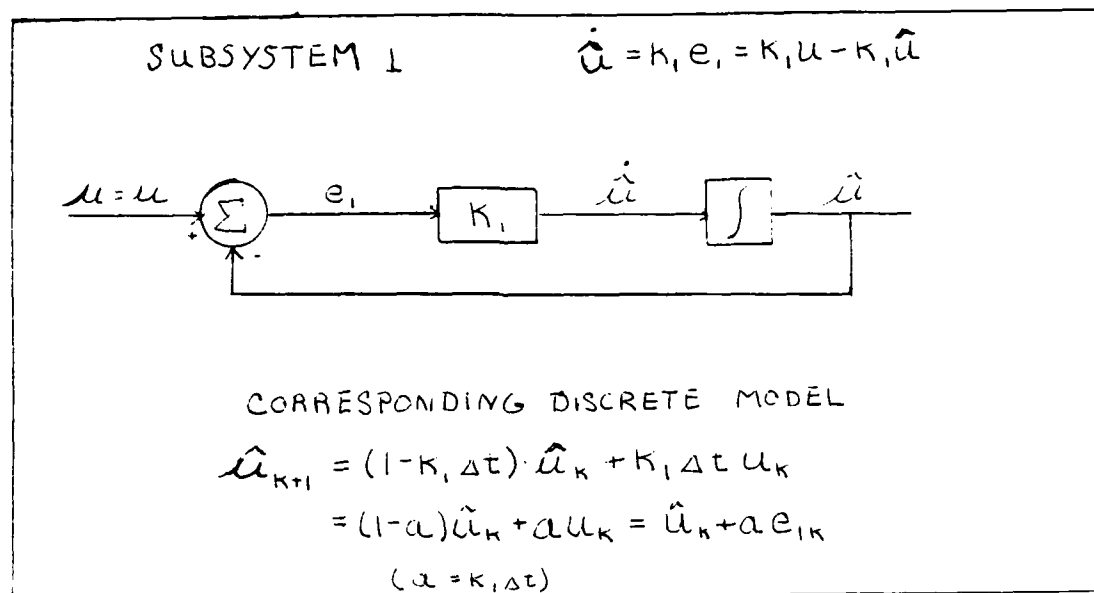


Figure 6.5 Subsystem 1

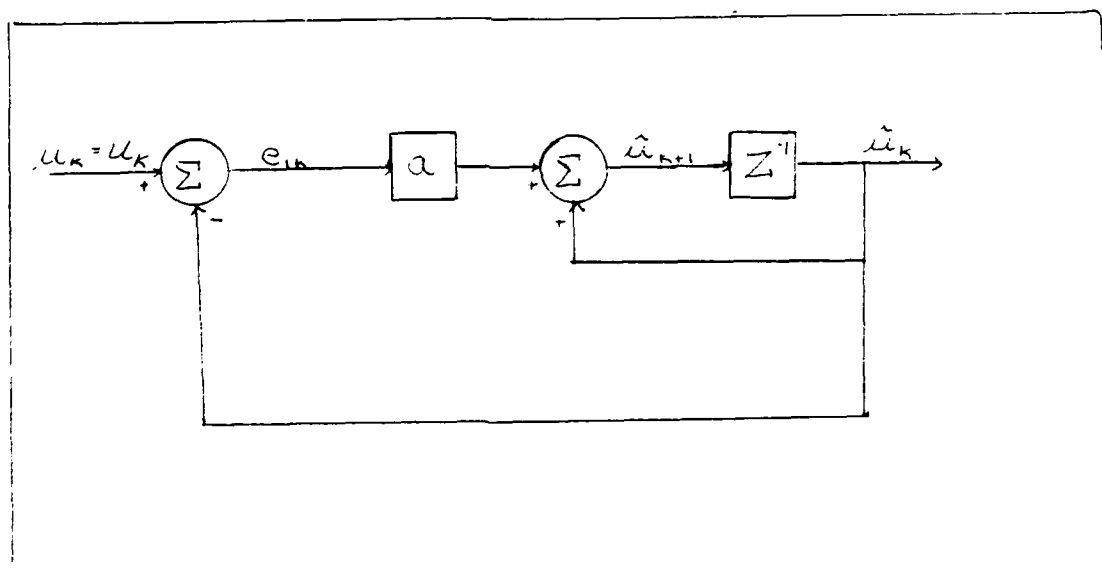


Figure 6.6 Discretized Block Diagram

$$\frac{\partial(e_z)}{\partial(V-\hat{V})} = \dot{\hat{X}} - \hat{\Phi}\hat{U} = J$$

Figure 6.7 illustrates the observer. This result is also in accordance with the method proposed in [Ref. 6].

Defining $\nu = (\dot{\hat{X}} - \hat{\Phi}\hat{U})V$ as a new measurement the corresponding function h is $h = (\dot{\hat{X}} - \hat{\Phi}\hat{U})V$. The Jacobian is $J = \partial h / \partial V = \dot{\hat{X}} - \hat{\Phi}\hat{U}$.

In order to simplify the stability analysis the Jacobian, J , is replaced with the signum function, $\text{signum}(J)$. This is sufficient to guarantee the negative feedback of subsystem 2. Subsystem 2 is analogous to subsystem 1 and will be stable if $0 < K_2 \Delta t < 2$. Consequently this system also performs as positioning servo-mechanism and will track relatively slow varying inputs $V(t)$ with very small error.

The presented analysis leads to a definition of the decoupled observer. This observer is depicted in Table 22. Appendix D contains the computer simulation results.

Figure 6.8 is essentially the same as Figure 6.4 with $J_{11} = 0$ and $J_{12} = \text{signum}(J_{12})$. Therefore it is possible to consider this algorithm a simplification of the algorithm developed in [Ref. 7]. However, it should be pointed out that the decoupled observer can be derived directly through analysis of the two linear subsystems presented above.

TABLE 22
DISCRETIZATION

$$e_1 = \mu - \hat{U} = -h_1(\hat{U}, \hat{V})$$

$$e_2 = -\hat{V}(\hat{X} - \hat{U}) = \mu - h_2(\hat{U}, \hat{V})$$

$$\dot{\hat{U}} = K_1 e_1$$

$$\dot{\hat{V}} = K_2 \text{Sygn}(J_{22}) e_2$$

After discretization this becomes

$$\hat{U}_{k+1} = \hat{U}_k + K_1 \Delta t e_{1,k}$$

$$\hat{V}_{k+1} = \hat{V}_k + K_2 \Delta t \text{sygn}(J_{22}) e_{2,k}$$

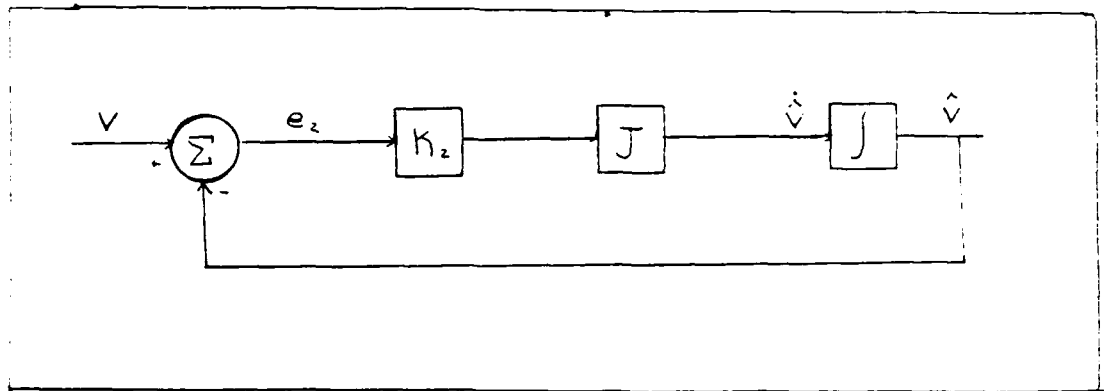


Figure 6.7 Subsystem 2

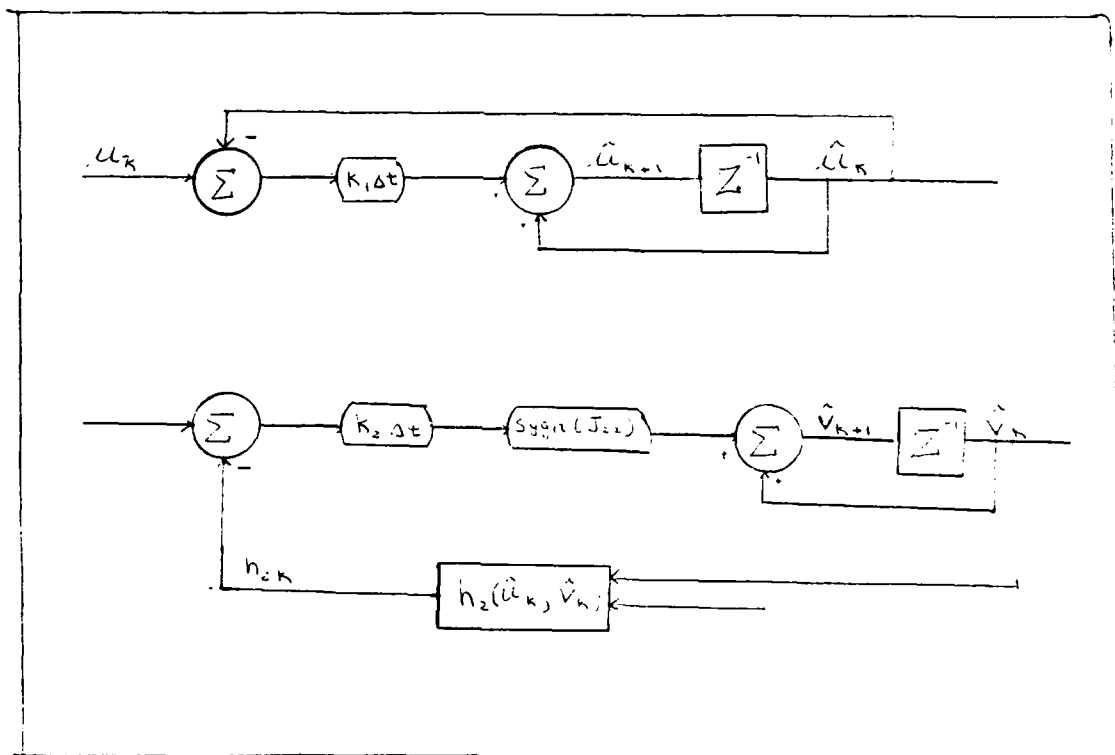


Figure 6.8 Decoupled Observer

In the decoupled model it is easier to control gains since the J_{12} element does not affect stability. It is noted that slightly more oscillatory behavior is present at the beginning of the simulation. This is not unusual for gradient type algorithms.

Satisfactory results for the product $K\Delta t = 0.1$ are expected if the observer is analyzed from the sampling theorem point of view. This presupposes that both continuous subsystems possess only one time constant $\tau = 1/K$. The sampling theorem requires that $t < \tau/2$ and $4tK < 0.5$.

Experience has shown that the best results for the one-step integration are obtained if the integration step (sampling time) is ten times less than the smaller time constant in the system. This means $4t = 0.1(1/K)$ and $4tK = 0.1$.

The sampling theorem is violated if $4tK=1$. As a consequence the observer requires much more time to extract sufficient information from the measurement and to start state tracking. The simulation results demonstrate that when the product $4tK$ equals unity convergence starts after fifty seconds. This is approximately ten times slower from previous experiments where the sampling theorem is satisfied.

In the case of $4tK = 0.01$ the system pole is very close to the unit circle. Therefore, convergence is relatively slow.

As demonstrated by the various computer generated graphs, the simulation results for this system are satisfactory. Therefore the selected coordinate system is proven acceptable.

VII. CONCLUSIONS AND RECOMMENDATIONS

The objective of this thesis is twofold. The first part of the thesis involves finding a suitable coordinate system in which to establish a satellite tracking model. The second part of the thesis uses this coordinate system to obtain an observability analysis and design an observer. This latter portion is the main thrust of the thesis.

The satellite model is based on the coordinate system developed in chapter three. The model is simplified yet not unrealistic. The main limiting assumption confines both the satellite and target to a constant speed and heading. An unchanging direction is important due to the desire to maintain a constant angle α . These restrictions imposed on the satellite are explained in detail in chapter three. Satellites and targets (aircraft) would normally travel a great circle path which requires a constant bearing. Therefore, the assumption is valid. This basic premise resulted in the spherical triangle that forms the basis of the system presented in Table 5. Once the basic model became established an observability analysis was accomplished in chapter four. The basic observability theories developed in [Ref. 6] (for mechanical springs) has been successfully applied to satellite observability. The system proved to be observable in the wide sense.

Further studies in the area of satellite tracking and observability are highly recommended. A more realistic satellite model could be devised in these studies. To improve the accuracy of the satellite motion equations the earth must no longer be assumed spherical and the satellite's orbit must no longer be confined to simple circular orbit. This leads to a different coordinate system by necessity. Relative coordinate systems should be explored in more detail. Appendix B discusses this briefly. A possible approach involves using the Euler equations of motion. A target position with respect to a satellite prime axis could be transformed via pitch, yaw and roll to a satellite normal axis. Enhanced satellite tracking studies should include a target that is not confined to a constant heading. The target should be allowed to alter course to further complicate the coordinate system and observer model. Both the satellite and target should be subject to random disturbances. This leads to the development of stochastic models. References 6 through 8 are highly recommended to anyone pursuing this course of research.

This thesis has successfully developed a model for satellite tracking. The system has been determined to be observable and an observer has been designed. The observer model has been successfully simulated.

APPENDIX A

ELEMENTS OF ORBIT

Satellites travel in elliptical orbits. Figure A.1 depicts a basic ellipse. The distances a , b and c are related by equation A.1.

$$c^2 = a^2 - b^2 \quad (A.1)$$

In this equation:

- a = semi-major axis
- b = semi-minor axis
- c = distance between foci

Eccentricity is also a parameter often used in connection with elliptical orbits. Eccentricity, e , is a measure of the elongation of the ellipse. Equations A.2 and A.3 relate eccentricity to previously defined parameters.

$$e^2 = 1 - (b/a) \quad (A.2)$$

$$c = ae \quad (A.3)$$

Other elements include apogee and perogee. Apogee is that point on the orbital ellipse where the satellite is furthest from the earth (focal point). The perigee is that point where the satellite passes closest to the earth. These new parameters are related to a and e by equations A.4 and A.5.

$$\text{apogee distance} = d_a = a(1+e) \quad (A.4)$$

$$\text{perogee distance} = d_p = a(1-e) \quad (A.5)$$

Any two of the above six parameters can define an ellipse. For the special case of a circle; $e = 0$, $d = d$, $c = 0$ and $a = b$.

To describe satellite motion more information is needed. The inclination angle, i° , is the angle of intersection between the orbital plane and the earth's equatorial plane. Figure A.2 illustrates. Information on the period of revolution of the satellite is needed as well as knowledge of the precise time that the satellite passes it's apogee or perogee.

Some references use information on the ascending node to determine satellite paths and positions. Figures A.3 and A.4 illustrate the relationships. [Ref. 5] uses the parameters in table A.1 as the necessary elements of orbit.

TABLE A.1

T - period (in minutes)	w - argument of perogee
i - angle of inclination	e - eccentricity
λ - SSP longitude at perogee	t - time at perogee

The elements listed in table A.1 completely describe the theory of satellite motion. Perturbations are ignored. In practice the motion of a satellite is very nearly described by these elements of orbit.

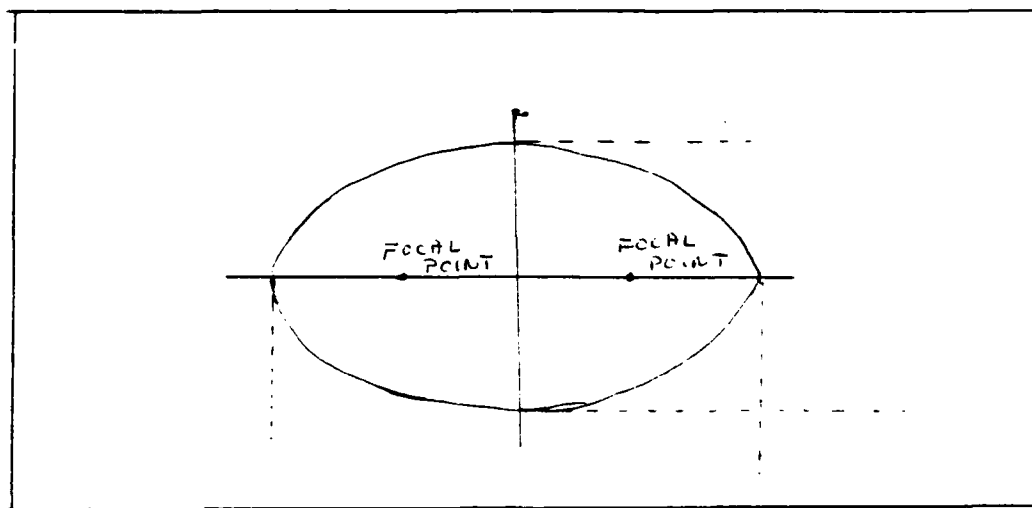


Figure A.1 Basic Ellipse

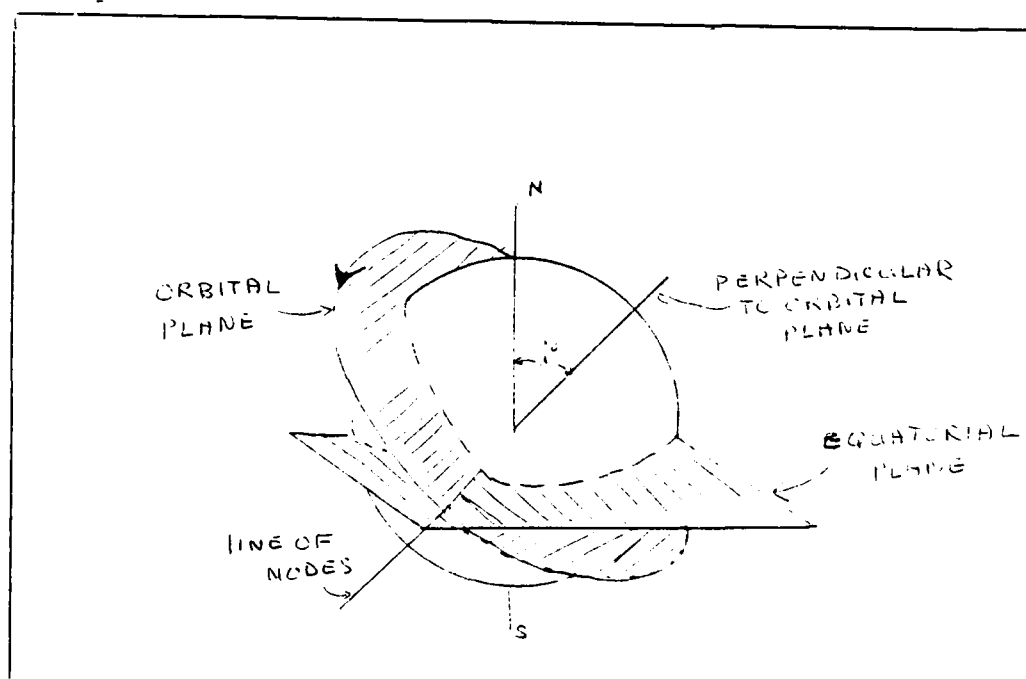


Figure A.2 Orbital Plane

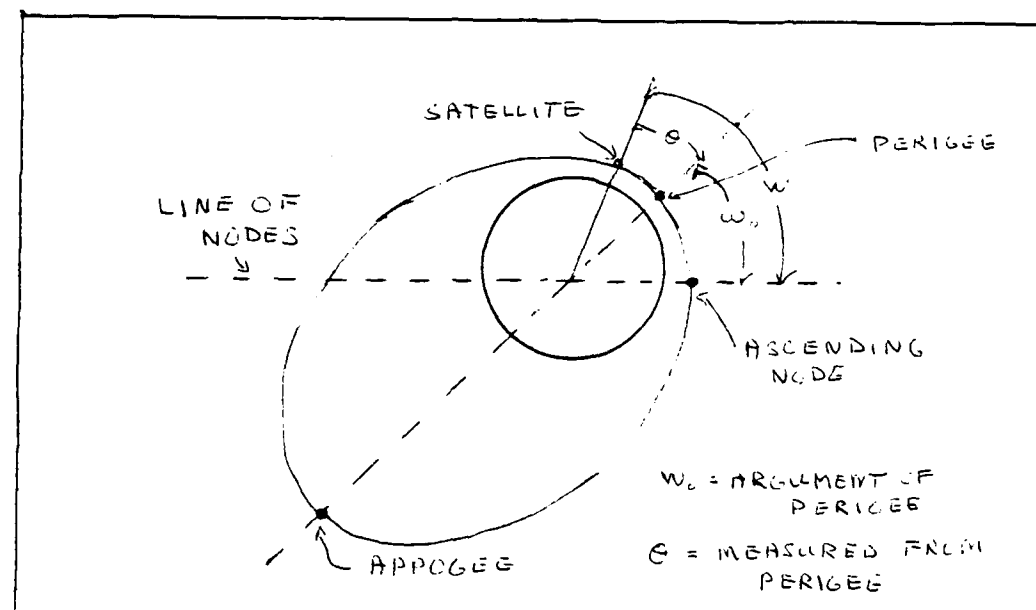


Figure A.3 Elliptical Orbit Diagram

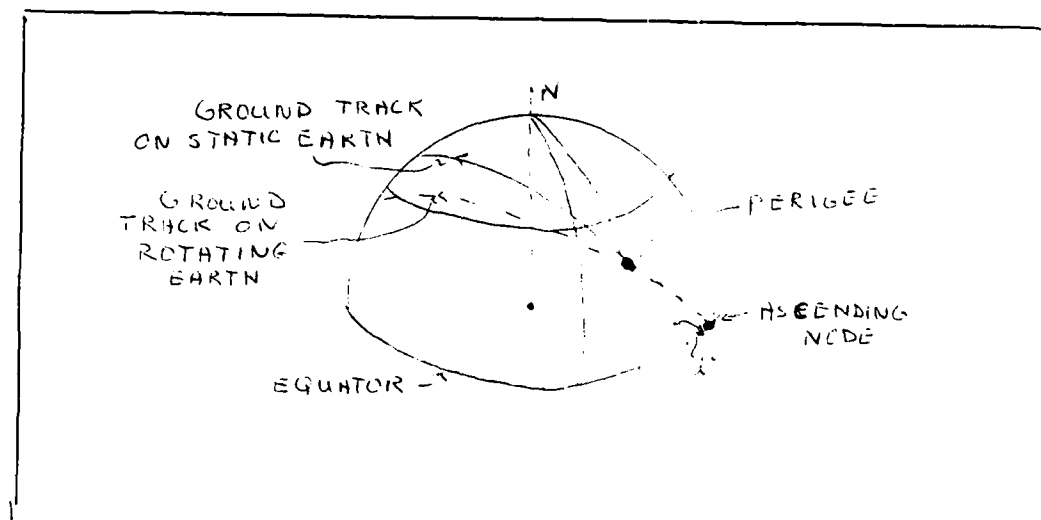


Figure A.4 Ground Tracks and Ascending Node

APPENDIX B

RELATIVE MOTION

The general theory of relative motion is developed using simple frames of reference. An object in frame A moves with respect to that frame. Frame A moves with respect to the fixed frame B. These frames are considered to be coordinate systems or sets of reference axes. Figure B.1 depicts an object in the prime system. The X-Y axes represent the fixed system. In figure B.2 the prime system moves with respect to the fixed system a distance d . The object in the prime system moves a distance d' within its system. Therefore the object moves a distance $d_{TOTAL} = d + d'$ with a velocity $V_{TOTAL} = V + V'$.

Further studies concerned with satellite tracking should involve relative motion. The fixed coordinate system is a three dimensional system with its origin at the center of the earth. The center of mass of the satellite is the origin for the relative or prime coordinate system. The prime system orbits the fixed system.

The target is detected by the satellite and its motion is therefore measured with respect to the satellite's prime coordinate system. These relative coordinates can be

related to the fixed coordinate system by a suitable matrix transformation.

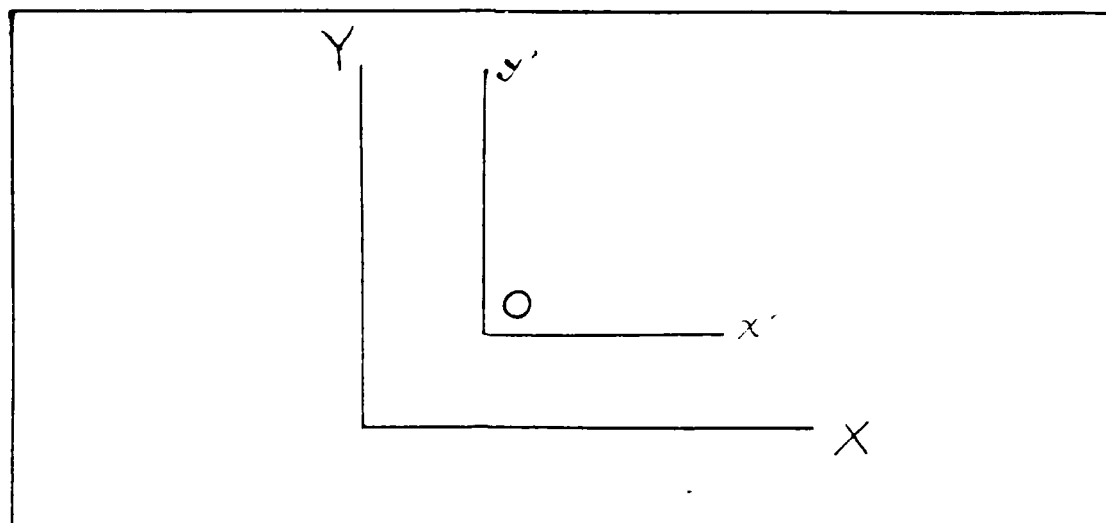


Figure B.1 Two Frames of Reference

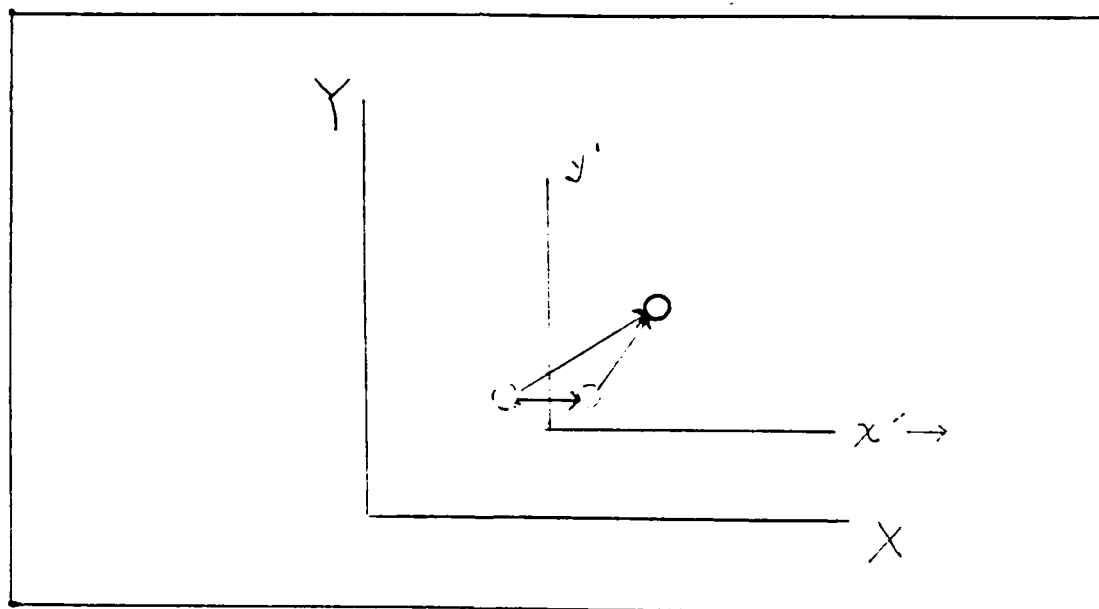


Figure B.2 Relative Motion

APPENDIX C

ORIGINAL MODEL SIMULATION RESULTS

This appendix contains the simulation for the original model. These graphs depict the states X and \tilde{X} . Figure 6.4 presents the block diagram of the model simulated. The simulations are run for 10 seconds and 500 seconds. This insures that a variety of suitable graphs are available for analysis. In order to accompany test observer behavior several different gains and time increments are used in the simulations. Specific combinations of gain and time increment produce excellent results (as explained in chapter 6).

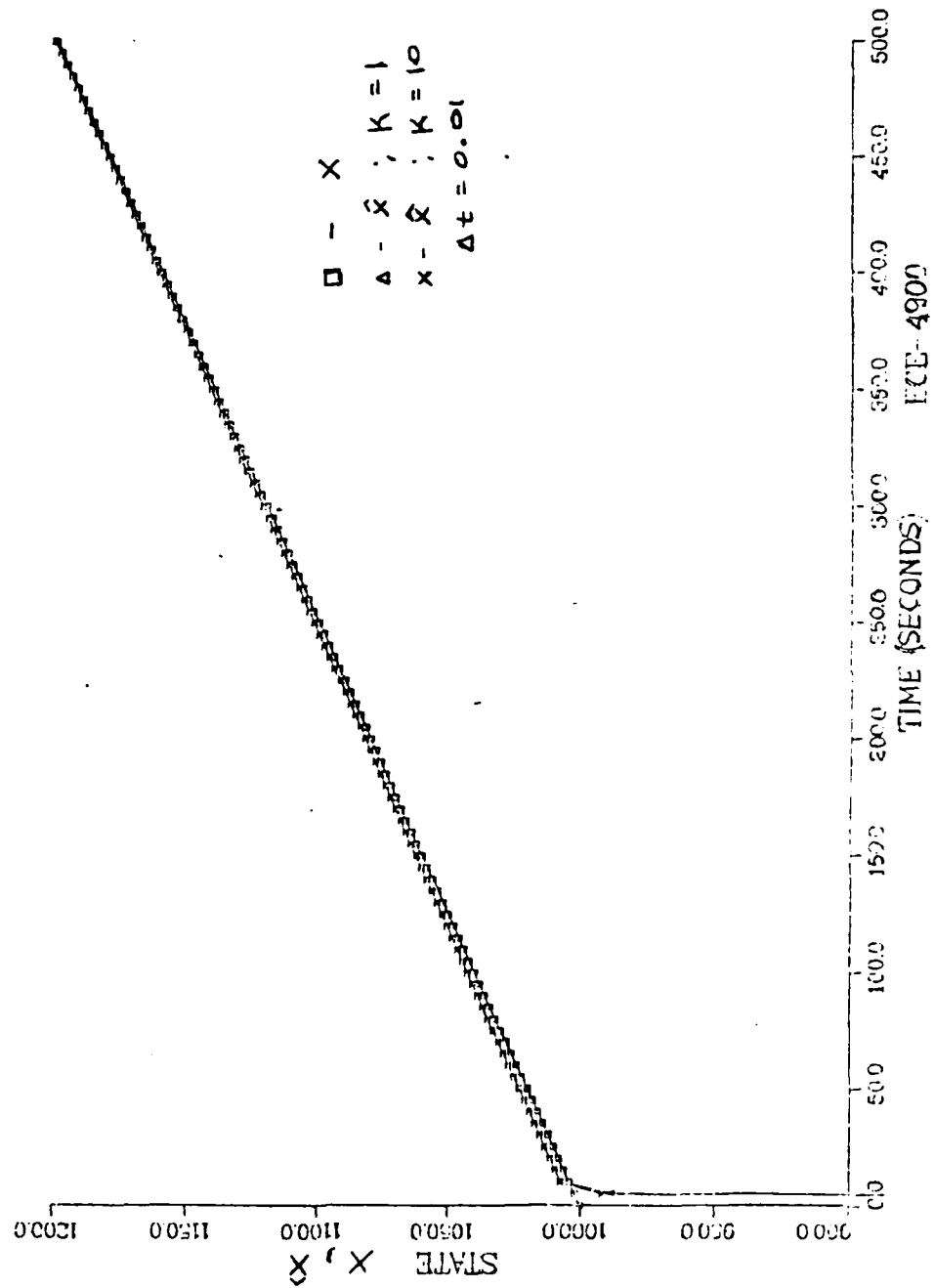
The observer model's ability to track a constant is recorded on eight graphs. The first two graphs (pages 112-113) depict state X for constant angular velocities and different gain values. The next two graphs (pages 114-115) depict state \tilde{X} for the same gains mentioned above. A gain (k) of ten is clearly beneficial for both X and \tilde{X} , since then $\Delta tk = 0.1$.

The following two graphs (pages 116-117) show two different time increments for state X , constant gain and constant angular velocities. The graphs on pages 118 and 119 display the same two time increments for state \tilde{X} . As

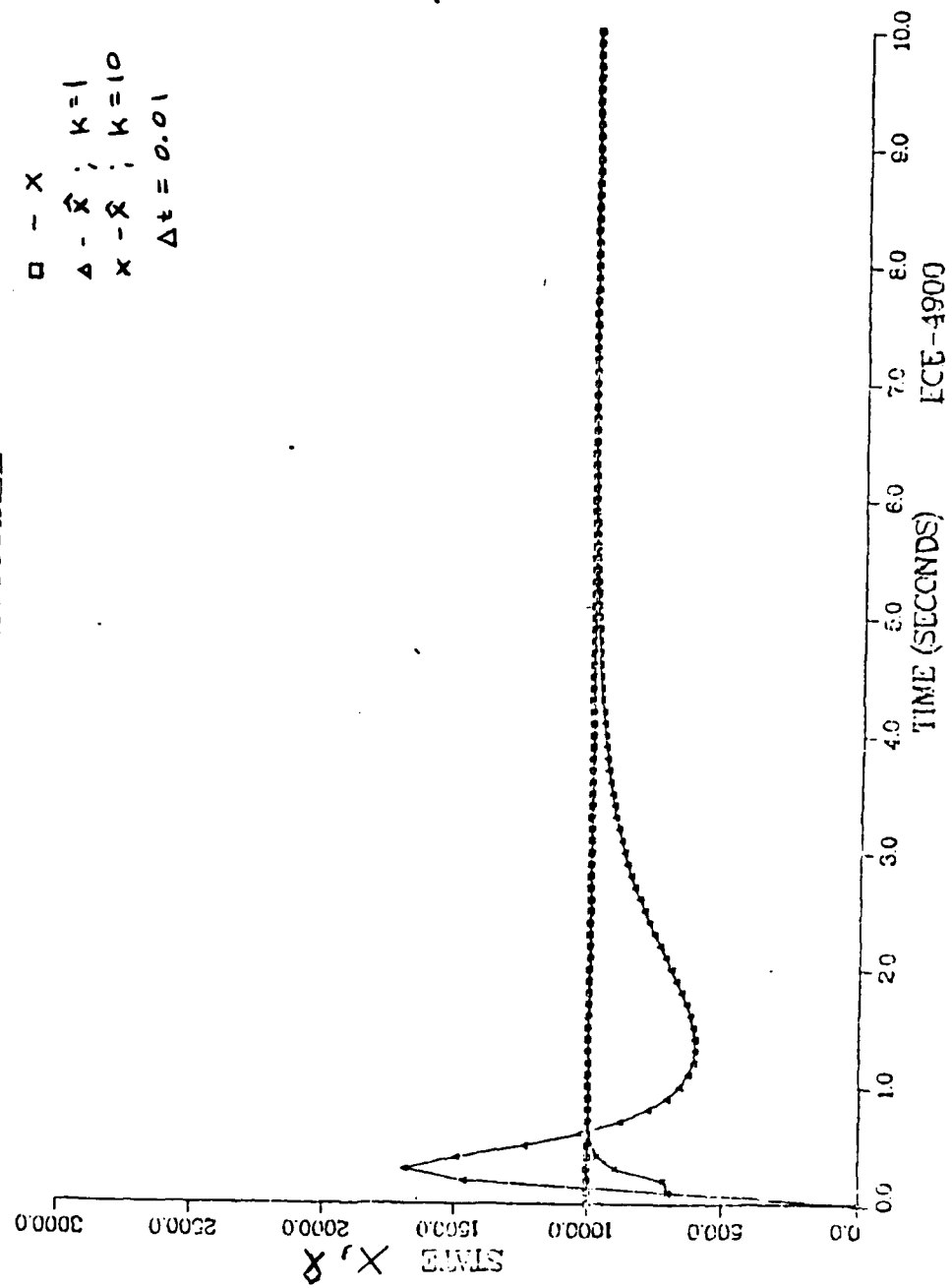
expected the smaller of the two time increments (0.01 seconds) gives a slightly better performance.

The last six graphs exhibit the model's time response to sinusoidal angular velocities. These are the results of the test used to determine the model's ability to track time varying functions. The first three of these graphs (pages 120-122) illustrate a target angular velocity of $.001 \cdot \cos(Dt)$ and a satellite angular velocity of $.0009 \cdot \cos(Dt)$. The variable D is varied in order to test observer response to different rates of change in angular velocities. The final graphs (pages 123-125) depict X and \dot{X} with a target angular velocity of $.005 \cdot \cos(Dt)$ and a satellite angular velocity of $.00045 \cdot \cos(Dt)$. The variable D is 0.01 in this simulation. This results in sinusoids of smaller amplitudes and longer periods. The results of tracking the sine wave are very satisfactory. It is noted that the relative error for both states is very small.

ORIGINAL MODEL

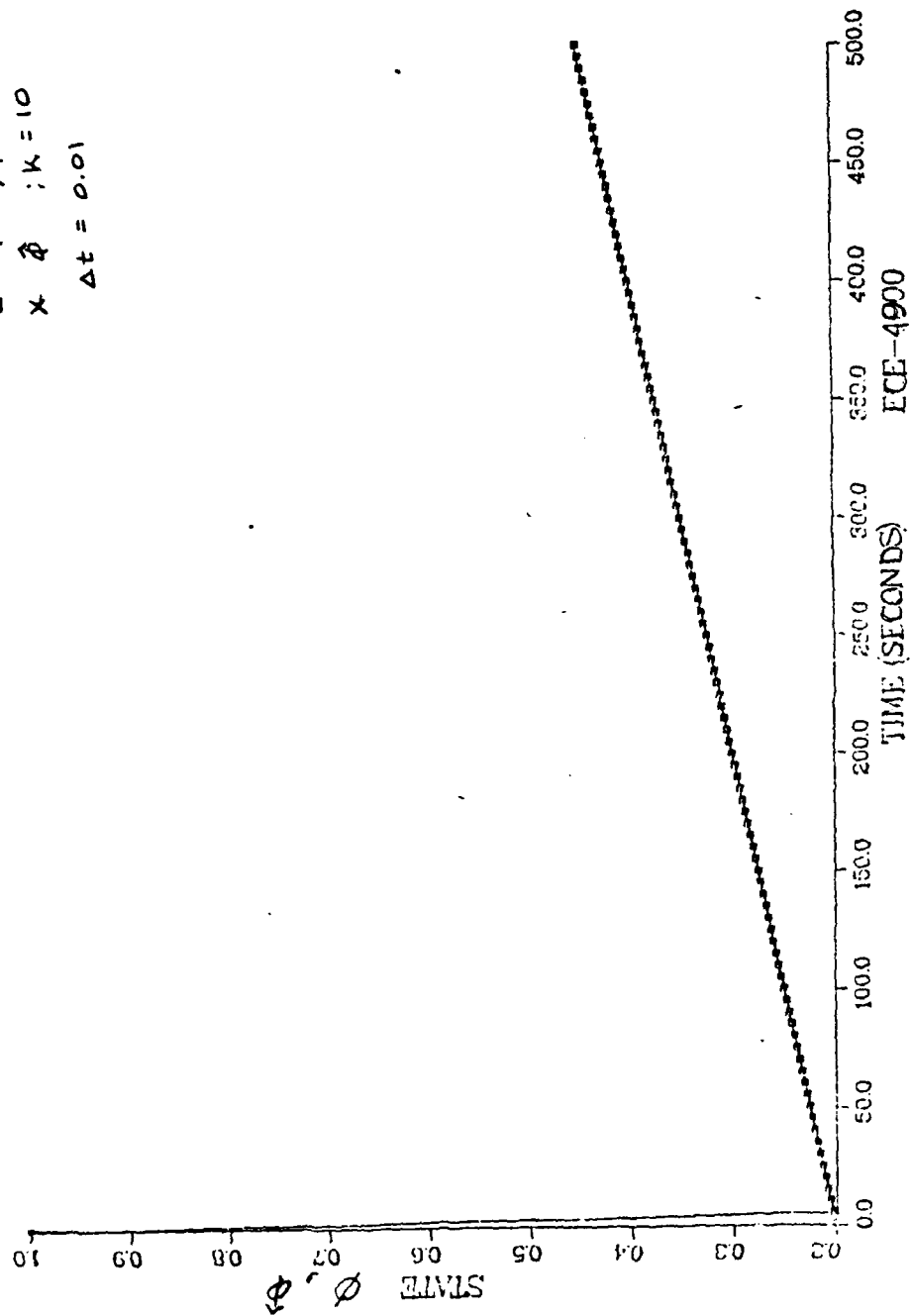


ORIGINAL MODEL



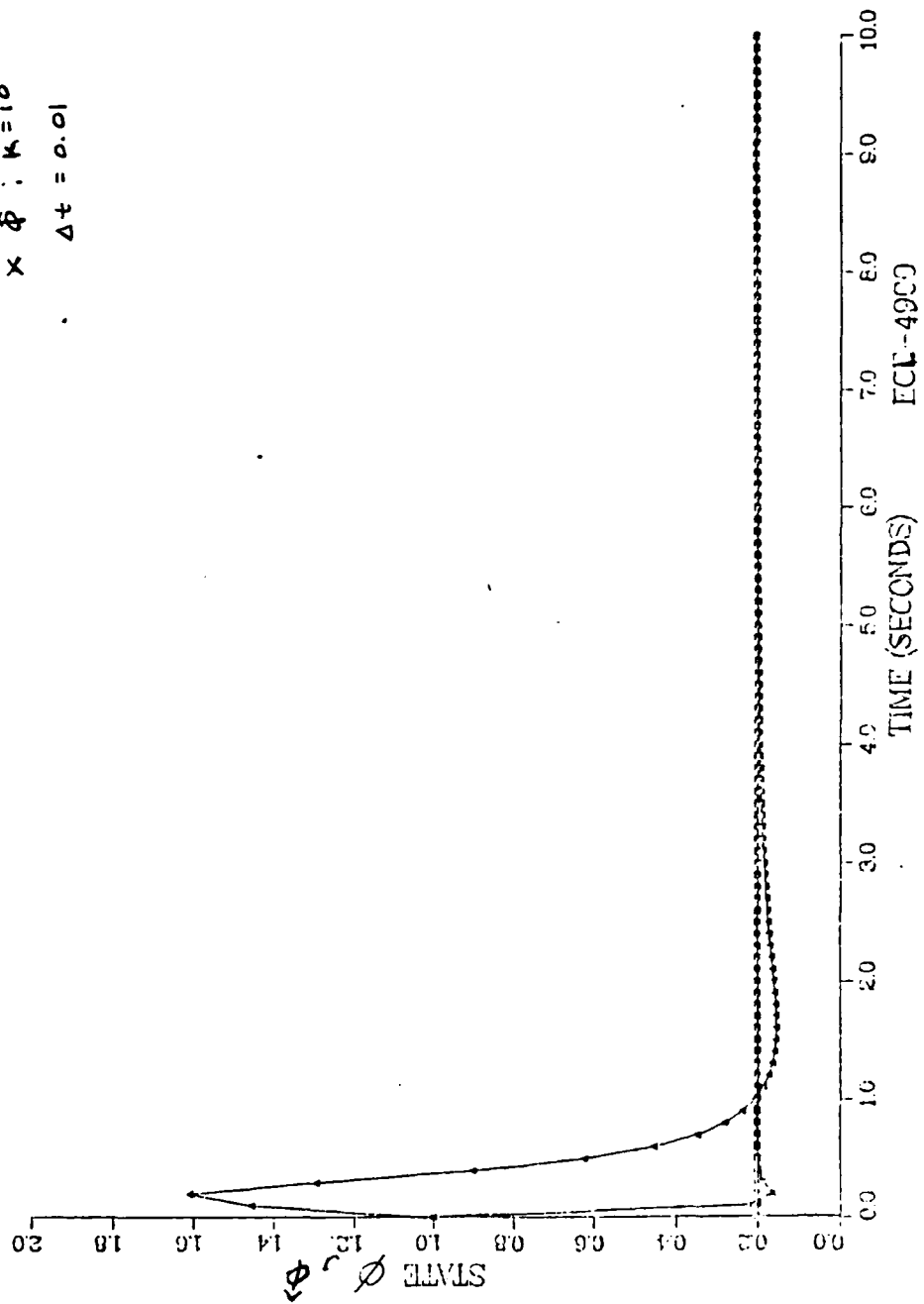
ORIGINAL MODEL

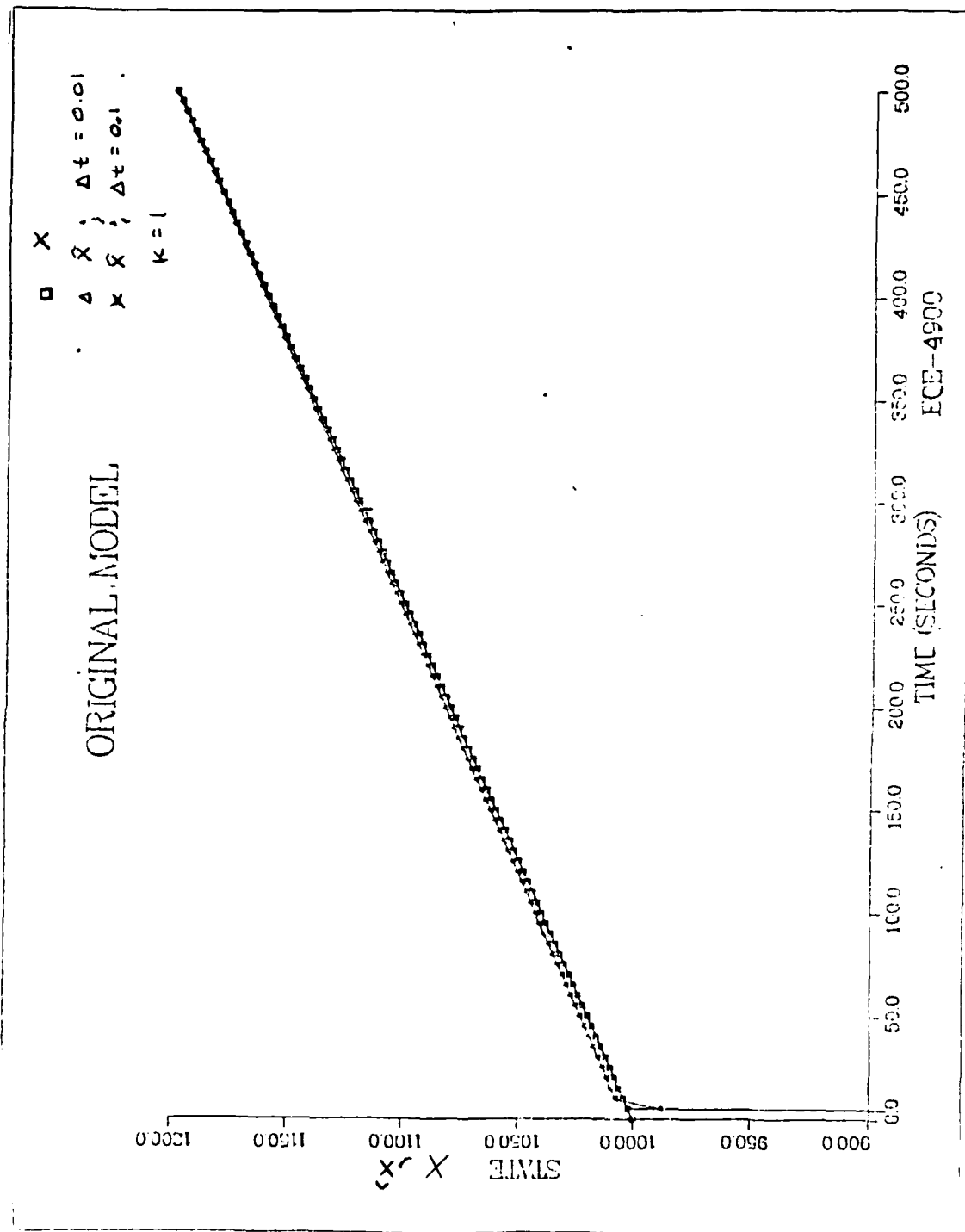
ϕ
 $\hat{\phi}$; $K=1$
 \times $\hat{\phi}$; $K=10$
 $\Delta t = 0.01$



ORIGINAL MODEL

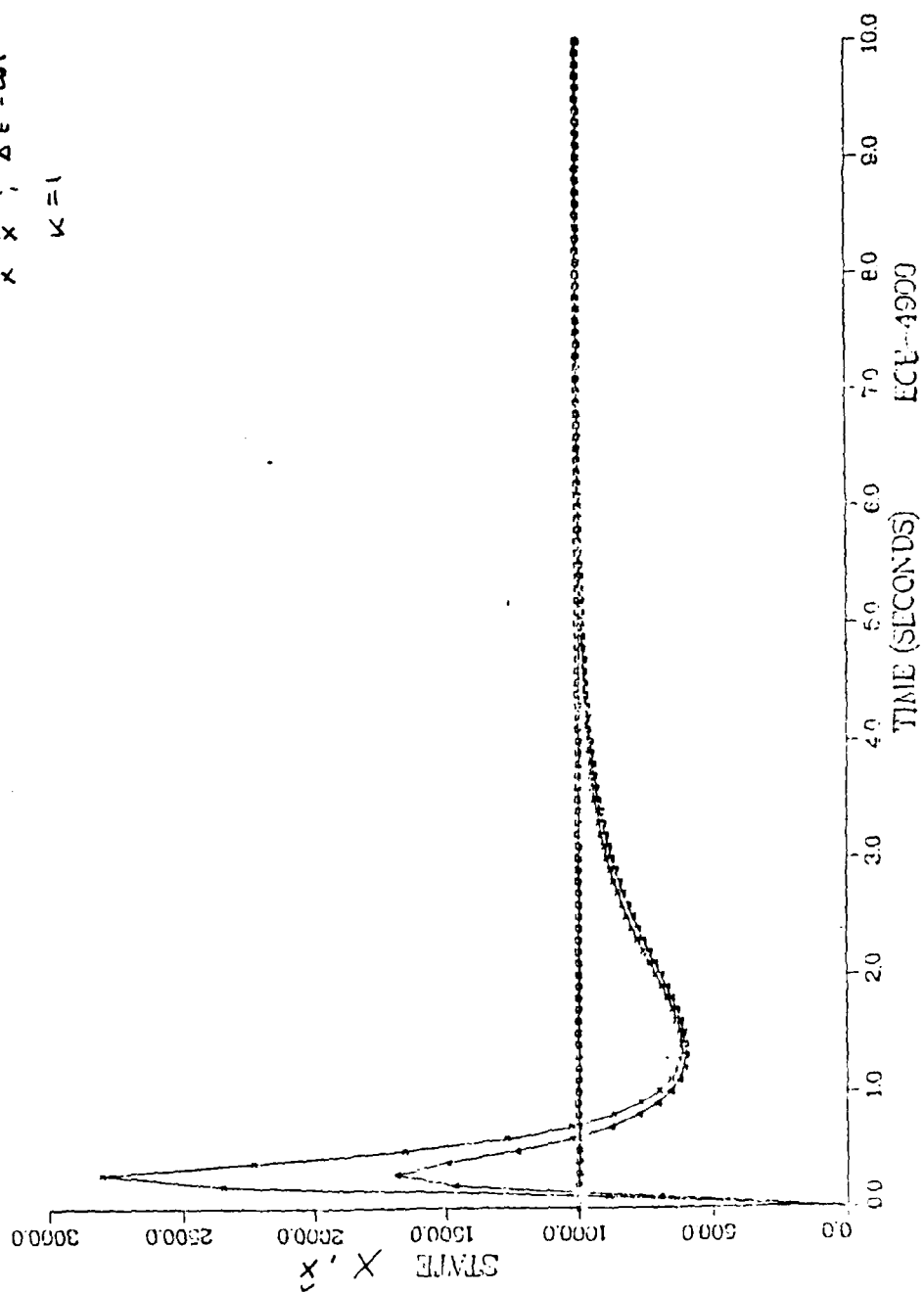
$\square \phi$
 $\Delta \hat{\phi} ; k=1$
 $\times \hat{\phi} ; k=10$
 $\Delta t = 0.01$

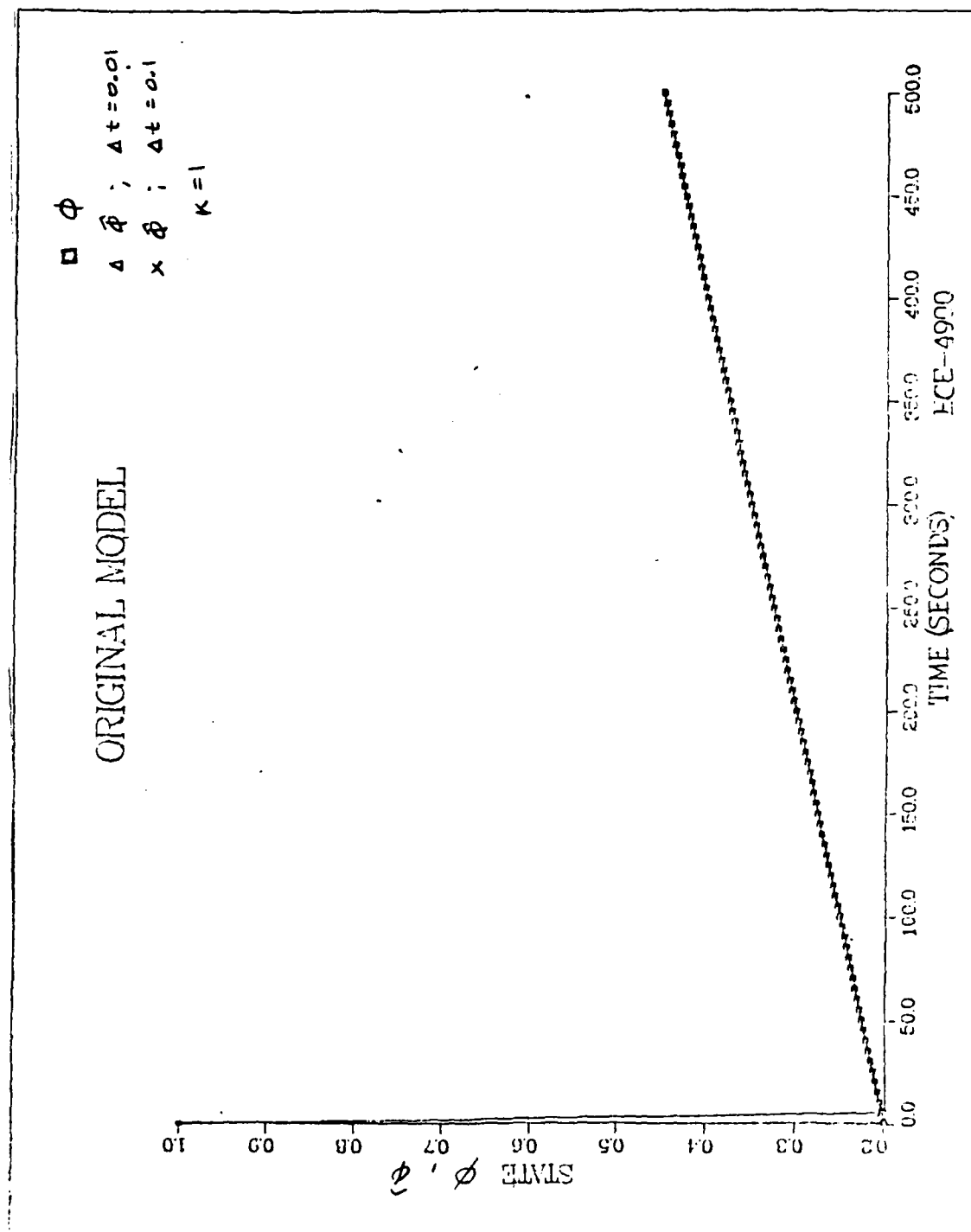




ORIGINAL MODEL

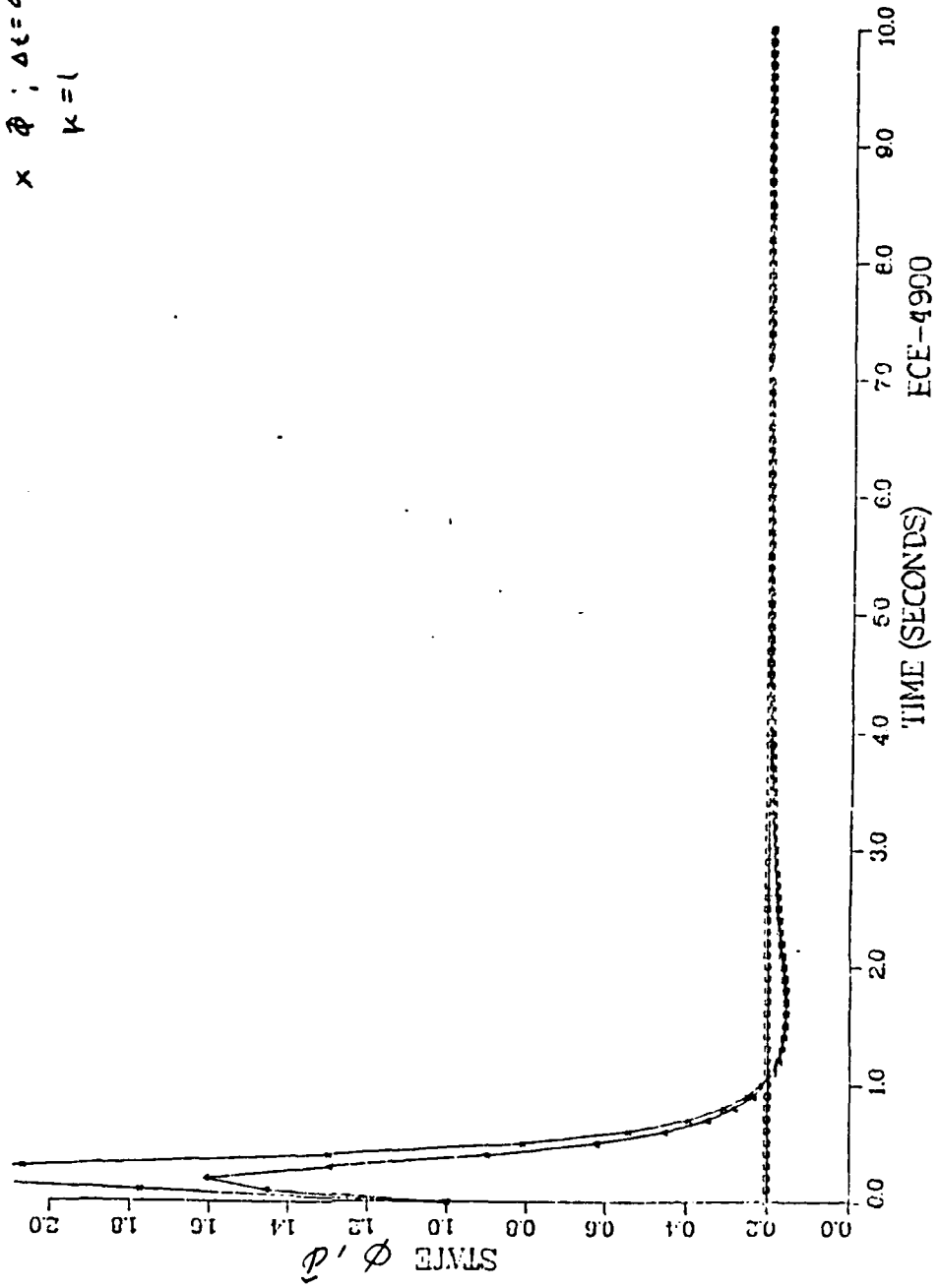
\square X
 Δ \hat{X} ; $\Delta t = 0.01$
 \times \hat{X} ; $\Delta t = 0.1$
 $K = 1$



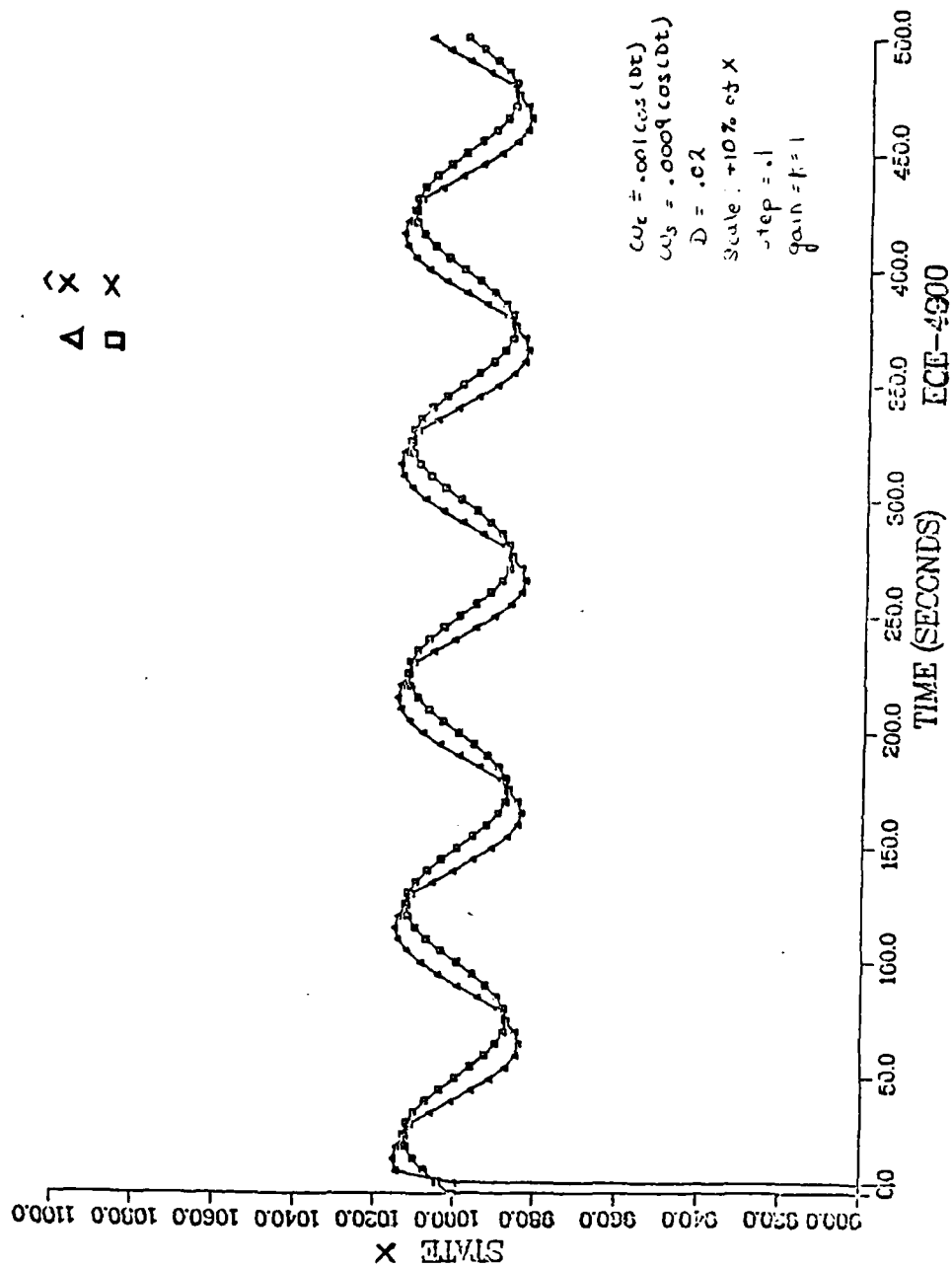


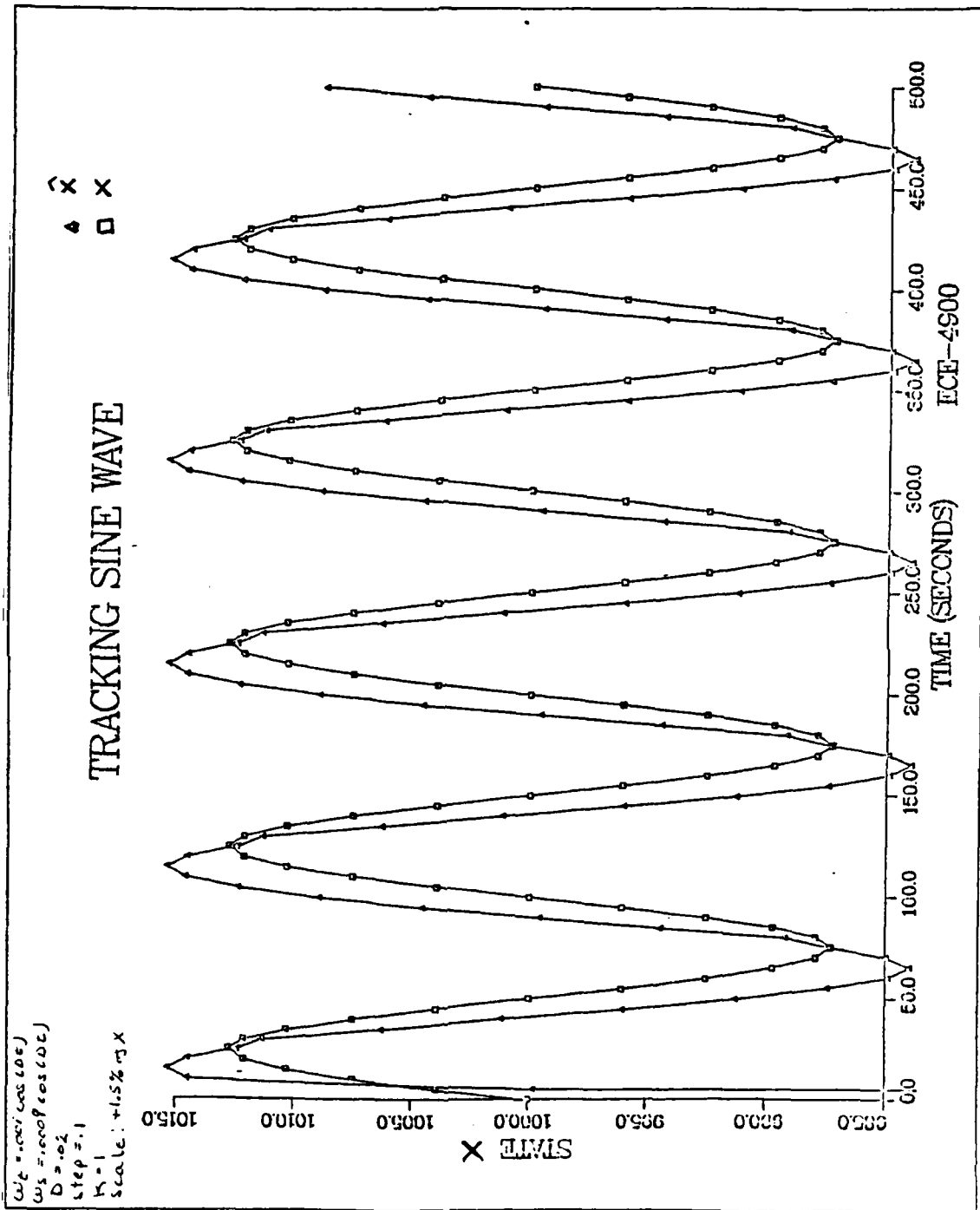
ORIGINAL MODEL

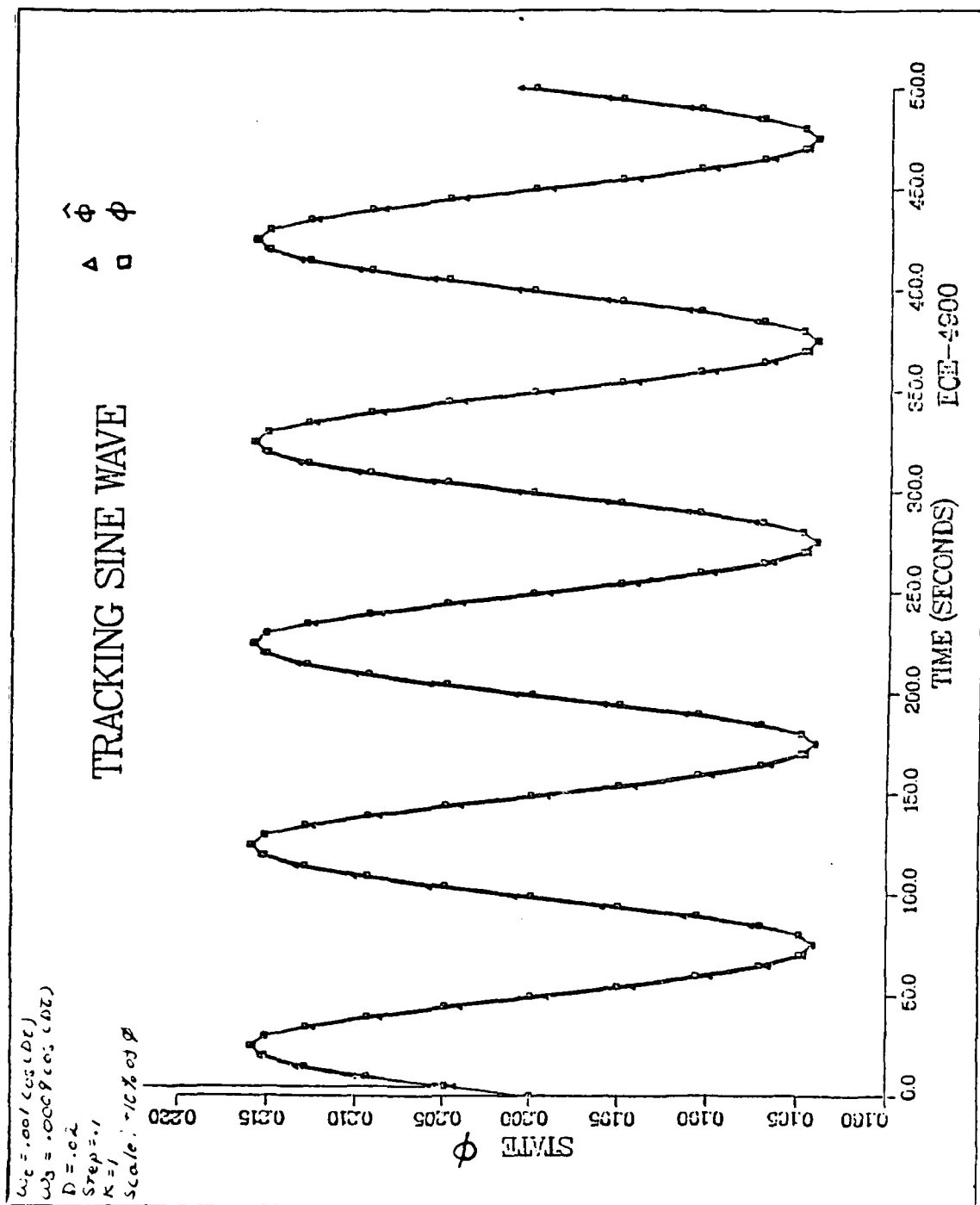
$\square \phi$
 $\Delta \phi ; \Delta t = 0.01$
 $\times \phi ; \Delta t = 0.1$
 $\kappa = 1$



TRACKING SINE WAVE

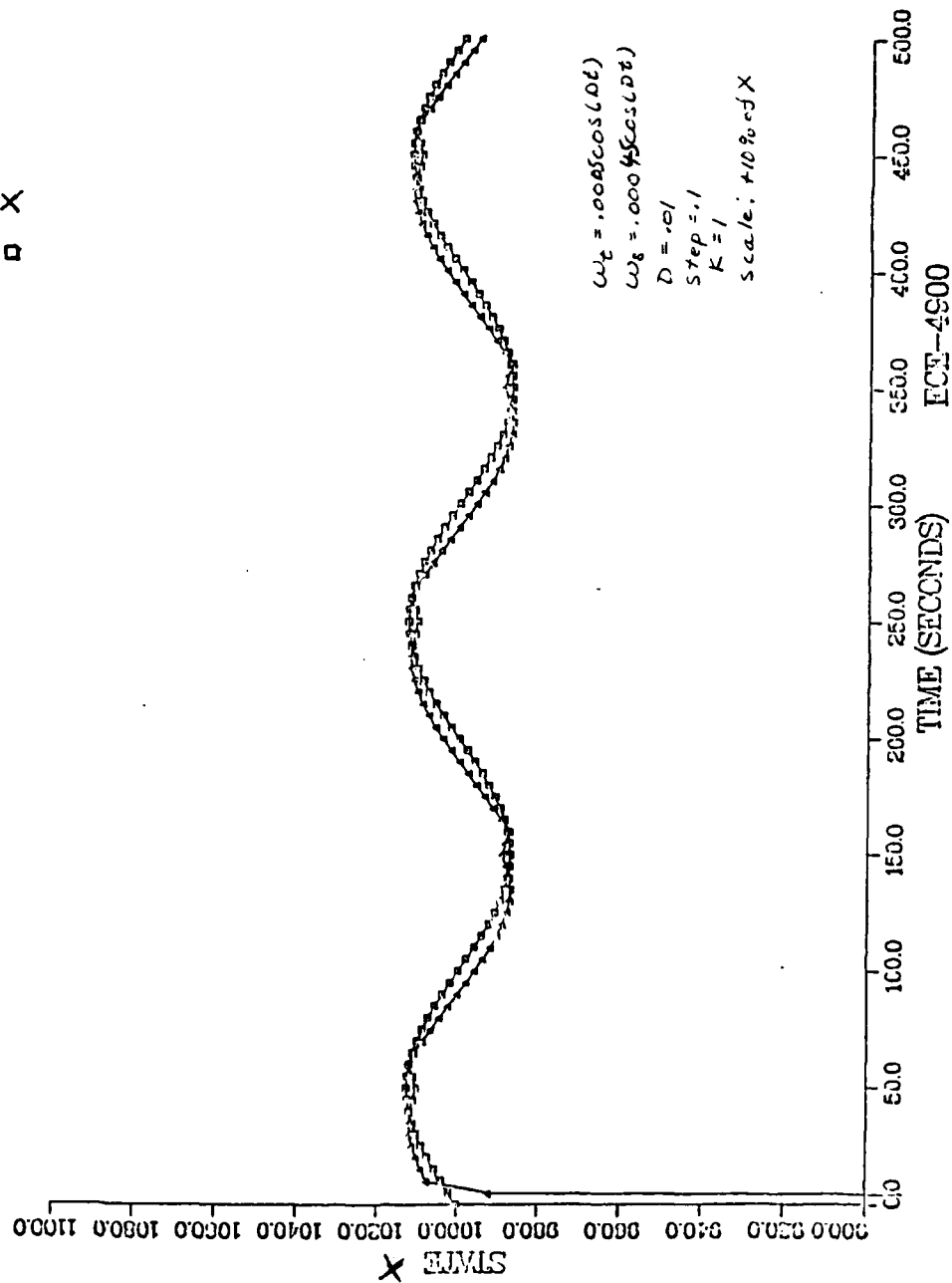






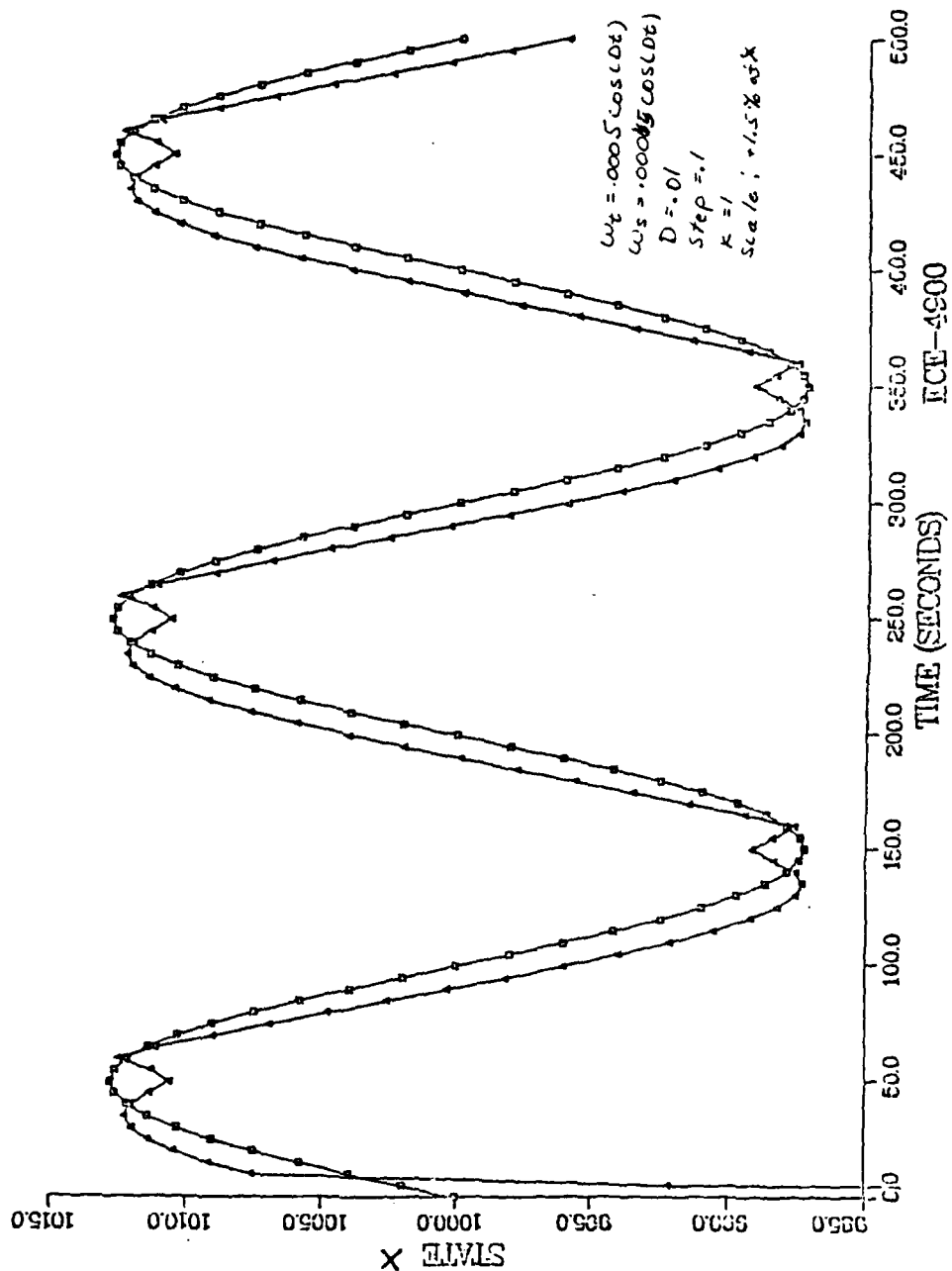
TRACKING SINE WAVE

△ \hat{x}
□ x



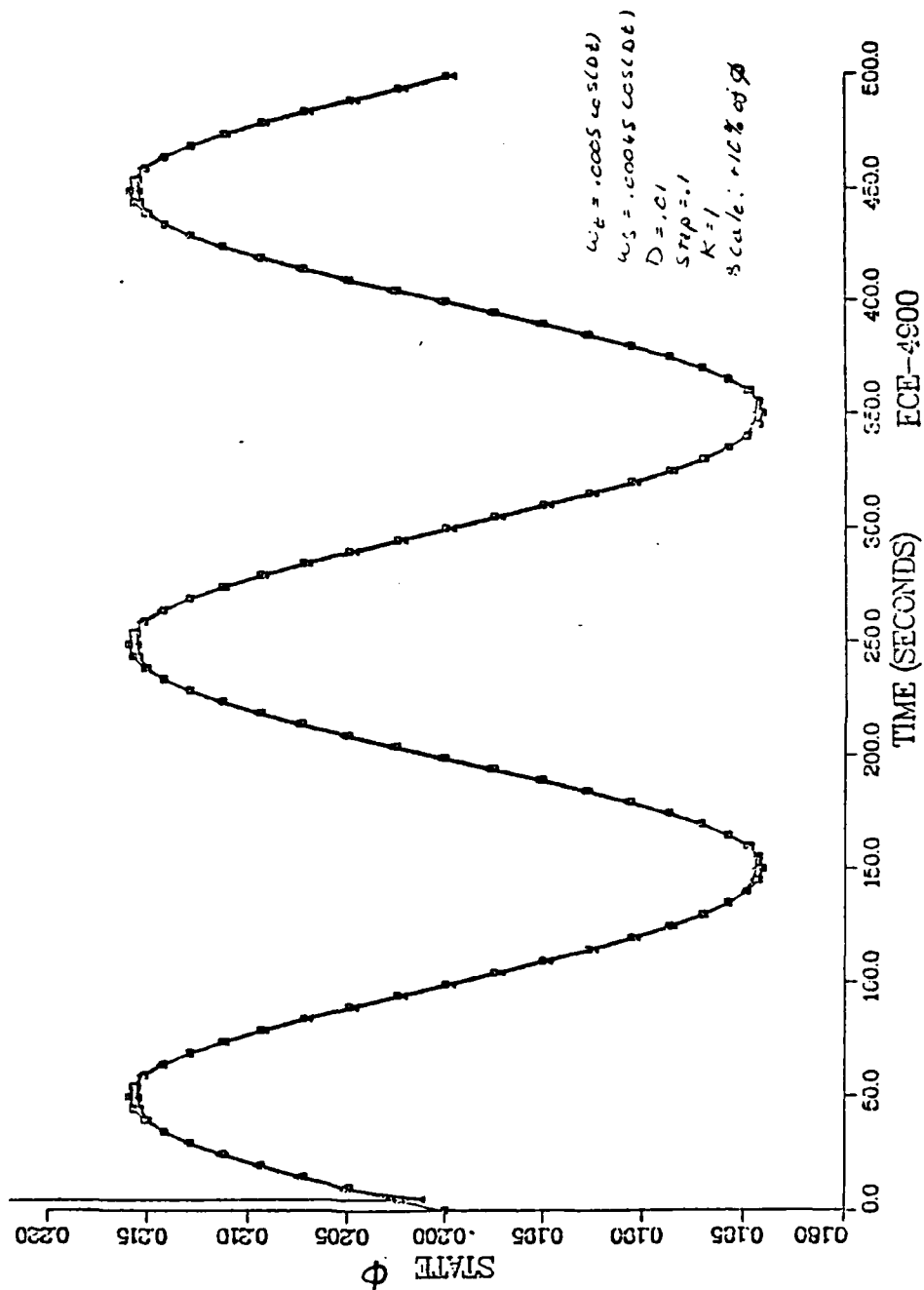
TRACKING SINE WAVE

\hat{x}
 Δ \square x



TRACKING SINE WAVE

$\hat{\phi}$
 ϕ



APPENDIX D

DECOUPLED MODEL SIMULATION RESULTS

These twenty graphs resulted from the decoupled model simulations (as described in chapter 6). Figure 6.3 presents a block diagram of the decoupled model. The first five graphs (pages 128-132) illustrate the time response for state X . The time increment, t , is held constant at 0.01 seconds. Several different gains were used on each graph. The state X was followed closely by \hat{X} . Different scales and simulation times are plotted to produce a variety of suitable graphs. A gain of ten consistently produces very good results in all five graphs.

The next group of five computer graphs (pages 133-137) exhibit state \dot{X} . As above, the time increment, t , is kept at 0.01 while the gain (k) is varied. The time response for the lower gains in particular are very satisfactory. The state \dot{X} is closely approximated by $\hat{\dot{X}}$.

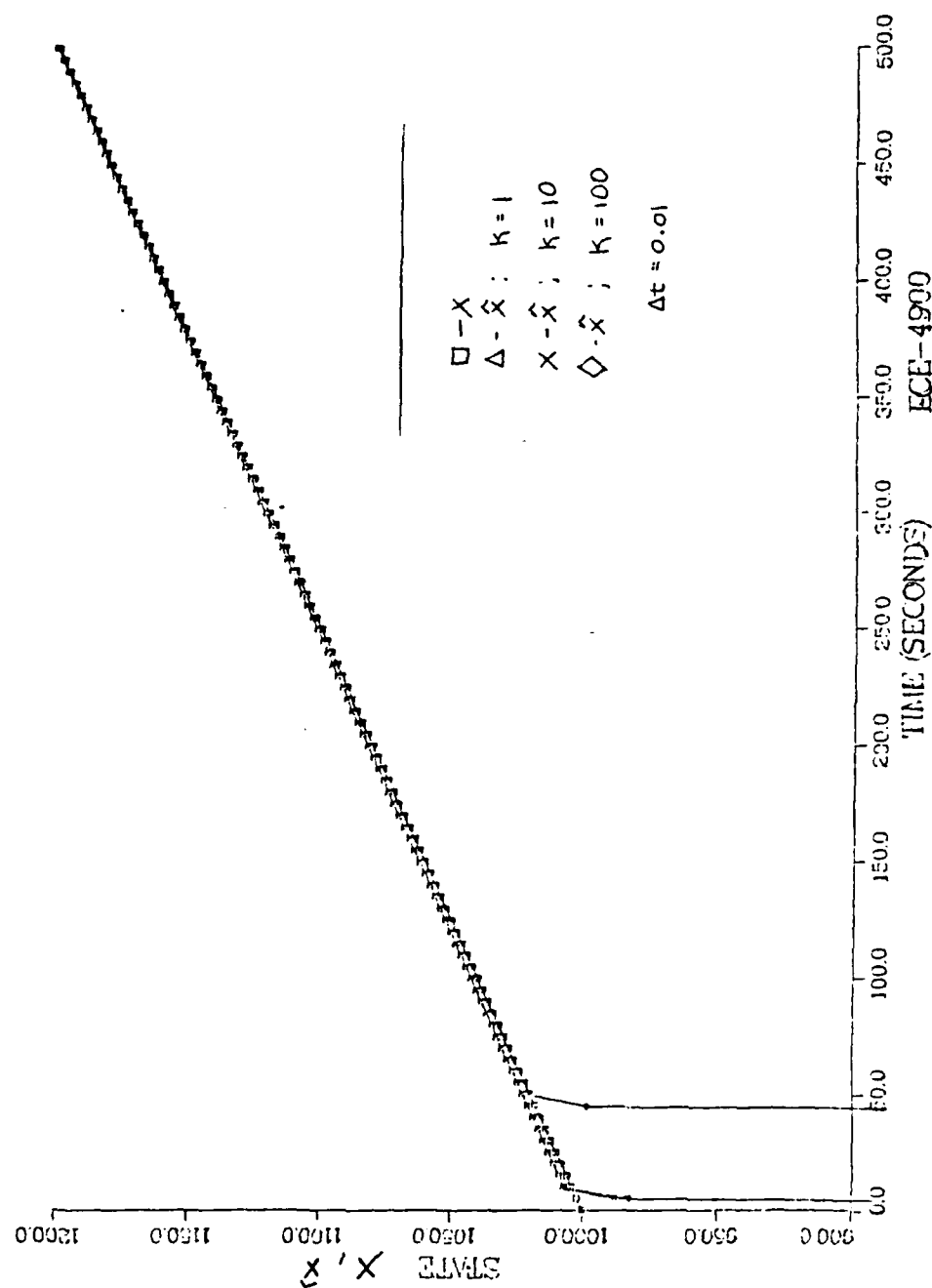
The third set of five graphs (pages 138-142) represent state X . This group of computer graphs holds the gain constant at one and allows the time increment to vary. As expected, smaller time increments (0.1 and 0.01) result in superior tracking capabilities.

The last set of five graphs (pages 143-147) show \dot{X} and \ddot{X} . The gain is kept at a constant value equal to one and

the time increment is varied. As before, the smaller time increments produce the best results.

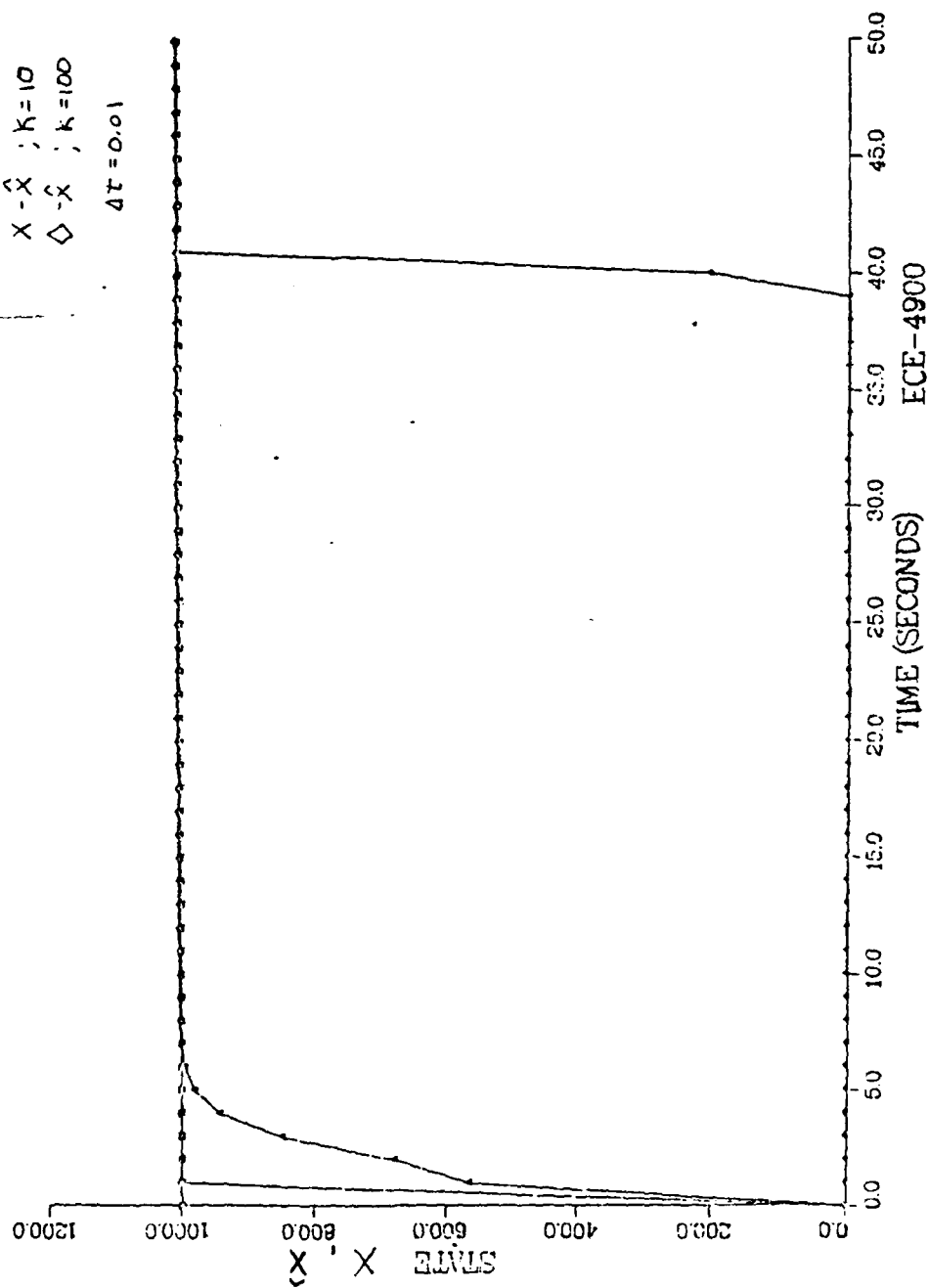
In all of the above examples, the approximated state (\hat{X} or $\hat{\Xi}$) closely tracks the actual state (X or Ξ). These simulation results are quite satisfactory.

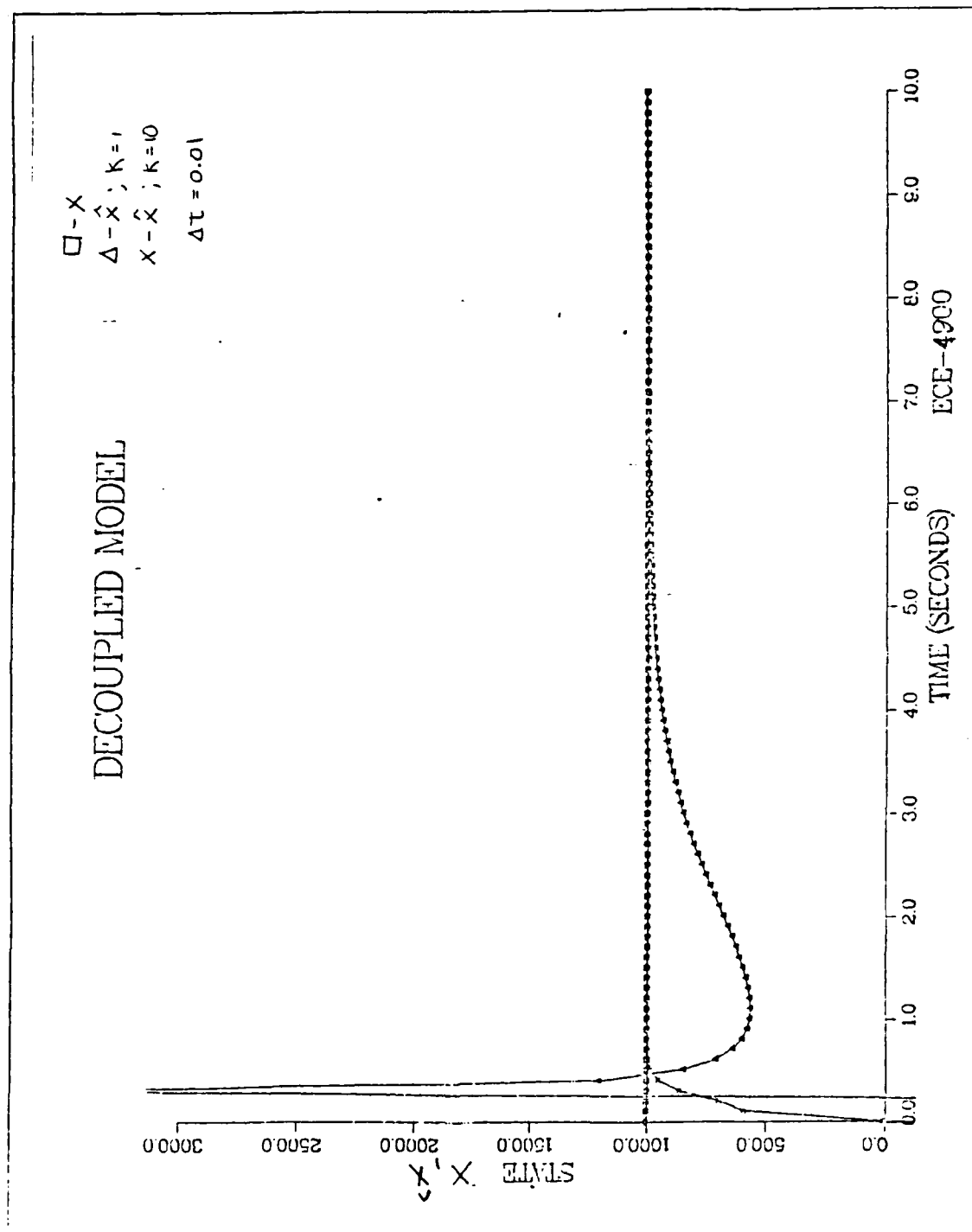
DECOUPLED MODEL



DECOUPLED MODEL

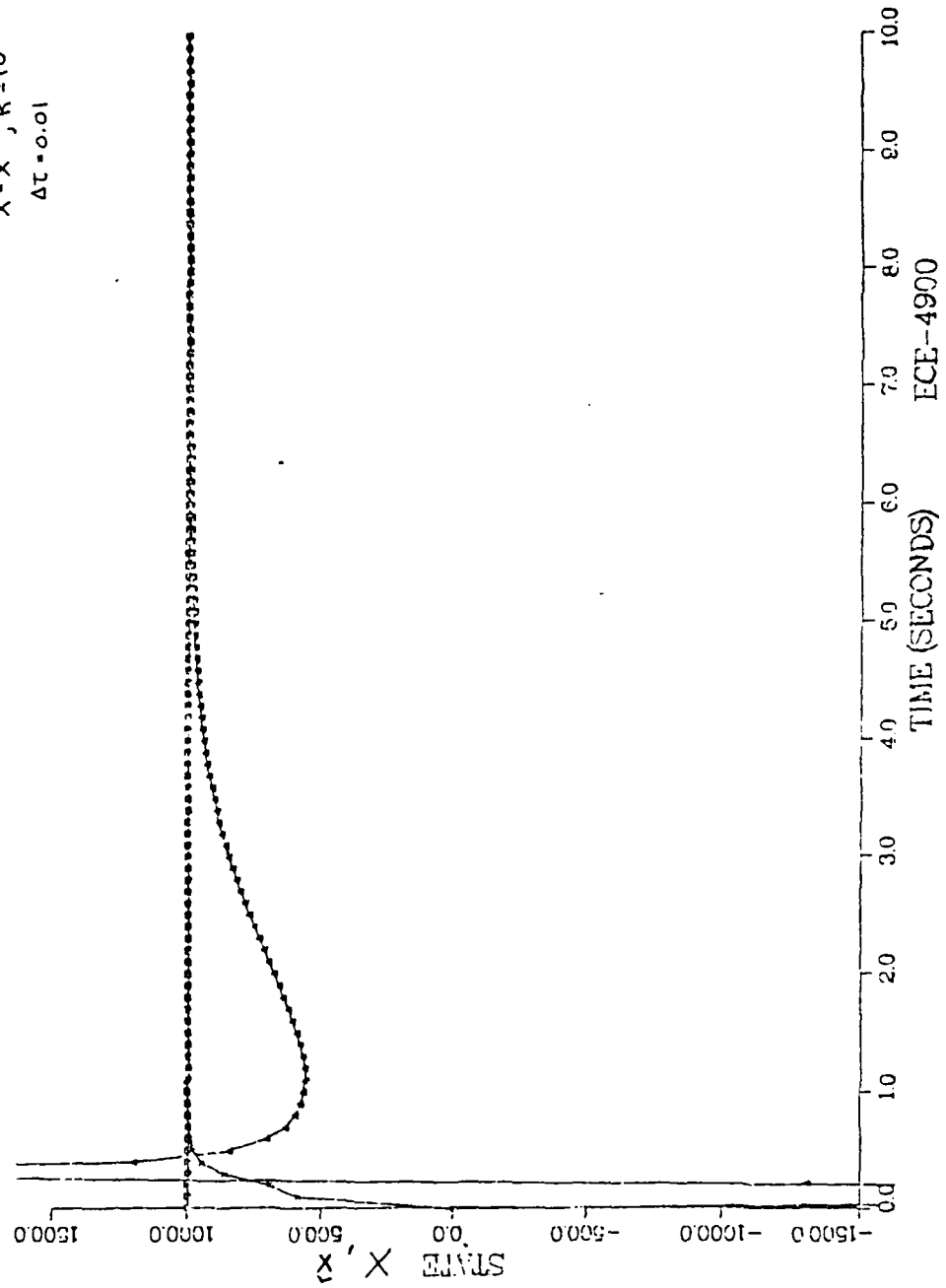
$\square - \hat{X}$; $k=1$
 $\Delta - \hat{X}$; $k=10$
 $\times - \hat{X}$; $k=100$
 $\diamond - \hat{X}$; $k=1000$
 $\Delta \tau = 0.01$





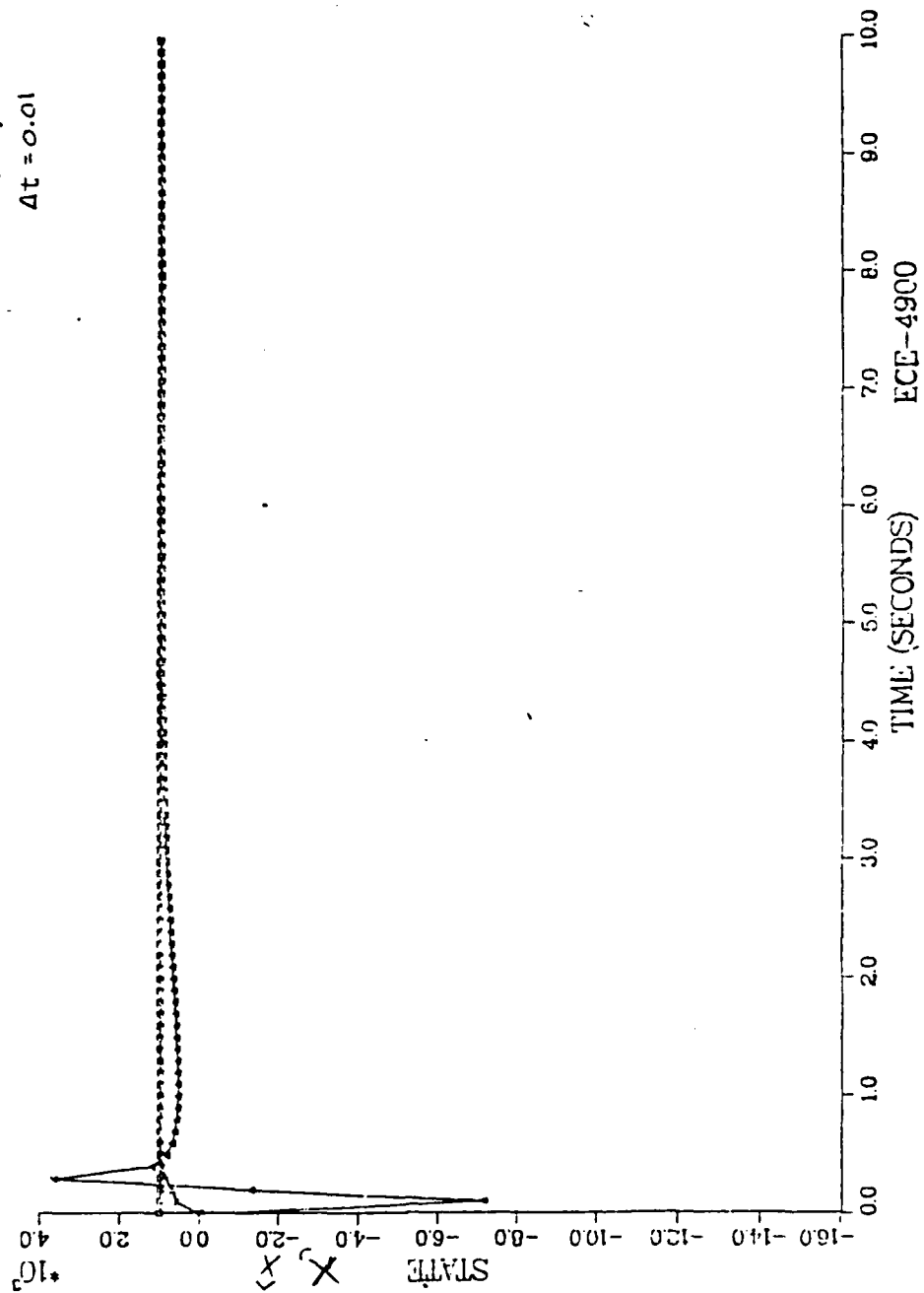
DECOUPLED MODEL

$\square - X$
 $\Delta - \hat{X} ; k=1$
 $\times - \hat{X} ; k=10$
 $\Delta \tau = 0.01$



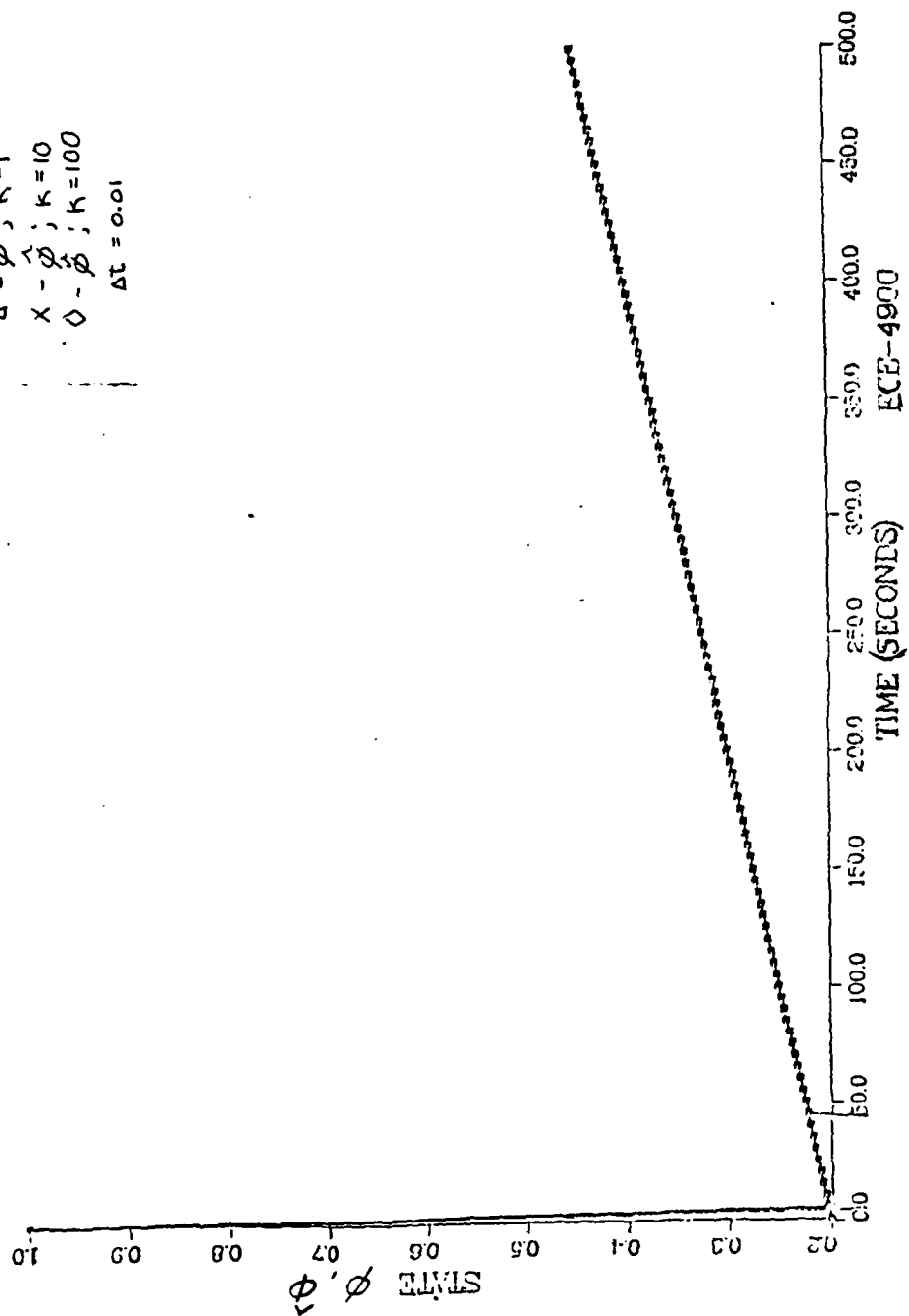
DECOUPLED MODEL

$\square - \hat{X}$
 $\Delta - \hat{X} ; k=1$
 $\times - \hat{X} ; k=10$
 $\Delta t = 0.01$



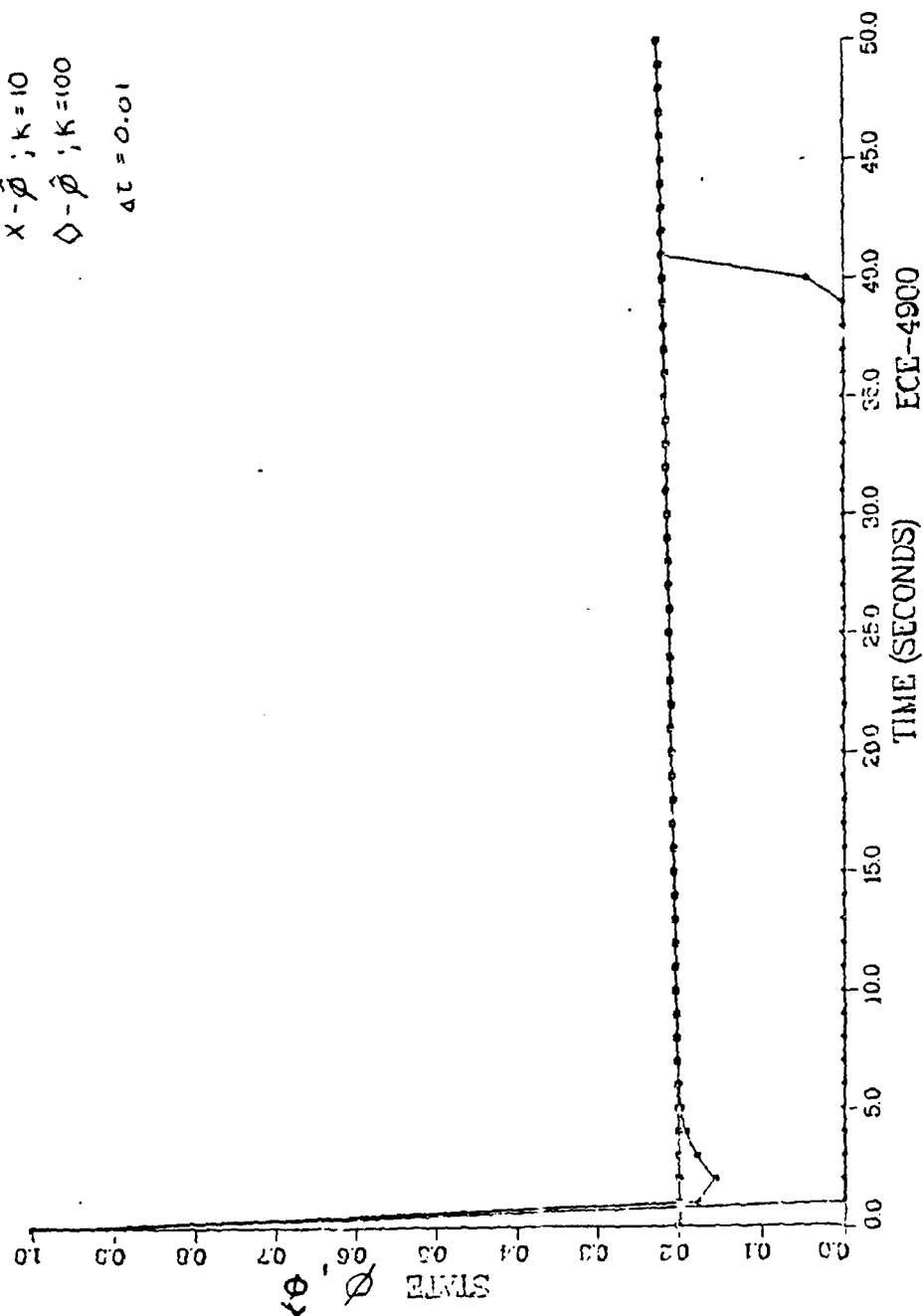
DECOUPLED MODEL

$\square - \phi$
 $\Delta - \hat{\phi}; K=1$
 $\times - \hat{\phi}; K=10$
 $\diamond - \hat{\phi}; K=100$
 $\Delta t = 0.01$



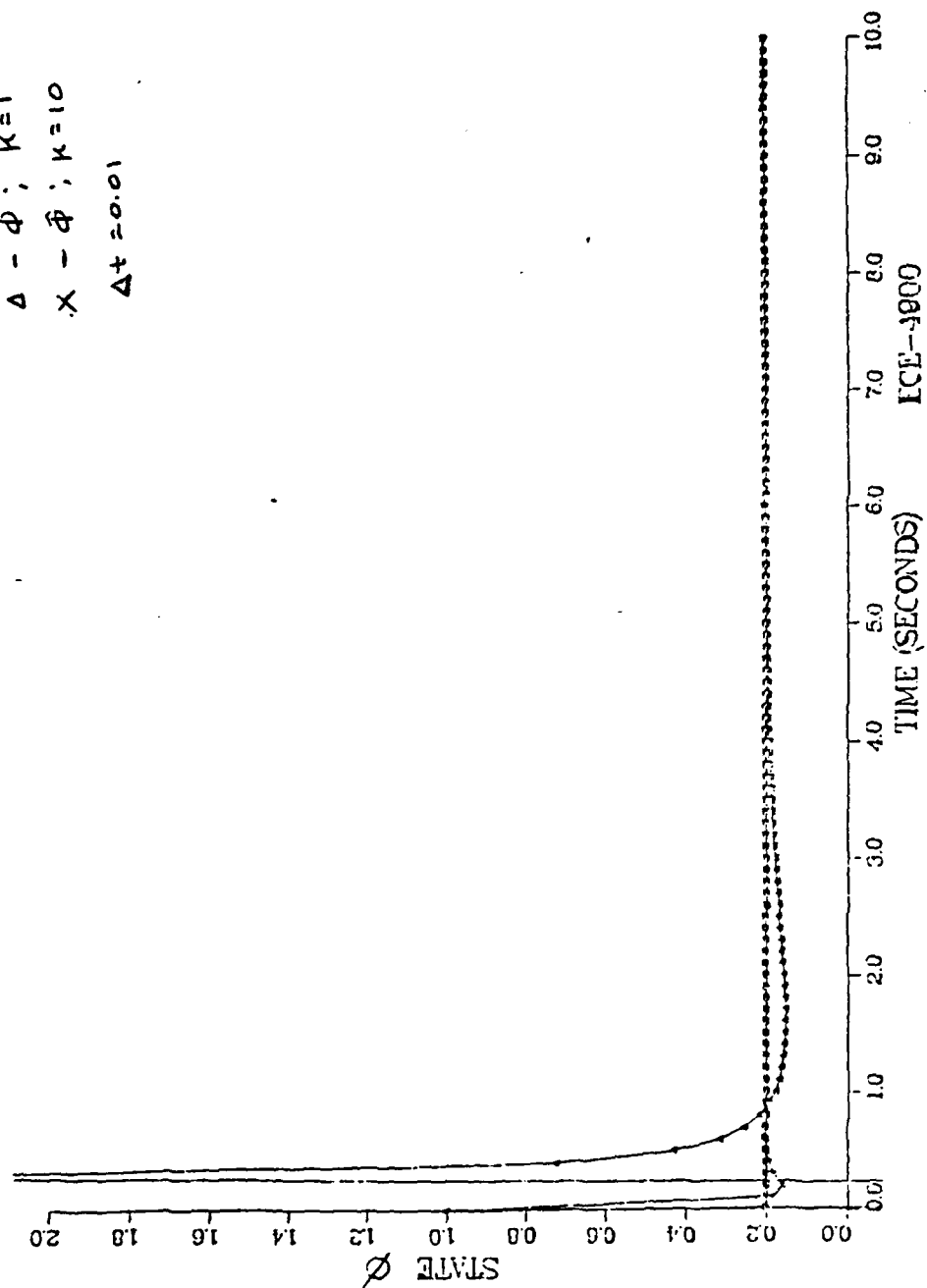
DECOUPLED MODEL

$\square - \phi$
 $\Delta - \hat{\phi}; k=1$
 $\times - \hat{\phi}; k=10$
 $\diamond - \hat{\phi}; k=100$
 $\Delta t = 0.01$



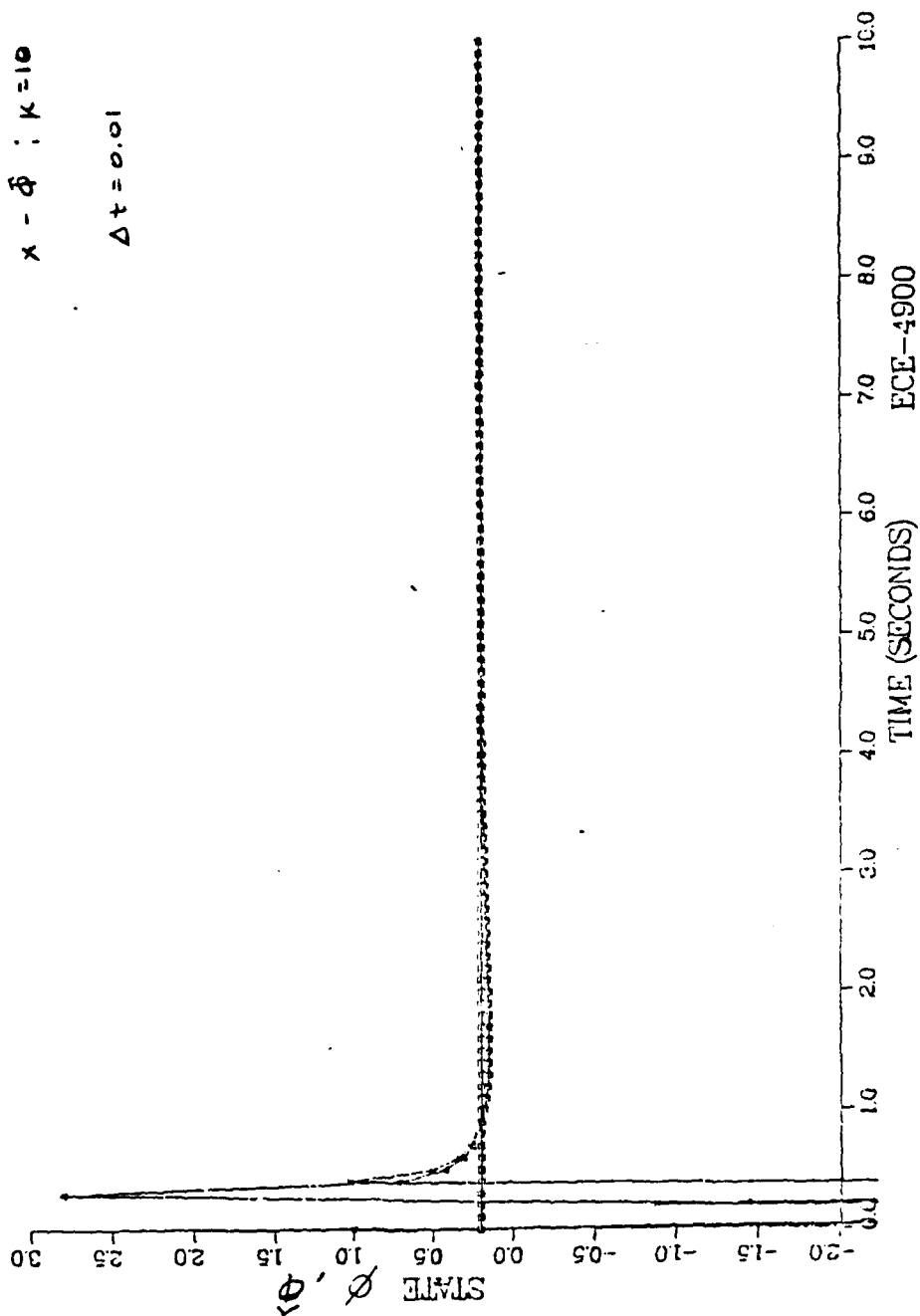
DECOUPLED MODEL

$\square - \phi$
 $\Delta - \hat{\phi}; K=1$
 $\times - \hat{\phi}; K=10$
 $\Delta t = 0.01$



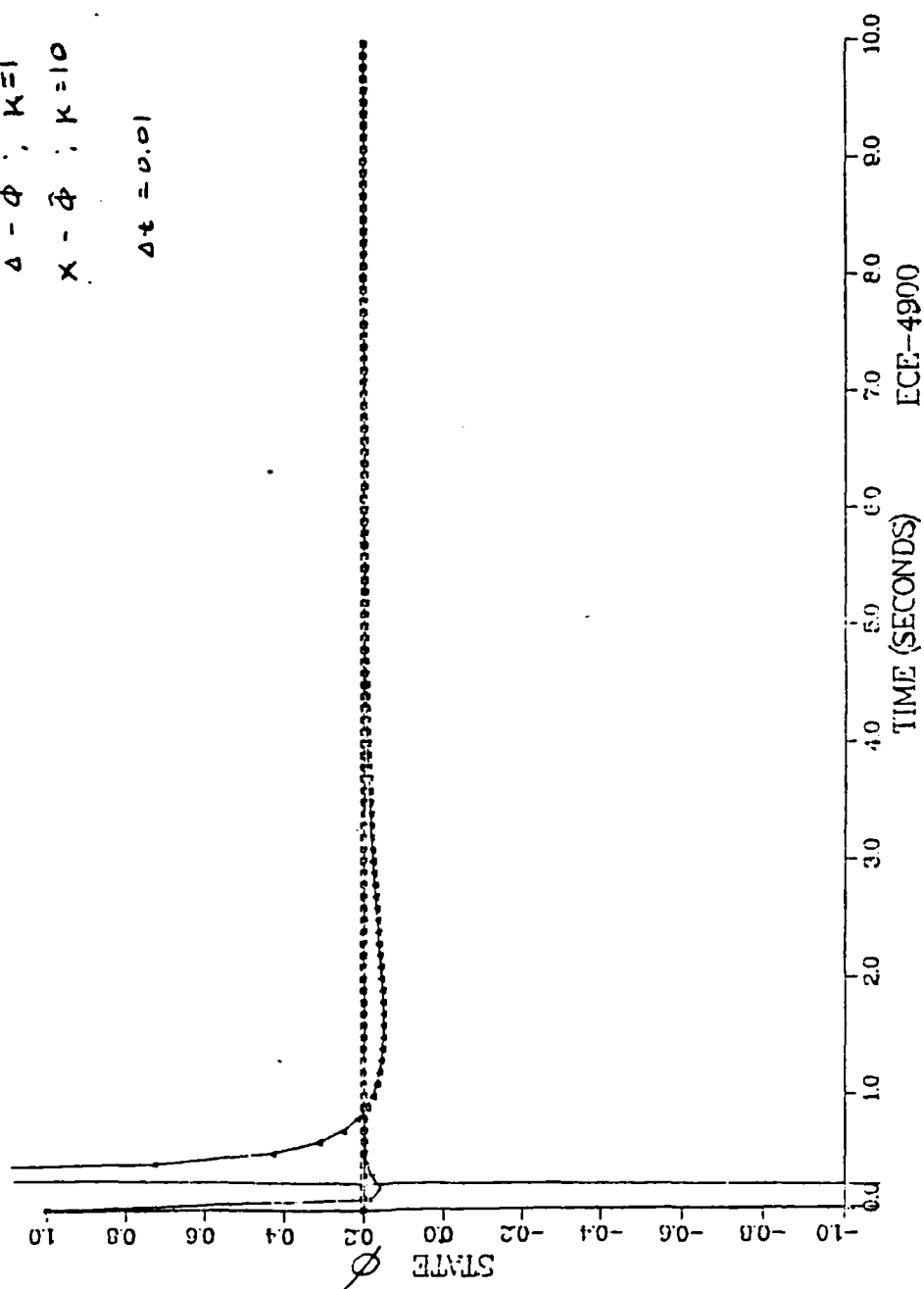
DECOUPLED MODEL

$$\begin{aligned} \square - \phi \\ \Delta - \hat{\phi} ; K=1 \\ \times - \hat{\phi} ; K=10 \\ \Delta t = 0.01 \end{aligned}$$

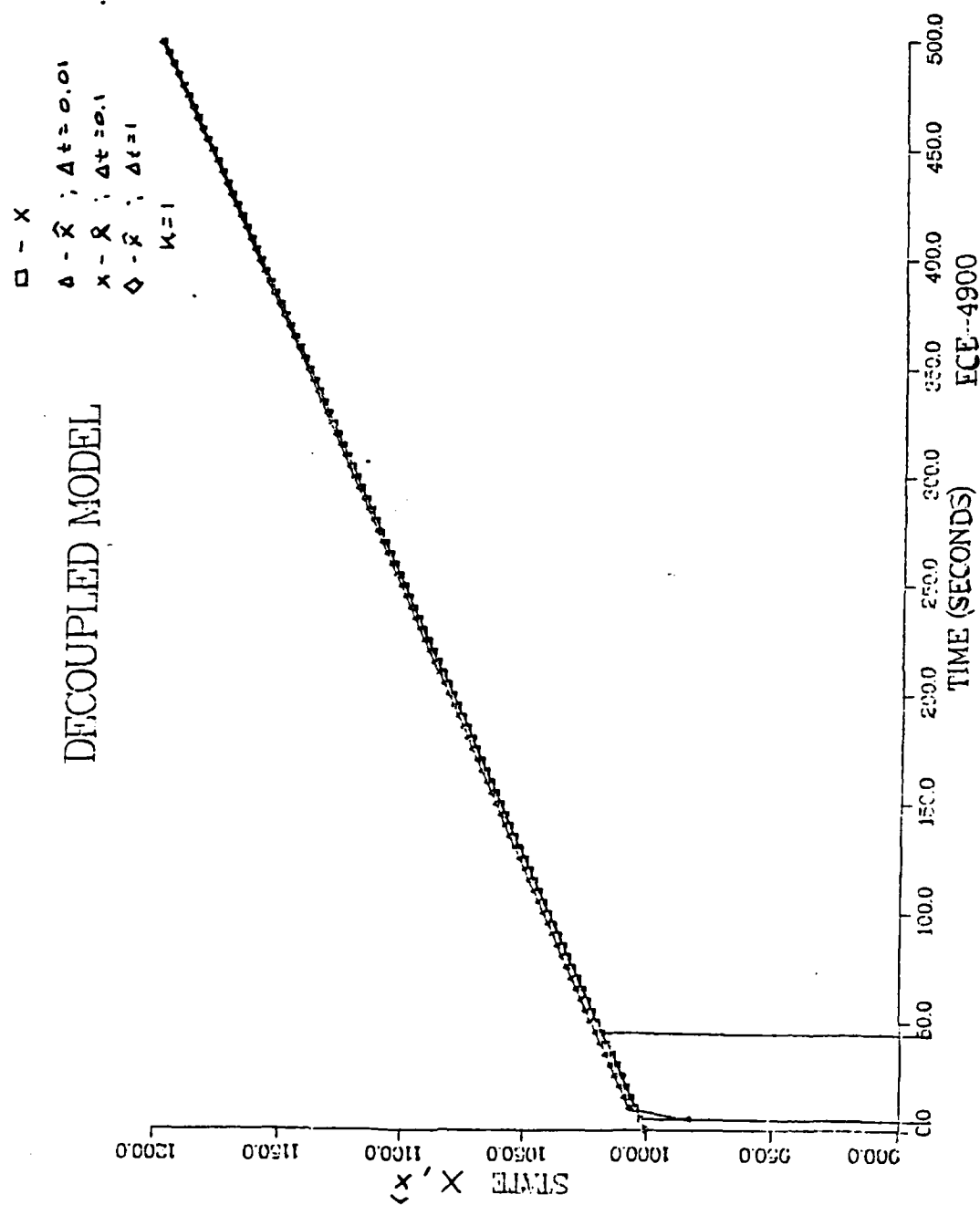


DECOUPLED MODEL

$\phi - \phi$
 $\Delta - \hat{\phi} ; \kappa = 1$
 $\chi - \hat{\phi} ; \kappa = 10$
 $\Delta t = 0.01$

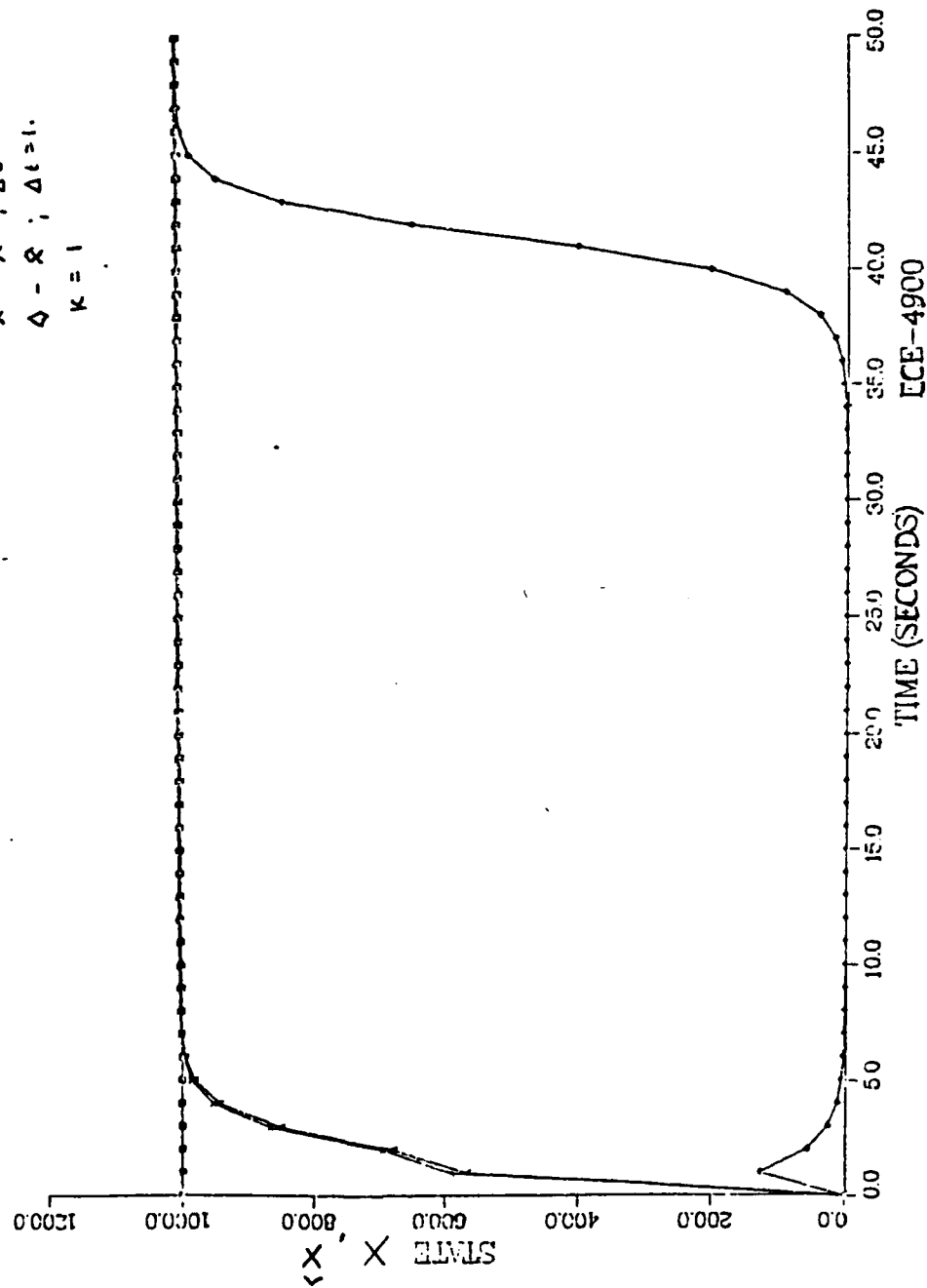


DECOUPLED MODEL



DECOUPLED MODEL

$\square - \hat{x}$
 $\Delta - \hat{x} ; \Delta t = 0.01$
 $\times - \hat{x} ; \Delta t = 0.1$
 $\diamond - \hat{x} ; \Delta t = 1.$
 $K = 1$



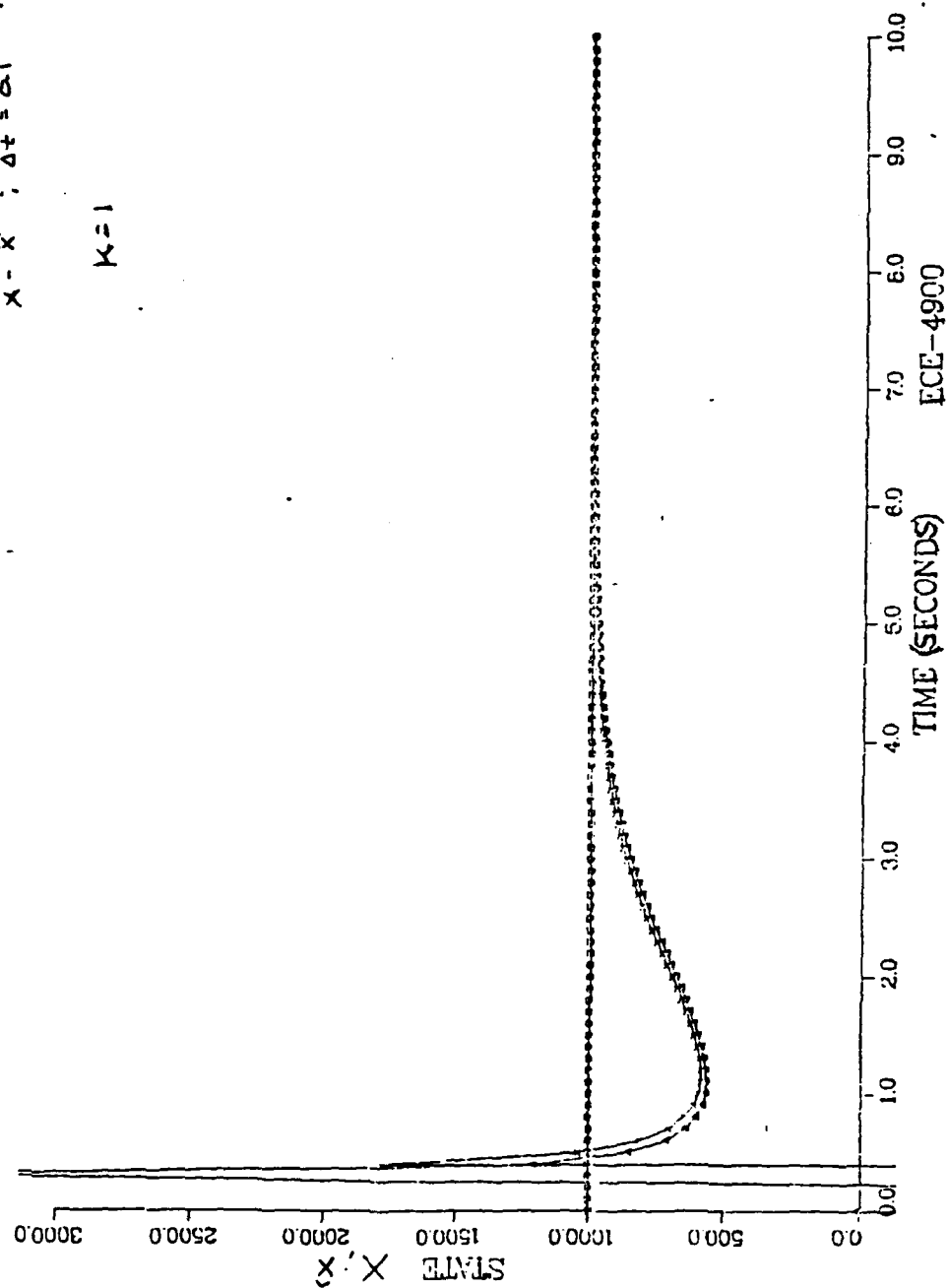
DECOUPLED MODEL

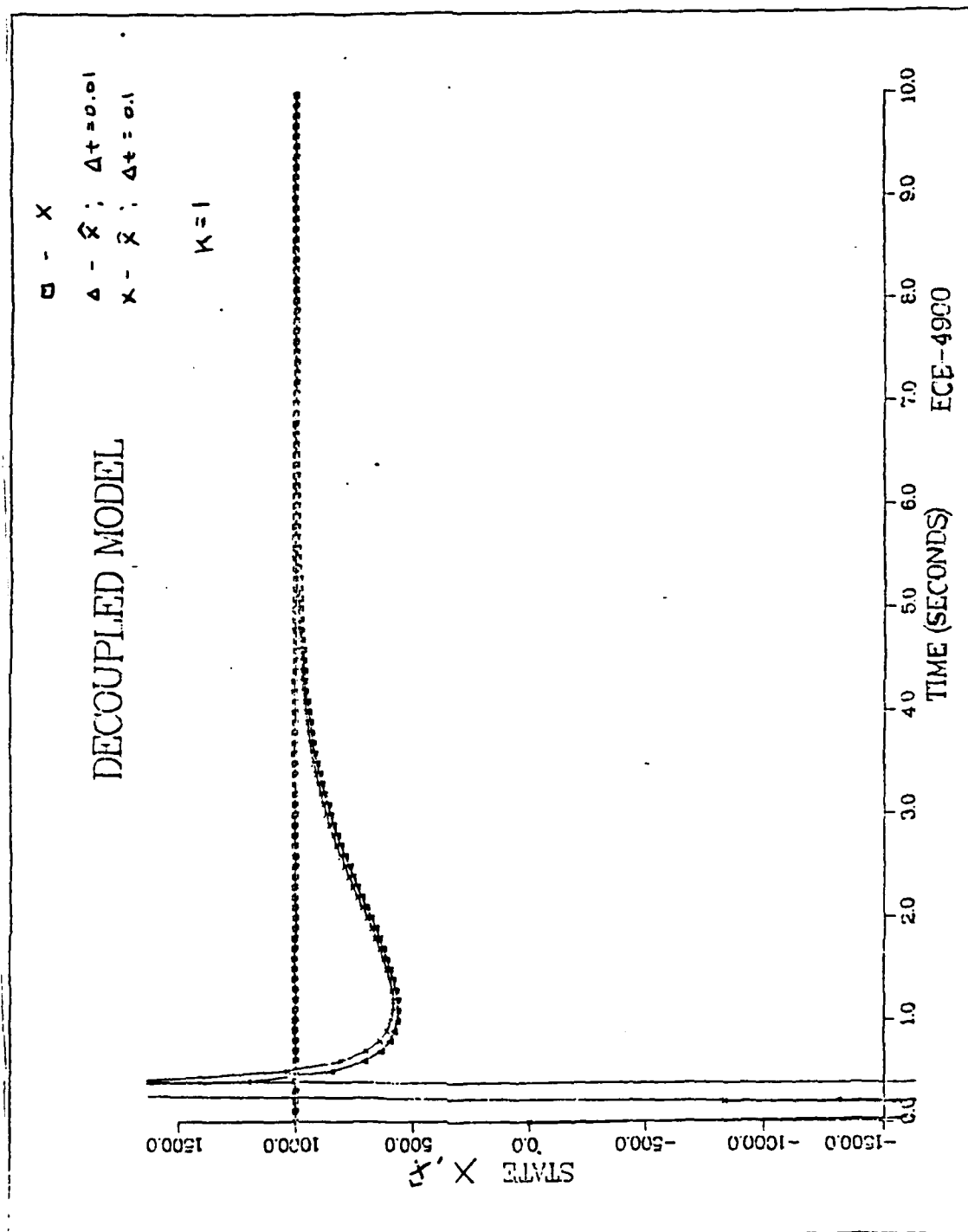
$\square - \hat{x}$

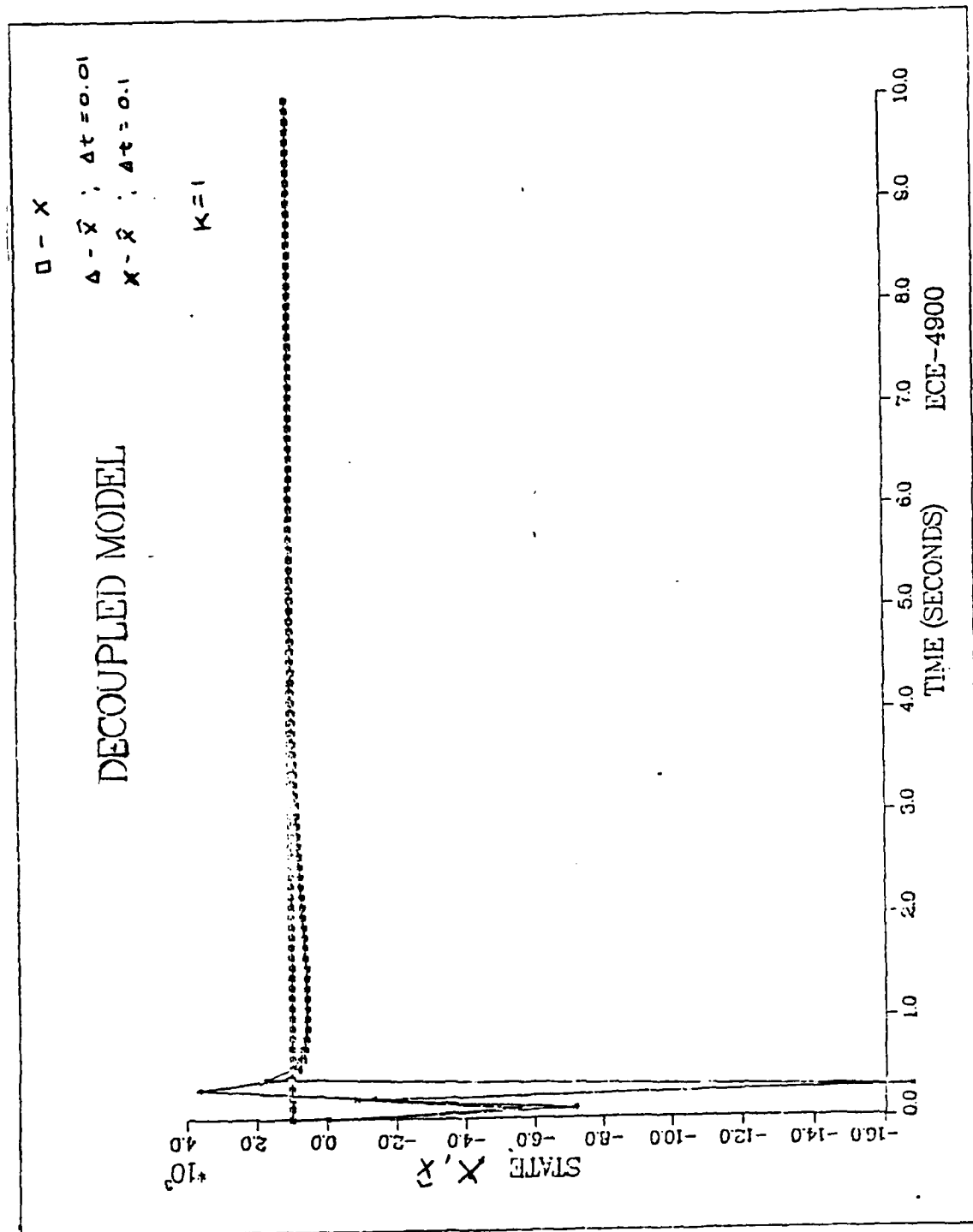
$\Delta - \hat{x} ; \Delta t = 0.01$

$\times - \hat{x} ; \Delta t = 0.1$

$K=1$

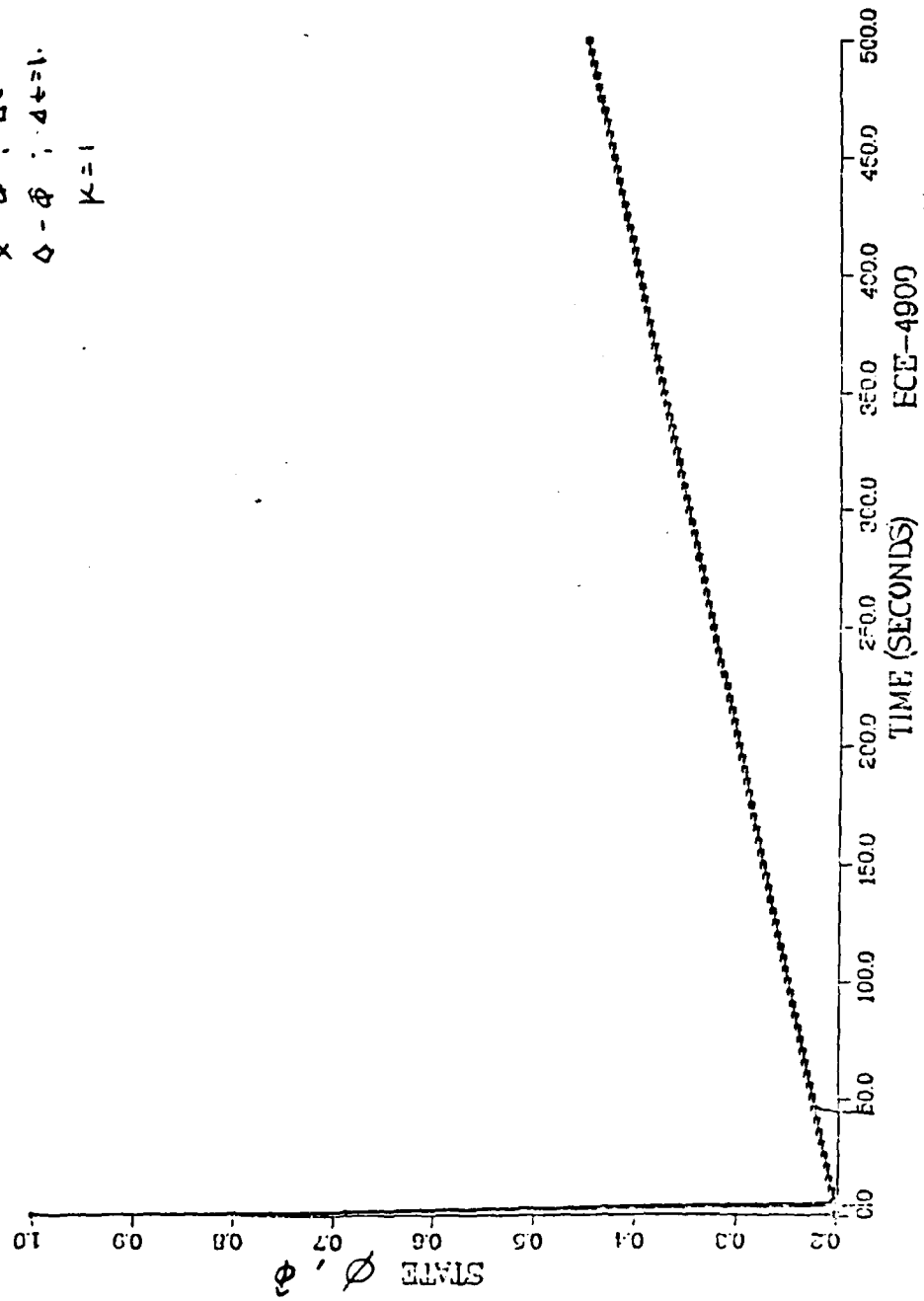






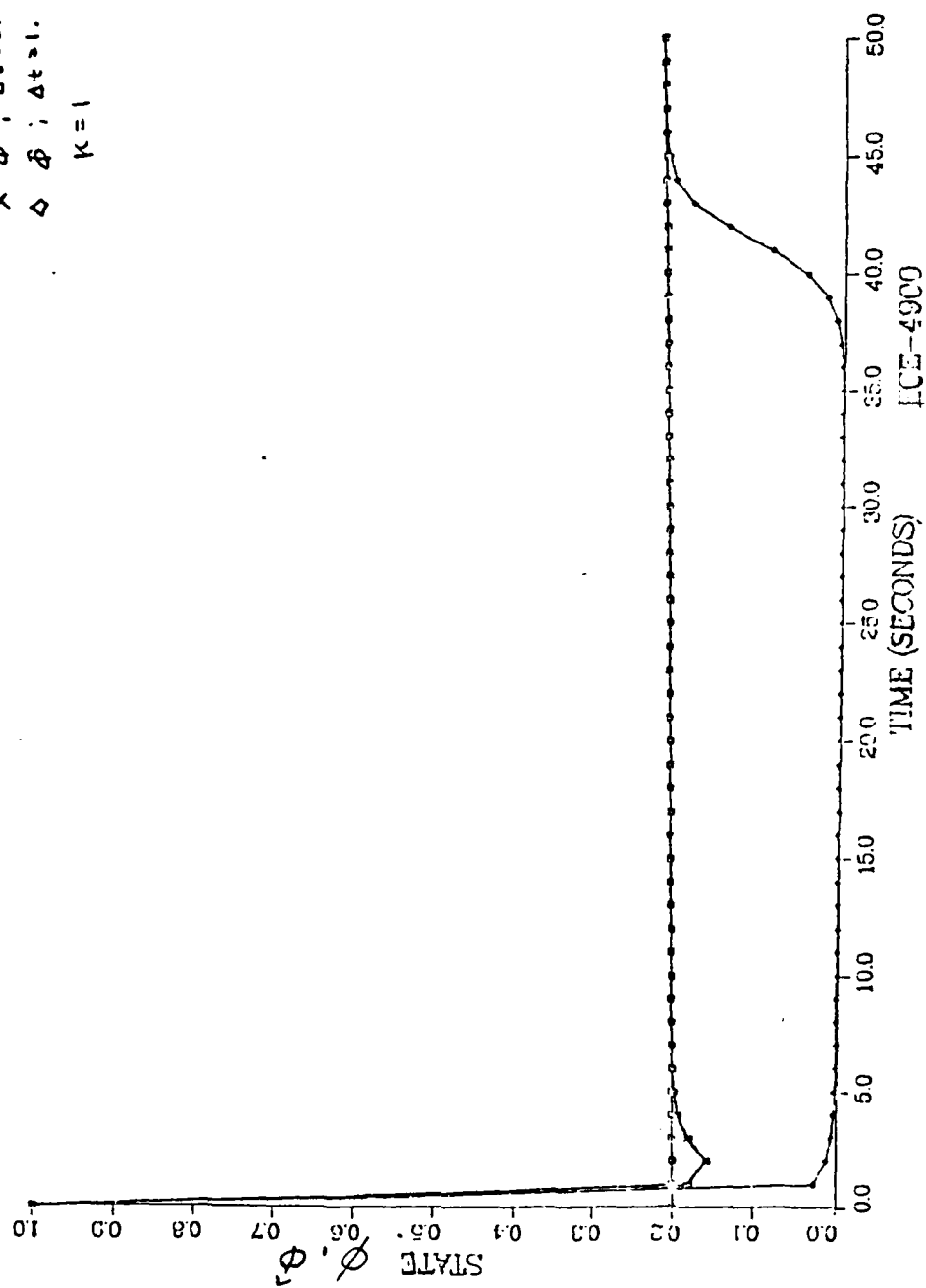
DECOUPLED MODEL

$\square - \phi$
 $\Delta - \hat{\phi} ; \Delta t = 0.01$
 $\times - \hat{\phi} ; \Delta t = 0.1$
 $\diamond - \hat{\phi} ; \Delta t = 1.$
 $\kappa = 1$



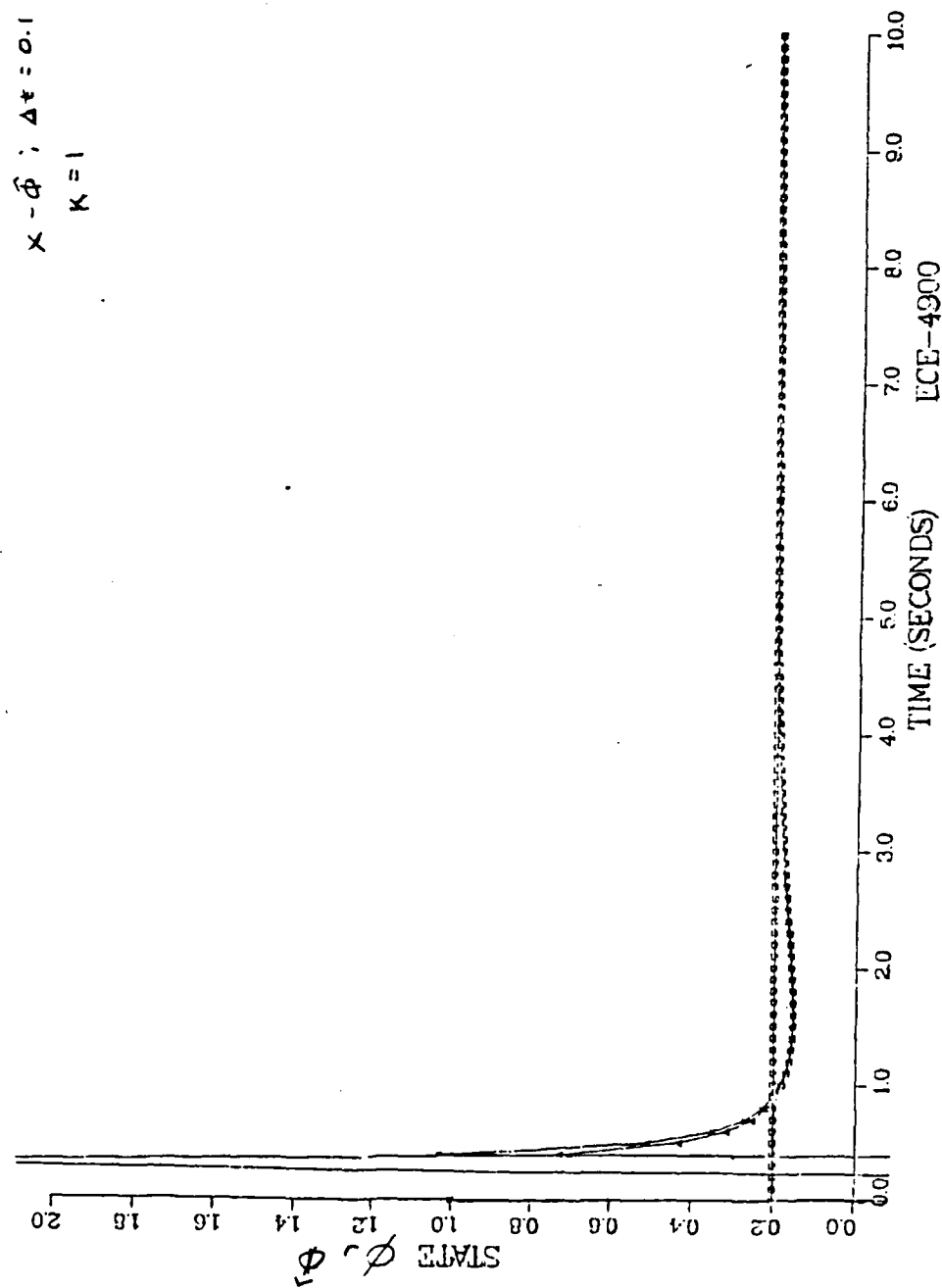
DECOUPLED MODEL

$\square \phi$
 $\Delta \phi; \Delta t = 0.01$
 $\times \phi; \Delta t = 0.1$
 $\diamond \phi; \Delta t = 1.$
 $K = 1$



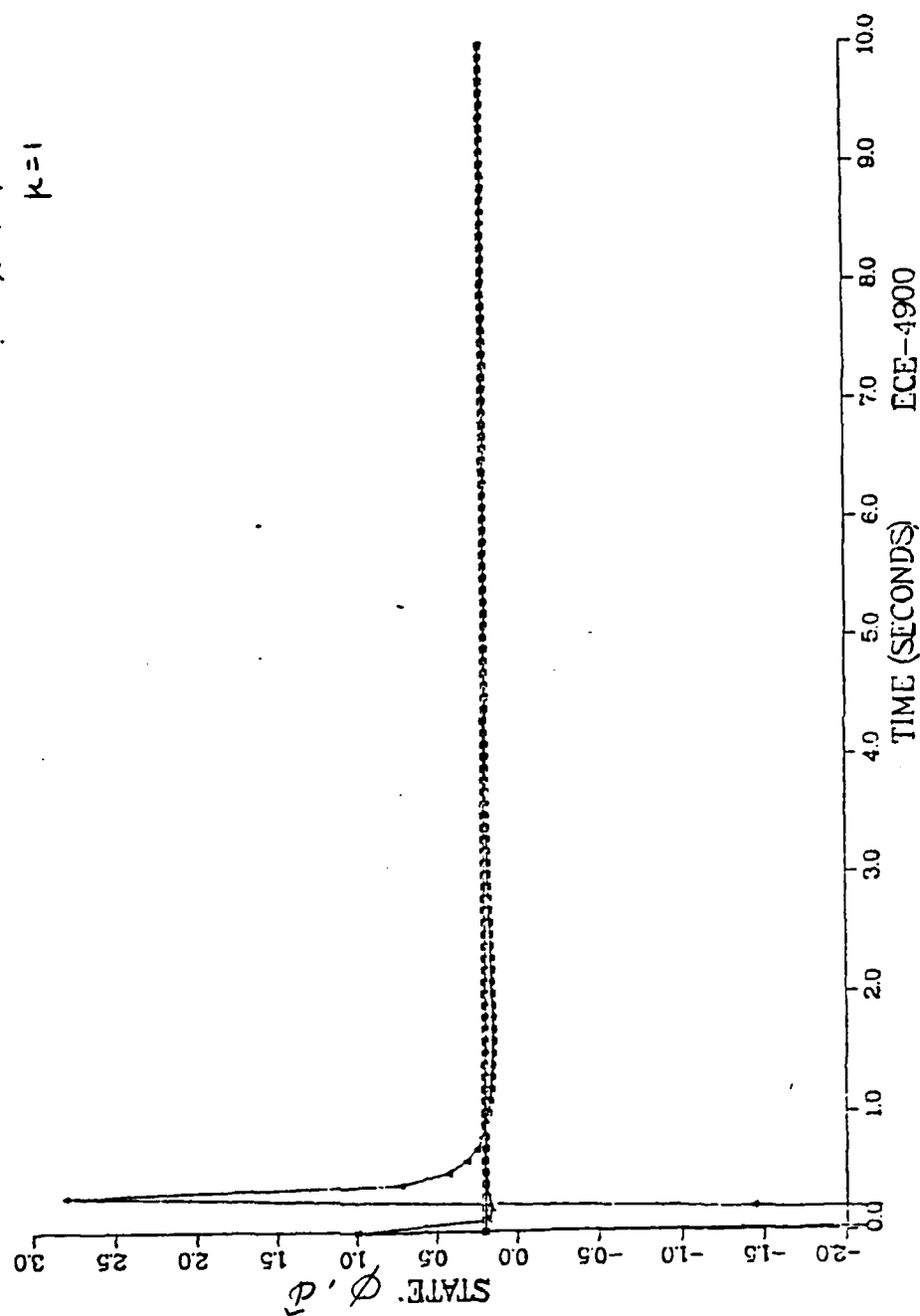
DECOUPLED MODEL

$\square - \phi$
 $\Delta - \hat{\phi} ; \Delta t = 0.01$
 $\times - \hat{\phi} ; \Delta t = 0.1$
 $K = 1$



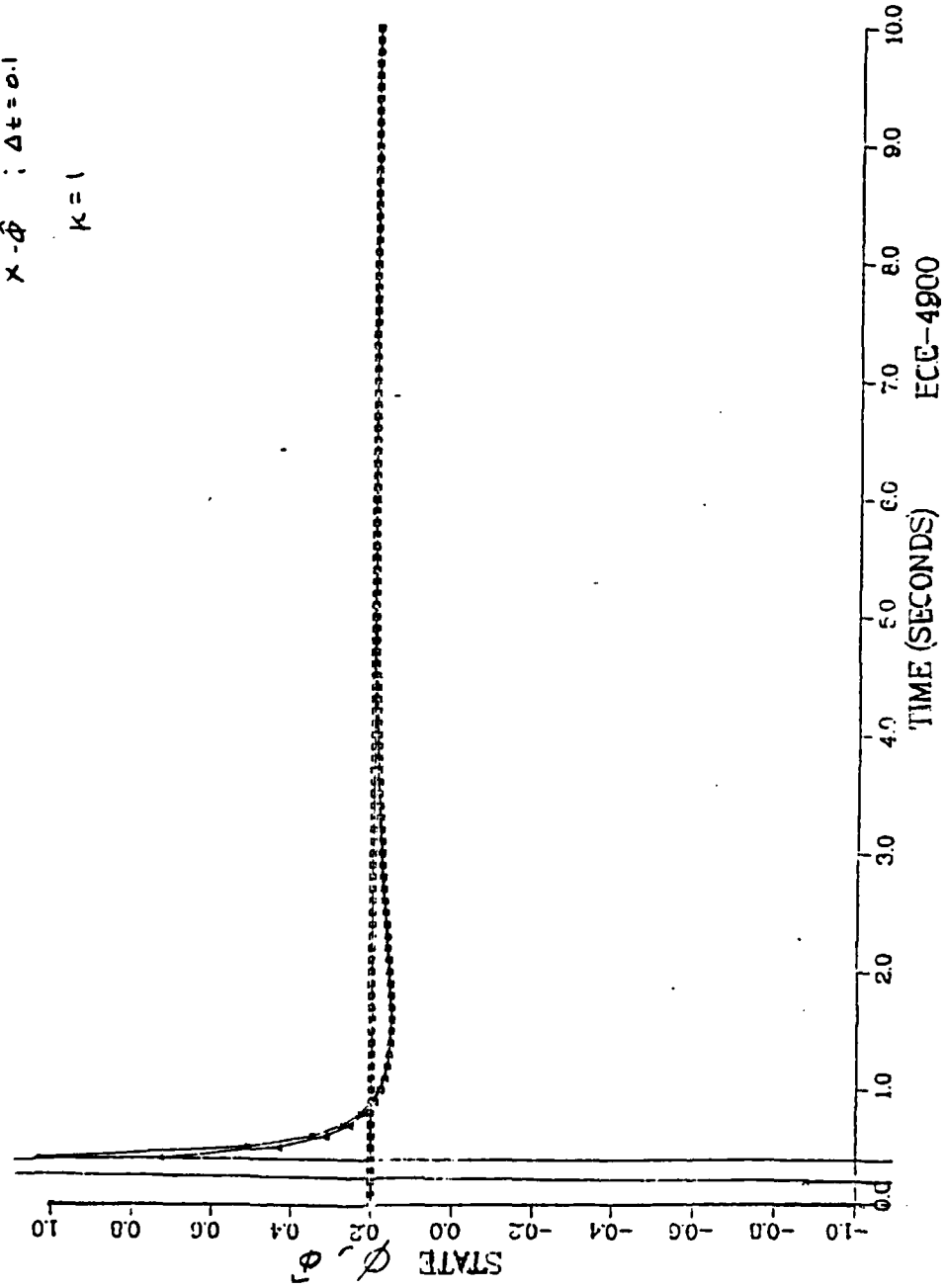
DECOUPLED MODEL

$\phi - \hat{\phi}$
 $\Delta - \hat{\Delta} ; \Delta t = 0.01$
 $X - \hat{X} ; \Delta t = 0.1$
 $K = 1$



DECOUPLED MODEL

$\phi - \hat{\phi}$
 $\Delta - \hat{\Delta}$; $\Delta t = 0.01$
 $\chi - \hat{\chi}$; $\Delta t = 0.1$
 $K = 1$



LIST OF REFERENCES

1. Abell, George O., Exploration of the Universe, 3rd ed., pp. 81-82, Holt, Rinehart and Winston, 1975.
2. Baily, John M., Liberal Arts Physics Invariance and Change, pp. 108-111, W. H. Freeman and Company, 1974.
3. Halliday, David and Resnick, Robert, Fundamentals of Physics, 2nd ed., pp. 252, 687-681, John Wiley & Sons Inc., 1981.
4. Deutsh, Ralph, Orbital Dynamics of Space Vehicles, pp. 268-283, Prentice-Hall, Inc., 1963
5. Naval Research Laboratory (NRL Report 7975), Orbital Mechanics of General Coverage Satellites, by John A. Eisele and Stephen A. Nichols, pp. 5-30, 1976.
6. C. S Hwang and R. R. Mohler, Nonlinear Observability and Mixed-Coordinate Bearing Only Signal Processing, Paper sponsored by ONR Contract No. N00014-81K-0814 and the NAVELEX Chair at the Naval Postgraduate School, pp 1-6. 1984.
7. W. A. Wolovich and H. Elliott, "A Computational Technique for Inverse Kinematics", Proceedings of 23rd Conference on Decision and Control, Dec. 1984, pp 1359-1361.
8. Bond, R. E. L., Target Observability for Satellite-Based Sensors, MSEE Thesis, Naval Postgraduate School, Monterey, California, March 1985.

BIBLIOGRAPHY

Davidoff, Martin R., The Satellite Experimenter's Handbook, The American Radio Relay League, 1984.

Eisele, John A., Astrodynamics, Rockets, Satellites and Space Travel, The National Book Company of America, 1967.

Feher, Kamilo, Digital Communications Satellite/Earth Station Engineering, Prentice-Hall Inc., 1983.

Guidance and Control-II, Progress in Astronautics and Aeronautics - Volume 13, eds., Robert C. Langford, and Charles J. Mundo, Academic Press, 1961.

Guidance and Control of Aerospace Vehicles, ed., Leondes, Cornelius T., McGraw-Hill Book Company, Inc., 1963.

Hewitt, Paul G. Conceptual Physics ...a New Introduction to Your Environment, 2nd ed., Little, Brown and Company (inc.), 1974.

King-Hele, Desmond, Satellites and Scientific Research, Dover Publications, Inc., 1962.

Landau, Yoan D., Adaptive Control: The Model Reference Approach, Marcel Dekker, INC., 1979.

Ordway, Richard J., Earth Science and the Environment, D. Van Nostrand Company, 1974.

Schlack, A. L. and Sandor, Bela I., Learning and Reviewing Aid for Dynamics, Prentice-Hall, Inc., 1983.

Strahler, Arthur N., Introduction to Physical Geography, John Wiley & Sons, Inc., 1965.

INITIAL DISTRIBUTION LIST

	No.	Copies
1. Library, Code 0142 Naval Postgraduate School Monterey, California 93943-5002	2	
2. Department Chairman, Code 62 Dept. of Electrical and Computer Engineering Naval Postgraduate School Monterey, California 93943-5000	1	
3. Professor Srbijanka Turajlic, Code 62TC Dept. of Electrical and Computer Engineering Naval Postgraduate School Monterey, California 93943-5000	2	
4. Professor Anthony Rigas, Code 62RX Dept. of Electrical and Computer Engineering Naval Postgraduate School Monterey, California 93943-5000	1	
5. Professor Ronald R. Mohler Dept. of Electrical and Computer Engineering Oregon State University Corvallis, Oregon 97331	2	
6. Captain James Kesler, SMC 2002 Naval Postgraduate School Monterey, California 93943	1	
7. Professor Roberto Cristi, Code 62CX Dept. of Electrical and Computer Engineering Naval Postgraduate School Monterey, California 93943-5000	1	
8. Lieutenant M. G. Mort Computer Science Department U. S. Naval Academy Annapolis, MD 21402-5002	3	

END

Dtic

7-86